ALGORITHMS TO PROCESS AND MEASURE BIOMETRIC INFORMATION CONTENT IN LOW QUALITY FACE AND IRIS IMAGES

RICHARD YOUMARAN

Thesis submitted to the
Faculty of Graduate Studies and Research
In partial fulfillment of the requirements
For the degree of Doctor of Philosophy in
Electrical and Computer Engineering

School of Information Technology
Faculty of Graduate and Postdoctoral Studies
University of Ottawa

Abstract

Biometric systems allow identification of human persons based on physiological or behavioral characteristics, such as voice, handprint, iris or facial characteristics. The use of face and iris recognition as a way to authenticate user's identities has been a topic of research for years. Present iris recognition systems require that subjects stand close (<2m) to the imaging camera and look for a period of about three seconds until the data are captured. This cooperative behavior is required in order to capture quality images for accurate recognition. This will eventually restrict the amount of practical applications where iris recognition can be applied, especially in an uncontrolled environment where subjects are not expected to cooperate such as criminals and terrorists, for example. For this reason, this thesis develops a collection of methods to deal with low quality face and iris images and that can be applied for face and iris recognition in a non-cooperative environment. This thesis makes the following main contributions:

I. For eye and face tracking in low quality images, a new robust method is developed. The proposed system consists of three parts: face localization, eye detection and eye tracking. This is accomplished using traditional image-based passive techniques such as shape information of the eye and active based methods which exploit the spectral properties of the pupil under IR illumination. The developed method is also tested on underexposed images where the subject shows large head movements.

II. For iris recognition, a new technique is developed for accurate iris segmentation in low quality images where a major portion of the iris is occluded. Most existing methods perform generally quite well but tend to overestimate the occluded

regions, and thus lose iris information that could be used for identification. This information loss is potentially important in the covert surveillance applications we consider in this thesis. Once the iris region is properly segmented using the developed method, the biometric feature information is calculated for the iris region using the relative entropy technique. Iris biometric feature information is calculated using two different feature decomposition algorithms based on Principal Component Analysis (PCA) and Independent Component Analysis (ICA).

III.   For face recognition, a new approach is developed to measure biometric feature information and the changes in biometric sample quality resulting from image degradations. A definition of biometric feature information is introduced and an algorithm to measure it proposed, based on a set of population and individual biometric features, as measured by a biometric algorithm under test. Examples of its application were shown for two different face recognition algorithms based on PCA (Eigenface) and Fisher Linear Discriminant (FLD) feature decompositions.

Acknowledgments

I would like to dedicate this thesis to my son, Alexandre and to my wife, Nadine who never stopped being a source of support and encouragement.

I would also like to take this opportunity and thank my supervisor, Dr Andy Adler, for his support, guidance and understanding. His comments and suggestions for further development as well as his assistance during writing this thesis are invaluable to me.

I would also like to thank my friends, Liepeng Xie and Yednek Asfaw for their constant support and help. We have had many useful discussions that played a major role in my learning process.

Finally, I want to express my deepest appreciation for my parents, my sister and my brother for being a constant source of loving support throughout the years.

Contents

List of Figures

Nomenclature

BI   Biometric Information

CMC   Cumulative Match Curve

DCAC   Discrete Circular Active Contour

DET   Detection Error Trade-off

EER   Equal Error Rate

FAR   False Accept Rate

FDA   Fisher Discriminant Analysis

FMR   False Match Rate

FNMR   False Non Match Rate

FRR   False Reject Rate

HD   Hamming Distance

ICA   Independent Component Analysis

IR   Infrared

LDA   Linear Discriminant Analysis

LoG   Laplacian of Gaussian

NC   Normalized Correlation

NIR   Near Infrared

PCA   Principal Component Analysis

ROC   Receiver Operating Characteristic

SVD   Singular Value Decomposition

SBI   System Biometric Information

WED   Weighted Euclidean Distance

Chapter 1

Introduction

1.1 Thesis Objectives

Biometrics is an emerging field of information technology that is crucial for human identification and verification. Biometric technologies measure and recognize human physical and behavioral characteristics for authentication purposes. Some of the most common physical characteristics include fingerprints, irises, and facial patterns. The use of face and iris recognition as a way to authenticate user's identities has been a major topic of research (Jain *et al.* (2004)). While many image processing algorithms exist for iris and face recognition, their performance is not completely reliable, especially in situations with variable lighting, and when dealing with low resolution images (Ma *et al.* (2004), Tajbakhsh *et al.* (2008)). Face and iris recognition algorithms are widely used; in most cases, images are taken from a cooperative individual under a controlled environment in order to provide satisfactory results (Ma *et al.* (2004)). Present iris recognition systems require that subjects stand close (< 2m) to the imaging camera and look for a period of about three seconds until the data are captured (*International Biometric Group* (2005)). This cooperative behavior is required in order to capture good quality images for accurate recognition. This will eventually restrict the amount of practical applications where iris recognition can be applied, especially in an uncontrolled environment where subjects are not expected to cooperate. Hence, these techniques have

limited capability of identifying non-cooperative subjects for applications such as surveillance, where the observed individuals are non-cooperating and/or non-habituated to the technology.

For this reason, this thesis aims on developing a new system that is composed of a collection of methods that deal with low quality face and iris images and that can be applied for face and iris recognition in a non-cooperative environment. Hence, the developed techniques can be used for automatically detecting and recognizing human subjects via their face and iris traits using images taken at a long distance without any subject cooperation.

Images taken from a non-cooperating individual at-a-distance in a very dynamic environment tend to include more distortions and noise (i.e. low quality underexposed images, obstructions by eyelids or eyelashes and reflections). For the terms of our work and of this thesis, all these factors are considered as *noise* and the processed images are described as *low quality*.

The thesis objectives consist of the following:

i.   Using infrared illumination to improve eye and face tracking in low quality and underexposed video images where subject is moving.

ii.   Improved identification of iris and eyelash features in low quality images where a major portion of the iris is occluded by eyelash noise, eyelid or specular reflections.

iii.   Measuring information content in biometric iris and face features.

iv.   Measuring biometric sample quality in terms of biometric information for face features.

1.2 Thesis contributions

The major thesis contributions include:

i.   For eye and face tracking in low quality images, a new system is developed using the "Bright-pupil" effect — specular reflection from the retina of human eyes under co-axial infrared illumination (Haro *et al.* (2000), Morimoto *et al.* (1998)). By using IR illumination, it is possible to get information from which the eye positions in the image can be calculated. Our algorithm consists of three parts: face localization, eye detection and eye tracking. This is accomplished using traditional image-based passive techniques such as shape information of the eye and active based methods which exploit the spectral properties of the pupil under IR illumination. We also address the problem of processing eye image containing weak reflections due to occlusion or eye closure using adaptive thresholding techniques to extract the eye contour. The developed method is also tested on underexposed images where the subject shows large head movements.

This work resulted in the following publications:

- *Conference paper in the 24th Queen's Biennial Symposium on Communications, QBSC 2008, Kingston, Canada, June 24 - June 26 (*Youmaran *et al.* (2008)).

- *Conference paper in Canadian Conference of Computer and Electrical Engineering (CCECE), Ottawa, Canada, May 7-10 (*Youmaran *et al.* (2006))

ii.   A new technique is developed for accurate iris segmentation using low quality iris images. A major portion of the iris is occluded with eyelash, eyelids and/or specular reflections. Most existing methods tend to overestimate the occluded regions, and thus lose iris information that could be used for identification. For this reason, the new method addresses most of these issues by using a collection of image processing techniques such as: non-linear image enhancement, edge detection, morphological operators, Hough transform, intensity gradient based algorithm and a block mean and variance method using region's local statistics.

This work resulted in the following publication:

- *Conference paper in the 24th Queen's Biennial Symposium on Communications, QBSC 2008, Kingston, Canada, June 24 - June 26 (*Youmaran *et al*. (2008)).

iii.   For face recognition, an approach is developed to measure biometric feature information and the changes in biometric sample quality resulting from image degradations. A definition of biometric feature information is introduced and an algorithm to measure it proposed, based on a set of population and individual biometric

features, as measured by a biometric algorithm under test. Examples of its application were shown for two different face recognition algorithms based on PCA (Eigenface) and FLD feature decompositions. Subsequently, we introduced a measure of information loss as a function of image degradation.

This work resulted in the following publications:

- *Journal paper in Pattern Analysis & Applications, 12:261-270 (*Adler *et al.* (2009)).

- *Book chapter in Biometrics: Theory, Methods, and Applications N.V. Boulgouris, K.N. Plataniotis, and E.Micheli-Tzanakou (Eds), In press: Wiley/IEEE2008 (*Youmaran *et al.* (2008)).

- *In Biometrics Consortium Conference 2006, Sep. 19-21, Baltimore, MD, USA (*Youmaran *et al.* (2006)).

- *Conference paper in Canadian Conference of Computer and Electrical Engineering (CCECE), Ottawa, Canada, May 7-10 (*Youmaran *et al.* (2006)).

iv.   For iris recognition, a new algorithm is developed to calculate biometric information for a set of iris features using the relative entropy measure developed in this thesis (section 5.2). The developed algorithm is divided in the following steps:

i. Distribution modeling of iris biometric features, ii. Relative entropy calculations, iii. ICA iris feature extraction and biometric information calculation. The iris regions used in the entropy calculation are obtained using the enhanced iris segmentation techniques developed in section (4.2).

1.3 Thesis outline

Chapter 2 presents a review of Biometrics. It includes a brief description of current biometric technology related to face detection, face recognition and iris recognition. It also describes some of the face detection and recognition algorithms that are used in similar applications.

Chapter 3 presents a new system for face detection and tracking that is designed for low quality video images using a Kalman filter type tracker. The technique extracts and tracks face and eye positions from surveillance type images with infrared strobe taken under poor illumination. In the case where many reflections occur, the algorithm will find all possible eye locations and presents the best solution using multi-stage classification techniques. The algorithm is tested using 1800 images taken from two different IR image databases.

Chapter 4 presents a new technique for eyelash noise detection, accurate iris boundary extraction and ideal iris segmentation. The proposed techniques locate the iris region using logarithmic image enhancement and the Hough transform techniques, locate the iris boundary, extract the exact iris contour, detect eyelashes based on the local image statistics and block intensity and propose an improved iris model for accurate iris recognition. The developed method overcomes the limitations encountered in other iris segmentation and eyelash detection techniques such that it detects accurately separable and multiple eyelashes, extracts the exact iris contour and is illumination invariant. The

performances of the enhanced method are studied and compared to the existing Masek's technique implemented based on Daugman's work (Masek (2003), Daugman (2003)).

Chapter 5 presents a new approach to measure biometric feature information and the changes in biometric sample quality resulting from image degradations. A definition of biometric feature information is introduced and an algorithm to measure it proposed, based on a set of population and individual biometric features, as measured by a biometric algorithm under test. Examples of its application were shown for two different face recognition algorithms based on PCA (Eigenface) and FLD feature decompositions. Subsequently, a new measure of information loss as a function of image degradation is introduced.

This chapter presents a new approach to measure biometric feature information using the segmented iris region from chapter 4. A definition of iris biometric feature information is introduced and an algorithm to measure it proposed, based on a set of biometric iris features. Biometric information (in bits) is calculated for iris using two different feature decomposition spaces. First, biometric information is computed on PCA features and then using ICA feature decomposition scheme. Since iris features tend to be non-Gaussian, biometric information using ICA features seems to be a more accurate measure since ICA maximizes non-Gaussianity.

Finally, chapter 6 concludes this thesis by summarizing the work proposed in it and discussing possible future applications where the developed methods can be used.

1.4 Image databases

The following image databases are used to test the methods developed in this thesis (Figure 1.1).

Databases	Images	Description
Underexposed face images (Asfaw *et al.* (2002))	**600 images**	• IR illumination • Very low intensity images • Poor edge delineation • Subject moving • Differing pose (angle)
Aberdeen face images (Belhumeur *et al.* (1997))	**288 images** • 18 images per subject • 16 subjects • Resolution: 150×200	• Low quality • Non-uniform illumination • Various facial expressions • Out-of-focus
RPI ISL IR eye images (Wang *et al.* (2005))	**1200 images** • 9 subjects • Resolution: 320×240	• IR illumination • Challenging for tracking • Eye closure and occlusions • Rapid head movement • In/out – of plane rotation • Various Facial expressions • Non-uniform illumination
CASIA iris images (Chinese Academy of Sciences Institute of Automation. (2004))	**689 images** • 108 different classes • 6 or 7 images per class • Resolution: 320×280	• Noisy iris images • Eyelids and eyelash occlusions • Out-of-focus • Specular reflections • Lighting reflections

(a)
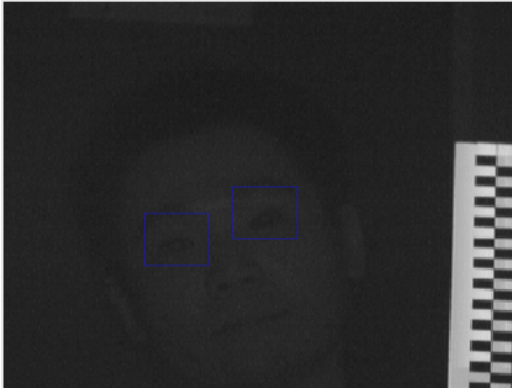
(b)

(c)
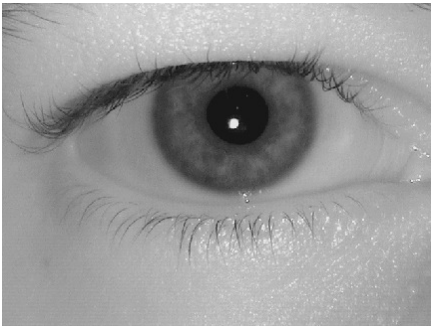
(d)

Figure 1.1: Images taken from (a) Underexposed, (b) RPI ISL IR, (c) CASIA and (d) Aberdeen databases, respectively.

Chapter 2

Biometrics review

2.1 Biometrics technology

Biometrics is an emerging field of information technology which aims to automatically identify individuals using their unique biological traits. By measuring the physiological and behavioral characteristics using the individual's biological samples, it has been shown that information characteristics of each individual can be extracted in order to verify the identity of that individual in a population. The main advantages of biometrics over other standard security systems are that biometric traits cannot be forgotten or lost. They are difficult to copy, share and distribute and they require the person to be present at the time of authentication. In most applications, a biometric system is a real-time identification system which requires the measurement of unique information (i.e. features) characterizing the individual being enrolled or tested and later comparing these samples against a database containing several candidates. Figure 2.1 shows a simplified block diagram representation of a biometric system. The first block (the sensor) acquires the necessary data to be processed and represents the interface between the real-world and the biometric system. Afterwards, the pre-processing block is used to remove artifacts and noise from the data using advanced image processing techniques that enhance the acquired information at the input of the system. Once the data are cleaned, the feature extractor creates feature vectors designed to be unique to each individual.

These features are used for the identification and matching process. Using these features, a template vector or image is then created for further processing. At the enrollment stage, the templates are stored in the database while during the matching (i.e. identification) phase, the extracted feature vectors are passed to a matcher that compares them to existing templates in the database. A similarity distance is then calculated using an algorithm which then sends a decision to the output of the biometric system allowing or restricting the individual for further operations. Depending on the context and the application, a biometric system can be either a verification/authentication (*Am I whom I claim I am*?) or an identification system (*Who am I*?) (Jain *et al.* (2004)). Verification implies making sure that the person, whose biometric information is already known in the system, is perhaps the one that he is claiming to be. This is a 1:1 match verification process which involves extracting new biometric features and then comparing them to the ones in the database in order to confirm or deny a person's claimed identity. On the other hand, identification involves establishing a person's identity. This involves extracting biometric information from the person and comparing them to the database. It is a 1: N match verification operation. It is a more computationally expensive process since most databases tend to contain a large number of templates.
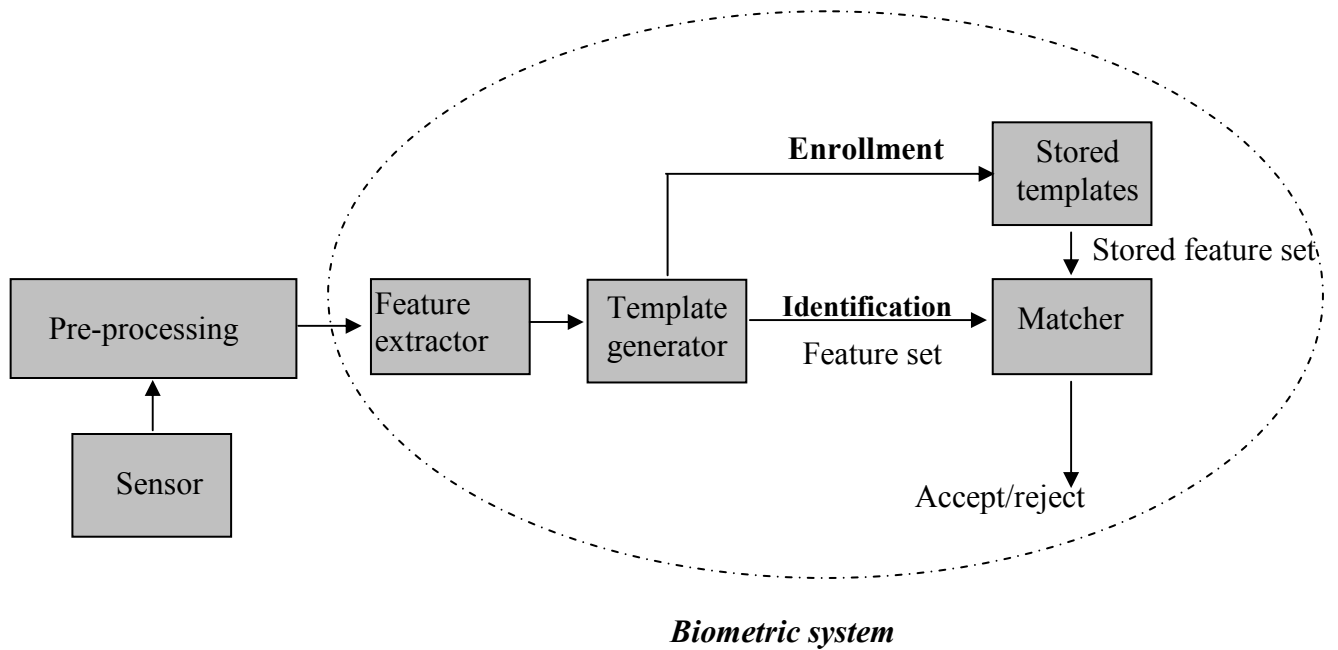
Biometric system

Figure 2.1: Evaluation Simplified block diagram representation of a biometric system

In order to analyze the performance of a biometric system, the probability distribution of genuine and impostor matching scores is examined. A genuine matching score is obtained by comparing two feature sets of the same individual while an impostor matching score is the result of comparing feature sets corresponding to two different individuals. If the matching score is higher than a certain threshold, it is then assumed that the two feature sets correspond to the same individual; otherwise, they are assumed to come from different subjects. Thus, there are two types of error that a verification biometric system can make (Jain *et al.* (2004)): (i) False rejection (*type I* error) which occurs when a genuine matching score does not exceed the threshold which means that a legitimate user is rejected and (ii) False acceptance (*type II* error) which occurs when an impostor matching score exceeds the threshold, meaning that an illegitimate user is accepted as someone else. False rejection tends to occur when the threshold in the Biometric System is selected to be more severe such as in facilities where high security is

required. For this reason, depending on the context, the biometric system must be calibrated according to the desired level of security. One example is credit card applications where it is important to keep the false reject rate low since it will not be convenient for a legitimate user to fail the authentication process when the system isn't properly calibrated.

In a biometric system, the probability that a genuine person is rejected is called false rejection rate (FRR), while false acceptance rate (FAR) is the probability that an impostor is accepted as legitimate (Figure 2.2). A receiver operating characteristic (ROC) curve plots the false reject rate (FRR) against the false accept rate (FAR) where FRR represents the percentage of genuine scores that do not exceed the threshold while FAR corresponds to the percentage of impostor scores that exceed the threshold chosen depending on the nature of the application (Figure 2.3). The point where FRR and FAR are equal is called the equal error rate (EER). The EER of a system can be used to give a threshold independent performance measure. The lower the EER is, the better is the system's performance, as the total error rate which is calculated as the sum of the FAR and the FRR at the point of the EER decreases. It is also important to mention that generally, in watch list applications, it is preferable that the biometric system produce a low FRR while in a high security context, the objective is to obtain a low FAR.

Besides these types of errors, in some cases, some individuals cannot provide good biometric data (i.e. poor quality fingerprint ridges) since they do not have the biometric feature from which there can be produced repeatable templates. The expected proportion of the population for whom the biometric system is unable to obtain good templates is called the failure to enroll rate (FTE). Similarly, a system may also be unable to capture

or locate an image of sufficient quality (Mansfield *et al.* (2002)). For example, this could

be because of worn, cut or unrecognizable prints as well as the quality of the captured

image is inadequate. In this case, the expected proportion of cases that failed to provide

good features is called the failure to acquire rate (FTAR).
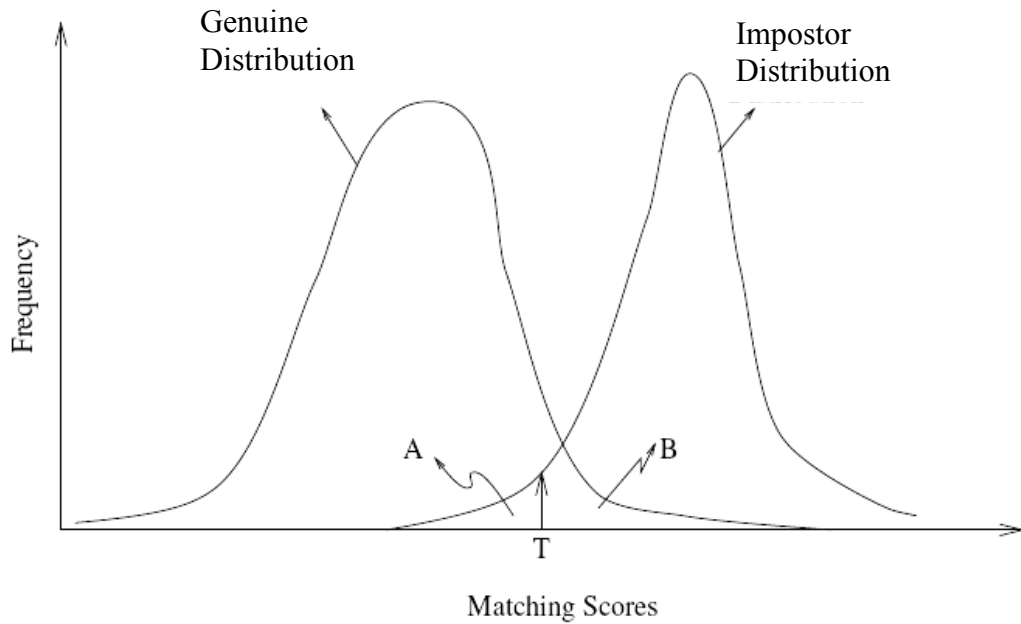
Figure 2.2: Evaluation of the matching accuracy of a biometric system. Histograms of the genuine and impostor matching scores are represented as well as the two types of errors that can arise in a biometric system given a matching score threshold (T). The areas A and B represent false accept rate (FAR) and false reject rate (FRR), respectively.
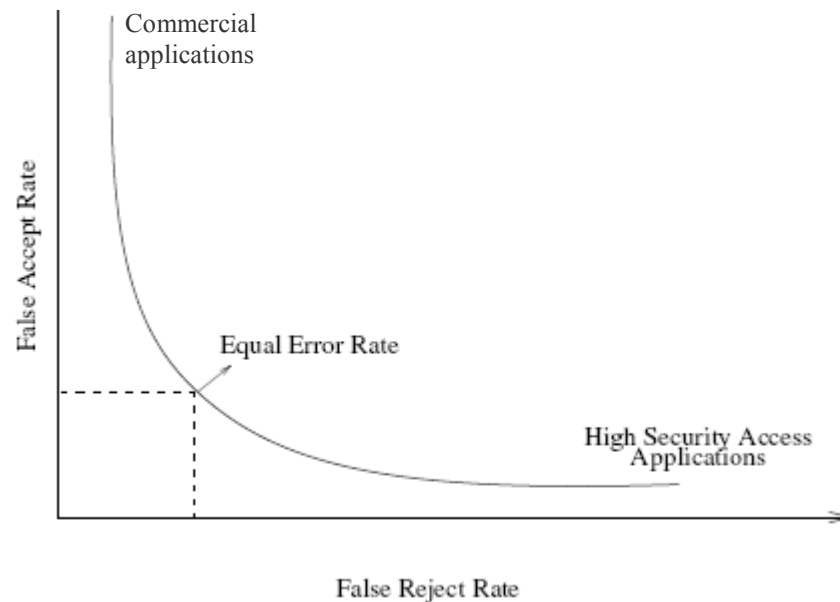
Figure 2.3: Receiver operating characteristic curve (ROC) showing the relation between false acceptance and false rejection in a biometric system.

2.2 Multimodal biometric systems

Most biometric systems deployed in real-world applications are unimodal since they rely on a single source of information for authentication (e.g., single fingerprint, iris or face). These systems suffer from different problems such as the presence of noisy data resulting for example from defective sensors, unfavorable ambient conditions, poor illumination, incorrect facial pose and many others. Some of these limitations can be overcome by including multiple sources of information for establishing identity. Those systems are called multimodal biometric systems and are expected to be more reliable due to the presence of multiple and independent biometric features. These systems can meet the severe performance requirements imposed by various real world applications by achieving higher accuracy and improved system's performance (Kuncheva *et al.* (2000)).

Also, since a single biometric feature can sometimes lead to *type I* and *type II* errors as well as higher failure to acquire (FTA) and failure to enroll (FTE) rates, a multimodal biometric system tends to be more reliable for the same application. For instance, fingerprints can be copied (Sandström (2004)) or altered by cuts and bruises (Jain *et al.* (2004)), a face recognition algorithm can result in too many false acceptances (Kosmerlj (2004)) and many other drawbacks exist in other biometric authentication schemes (Jain *et al.* (2004)). For this reason, a multimodal biometric system (Jain *et al.* (2004)) combines the use of more than one biometric feature to solve these issues. For example, the system can solve the problem of distinguishing between people with similar faces (i.e. identical twins) by using fingerprints as an additional biometric feature, while at the same time issues caused in a fingerprint biometric system by people having worn fingerprints and people missing fingers are handled by using face recognition. Furthermore, a multimodal system also provides anti-spoofing measures (Jain *et al.* (2004), Schuckers (2002)) by making it more challenging for an impostor to fool the system.

2.3 Properties of Biometrics

In order for a Biometric system to achieve good performance at the enrollment/authentication and at the matching levels, the following properties of biometric characteristics must be met:

- **Invariance**: The biometric characteristics should remain constant over a long period of time. This eliminates the need for updating the biometric feature

templates stored in the database, reduces the complexity of the system and improves the recognition rate. For example, facial characteristics may change over time due to aging while iris features remain constant throughout a person's lifetime (Jain *et al.* (2004)).

- **Measurability and Timeliness**: The process for extracting biometric samples should be simple and fast. This is very important for continuous authentication in applications where real-time identification is necessary. Extracted features in a biometric system must be measureable in order to automatically compare them to an expected norm. For example, in airports, biometric samples must be taken at a distance and computation must be done rapidly as subjects are walking by the gate.

- **Singularity/Uniqueness**: Biometric characteristics should have sufficient unique properties for different individuals in order to distinguish one person from another. This is true for all biometrics except that some of them, present more unique and accurate features compared to others (i.e. iris contains more information compared to hand geometry).

- **Reducibility**: In a biometric system, the extracted feature templates should be reduced in size for handling and storage purpose as long as information is impossible to duplicate. This becomes a crucial property especially when

information is transmitted across secure channels when the controller of the results is located in a remote area.

- **Reliability**: The biometric algorithm should ensure high reliability and integrity. It becomes very inconvenient and costly when a biometric system does not provide consistent results.

- **Privacy**: In a biometric system, the privacy of the individual cannot be violated in any way. Information about the identity of a person cannot leak out of the system and should remain confidential, otherwise, people will hesitate to use it.

All the properties mentioned above are important to all biometric characteristics (e.g. face, iris, fingerprint, hand geometry, etc…) and must be met in a biometric system in order to be able to provide an accurate way of authentication.

2.4 Classification of Biometric System

Biometric systems can be classified according to six perspectives (Dessimoz *et al.* (2005)) as follows:

- **Overt / covert:** An application is defined as overt if and only if the user is aware about the acquisition of his biometric data otherwise, the application is said to be covert which is in fact one of the most concerning public perception of a

biometric system since it is related to a privacy issue. In overt applications, there are fewer concerns with data acquisition and sample quality since images are taken in a controlled environment where subject is asked to cooperate during the data acquisition process. On the other hand, in a covert environment such as at an airport checkpoint where face images of passengers are captured and compared to a watch list without their knowledge, the quality of the captured images can be problematic since they are taken in an uncontrolled environment without any user cooperation.

- **Attended / non-attended**: The biometric recognition process is performed attended if the user is observed and guided by supervisors during the process. On the other hand, if the process is unsupervised, the process is considered to be non-attended. In attended applications, biometric samples tend to be of a better quality compared to the ones acquired in a non-attended system where subject cooperation is non-existent.

- **Standard / non-standard environment:** A standard environment involves that most conditions in the biometric system are controlled and the recognition takes place indoors within a constrained environment, otherwise, the use is called in non-standard environment. For example, customs and airport security systems are considered standard since the entire biometric recognition process is completed in a controlled environment.

- **Habituated / non-habituated:** If the majority of the users interact with the biometric system on a frequent/daily basis then the recognition is said to be performed in the habituated mode. On the other hand, when the system's usage frequency is low, the recognition is performed in the non-habituated mode. This is relevant to the degree of cooperation and training demanded from the users.

- **Public / private:** The application is considered to be public if the users are not employees or work within the association that owns the biometric recognition system. If the users are the employees, the application is then called private. An example of a private application is internal bank security where employees are asked to voluntarily present their biometric traits for authentication.

- **Open / closed:** The biometric application is considered to be closed if the system uses completely proprietary formats. On the contrary, when the system is able to exchange data with others, the system is then called open and privacy issues should be addressed properly.

Based on the above description of a biometric system, we classify the systems considered by this thesis as covert, non-standard, non-habituated, non-attended, public and open biometric recognition systems.

2.5 Biometric Sample Quality Measures

Biometric systems are designed to identify a person based on physiological or behavioral characteristics (Wayman (2001)). Some of the most popular biometric systems presently used include automatic fingerprint, iris, and face recognition systems. Currently, these systems are seeing an increasing level of interest in a wide variety of applications such as in national identification applications, criminal searches, airport security and for access control. Lately, a significant level of interest is seen in the development of standards for measurement of biometric quality. According to (ISO (2007)), biometric sample quality may be considered from the point of view of character (inherent features), fidelity (accuracy of features), or utility (predicted biometrics performance). In general, a good biometric quality measure should demonstrate that images evaluated as higher quality must be those that result in better identification of individuals, as measured by an increased separation of genuine and impostor match score distributions.

In addition, the genuine and impostor distribution separation can be improved through the use of a prior knowledge in large-scale biometric recognition systems. For example in face recognition, knowledge such as demographics, face image resolution, pose, expression, and eye/face detection confidence carry useful information that can improve biometric performance. Using the a priori knowledge, new sets of localized genuine and impostor distributions can be extracted out of the overall data. The Receiver Operator Characteristics (ROC) Curve from the localized genuine and impostor distributions can be used to determine its own optimal threshold. These local thresholds can then be combined to improve upon the optimal threshold of the generalized ROC curve.

Therefore, the use of quality measures should help address issues in biometric performance improvement encountered in large-scale biometric recognition systems. In today's literature, few works exist on automatic face quality measures. For example, a method described in (Kryszcuk *et al.* (2005)) is developed where poorly illuminated face image regions are segmented using statistical methods and the remaining face area left after segmentation is used as a quality measure to find the optimal decision threshold. Another method developed towards the use of quality measures for face verification is presented in (Kryszcuk *et al.* (2006)) where two face quality measures are used as evidence in the process of reliability estimation. The quality measures developed in that work are based on image contrast and normalized 2-D correlation with an average face template.

In section (5.3) of this thesis, a new biometric quality measure is proposed based on a new information theoretic framework. The new approach is developed based on the intuitive observation that a high quality biometric image is believed to have more useful information in identifying an individual compared to a low quality image. This suggests that the quantity of identifiable information decreases with a reduction in quality. Given a way to measure the decrease in information caused by a given image degradation, one can measure the associated decrease in biometric information.

2.6 Face recognition

Face recognition is one of the most common methods used for identifying humans due to its non-intrusive nature, as acquiring face images can be done at a distance. Recognizing

faces and facial expressions is becoming very important in many practical applications, such as in border control and airport security. The process flow in face recognition consists of four phases: capture of samples, feature extraction, template creation and matching. Several techniques exist for face recognition. Some techniques can be more suited than others depending on the application. Recent surveys and reviews on face recognition technologies are provided in (Zhao *et al.* (2003), Kong *et al.* (2005), Li and Jain (2005)). Some of the most popular face recognition techniques are the Eigenfaces (Turk *et al.* (1991)), local feature analysis (Chirillo *et al.* (2003) and Elastic Graph Matching (Zhang *et al.* (1997)).

Eigenfaces method is used to efficiently represent facial images using principal component analysis (PCA) where a set of images is represented using a set of orthonormal basis vectors. Each eigenface is derived from the covariance analysis of the face image population. A similarity measure is then created in order to measure resemblance between faces. Two faces are considered to be similar if the distance between their feature vectors is small in the eigenface feature space. The mathematical properties of the eigenface representation and the matching process have shown to perform well on face images taken in a certain controlled environment (Zhao *et al.* (2003)). Like most facial recognition techniques, the eigenface methods perform better in well-lit, frontal image capture scenarios (Turk *et al.* (1991)).

Local feature analysis (LFA) is a very popular method used in face recognition. It has the ability to accommodate for changes in facial expression and aging (Chirillo *et al.* (2003)). In LFA algorithms, a set of features such as geometrical metrics and distances are derived from the facial images and used as the basis for image representation and comparison. In

general, the eyes, nose, mouth, jaw line and cheeks are the most common used features in these methods and are usually represented by their position and dimensions. This technique performs generally well except that it has few drawbacks such that it highly depends on the environment where pictures are taken and on the quality of the images.

Another method used in face recognition is Elastic Graph Matching. This technique is known for its ability to provide face recognition that is invariant to affine transformations and changes in facial expressions (Wayman *et al.* (2005)). In this method, features are locally extracted at specific locations in the face image. Afterwards, the distances between these nodes are recorded for further processing. Based on the application that this method is used for, some features (i.e. nodes) are more reliable and important for face recognition than others. For this reason, the use of weights has been introduced in (Duc *et al.* (1999)) where more important features are assigned higher weights. Zhang *et al.* (1997) developed an extension of the Elastic graph Matching method where several images of the same individual taken at different angles are used for feature extraction. This technique (Elastic Bunch Graph Matching) showed better results because it is more robust to differences in posture and facial expressions.

Today, face recognition technology has evolved and it is used on three-dimensional face images (Philips *et al.* (2003)). This leads to significant improvement compared to the two-dimensional face recognition technology. A common drawback with the 2D face recognition technology is the inability for algorithms to accommodate for changes in illumination and pose (Pan *et al.* (2003)). In (Pan *et al.* (2003)), the developed 3D face

recognition method performed well for images taken under different pose lighting conditions however, the method doesn't handle variations in facial expressions very well.

The work presented in this thesis develops new methods and solutions to improve the performance of a face biometric system when dealing with low quality images. A variety of algorithms are developed to deal with face detection, face tracking, feature extraction, and pattern comparison using low quality face images. The developed methods make use of two different face recognition algorithms based on PCA (Eigenface) and Fisher Linear Discriminant (FLD) feature decompositions in order to measure biometric feature information (section 5.2). A definition of biometric feature information is introduced and an algorithm to measure it proposed, based on a set of population and individual biometric features. In addition, section (5.2.6) develops a new approach to understand and measure the changes in biometric sample quality resulting from image degradations. We begin with the intuition that degradations to a biometric sample will reduce the amount of identifiable information available. We then show that the biometric information for a person may be calculated by the relative entropy theory between the population feature distribution and the person's feature distribution and that the biometric information for a system is the mean for all persons in the population. In order to do this, we simulate degradations of biometric images and calculate the resulting decrease in biometric information. Results show a quasi-linear decrease for small levels of blur with an asymptotic behavior at larger blur (section 5.3).

2.7 Face tracking algorithms

Face tracking is a crucial part of most face processing systems. It requires accurate target (i.e. face) detection and motion estimation when an individual is moving. Generally, this process is required to facilitate the face region localization and segmentation necessary prior to face recognition. Accurate face tracking is a challenging task since many factors can cause the tracking algorithm to fail. Some of the major challenges encountered by face tracking systems are robustness to pose changes, lighting variations, and facial deformations due to changes of expression and face occlusion. These factors might cause the algorithm to lose track of the subject's face and drift (i.e. lose face detection for initialization). Face tracking techniques can be classified into two categories: tracking cues and motion estimation (Li *et al.* (2008)). Tracking cues include knowledge-based and learning-based techniques. The knowledge-based methods use prior information about the face area such as face contour, intensity, shape and face models in order to locate the face region in an image. These methods perform generally well, however, they seem to fail in situations where the subject's face is occluded by other objects, especially those of circular shapes. On the other hand, learning-based techniques attempt to model the face pattern using distribution functions in a probabilistic framework. These methods perform better than the knowledge-based techniques since they are not limited to the prior knowledge on face instead, they are known for their capability of developing learning models using training sets which perform better in challenging situations (Li *et al.* (2008)).

2.7.1 Knowledge-Based Classifiers

The following are some knowledge-based (i.e. tracking cue) methods applied for face tracking.

2.7.1.1   Face color model

In face tracking, using skin color in knowledge-based techniques provides important information that facilitates target detection based on the analysis of the previous image frame. Color information is a solid feature due to its robustness to image scaling, translation, rotation and stretching.

HSV color space model

HSV (Hue/Saturation/Value) space separates out hue (color) from saturation (color concentration) and from brightness (value) (Bradski (1998)). HSV can be thought of as describing colors as points in a cylinder (called a color solid) whose central axis ranges from black at the bottom to white at the top, with neutral colors between them. The angle around the axis corresponds to "hue", the distance from the axis corresponds to "saturation", and the distance along the axis corresponds to "lightness", "value" or "brightness". Color models are created by taking 1D histograms from the H-channel in HSV space. For face tracking via a skin color model, face areas are sampled by prompting users to center their face in an onscreen box to find skin areas for further color sampling. The hues derived from skin pixels in the image are sampled from the H-channel and binned into a 1D histogram. Once sampling completed, the histogram values are stored for future use. More robust histograms can be developed by sampling skin

hues. During operation, the stored skin color histogram is used as a model, or lookup table, to convert incoming video pixels to a corresponding probability value. This process is done for each video frame. Using this method, probabilities range in discrete steps from zero (probability 0.0) to the maximum probability pixel value (probability 1.0). For 8- bit hues, this range is between 0 and 255 (Dansheng (2009)).

Stochastic skin-color model

Skin color can be represented in the chromatic color space (Gejgu *et al.* (2003)). Chromatic colors (r, g), also known as pure colors in the absence of brightness are defined by the following normalization process:

$$r = R/(R + G + B) \tag{2.1}$$

$$g = G/(R + G + B) \tag{2.2}$$

Blue color is redundant after the normalization because $r + g + b = 1$. In (Kjeldsen *et al.* (1996)) it has been shown that chromatic skin-color has normalized Gaussian distribution. Therefore, a face color distribution can be represented by a Gaussian model, $N(m, \mu^2)$ where $m = (\bar{r}, \bar{g})$ with

$$\bar{r} = \frac{1}{N} \sum_{i=1}^{N} r_i \tag{2.3}$$

$$\bar{g} = \frac{1}{N} \sum_{i=1}^{N} g_i \tag{2.4}$$

and

$$\Sigma = \begin{bmatrix} \sigma_{rr} & \sigma_{rg} \\ \sigma_{gr} & \sigma_{gg} \end{bmatrix} \qquad (2.5)$$

where m and σ represent the mean and standard deviation, respectively.

In order to train the skin color model, a set of hand segmented images are required. From this, the likelihood of skin color for any pixel in the face image can be obtained. For example, the likelihood of skin color for a certain pixel transformed from RGB color space to chromatic color space with chromatic pair value (r, g) can be computed as follows:

$$P(r, g) = e^{(-0.5(x-m)^T \Sigma^{-1}(x-m))} \qquad (2.6)$$

where $x = (r, g)$. From this, a color image can be transformed into a grey scale image using the skin color model. Each pixel grey value represents the likelihood of the pixel belonging to the skin.

2.7.1.2   Texture model (LBP Cue)

Ojala *et al.* (1996) proposed a local binary pattern (LBP) operator as a powerful tool for describing image textures. The LBP operator applies a 3×3 mask to the image from which a binary number is computed by applying a threshold to the neighboring pixels (Dansheng (2009), Wang *et al.* (2008)). Once the threshold values are computed for every pixel in the image, the histogram of the labels is then used as a texture descriptor. One limitation to the LBP operator is the fact that it cannot capture larger texture in an

image due to the fact that it is limited to a 3×3 pixels area. Therefore, the LBP operator must be extended to different sizes and the use of circular masks becomes necessary.

2.7.1.3 Edge cue

Edged based models are other appearance-based classifiers that use face contours and local structures (i.e. eyes, nose, mouth contours) in a face image (Swaminathan *et al.* (2007)). In general, contours are extracted using the Difference of Gaussian (DOG) filters applied to the grayscale image. One limitation of these methods is the fact that they might fail when subject's face is occluded.

2.7.1.4 Facial shape

Ellipse fitting algorithms are used for face image classification (Gejgu *et al.* (2003)). In a face image, only blobs with elliptical shapes are retained for further processing. In general, face detection is applied on the first frame in a sequence of images and then blobs corresponding to faces are tracked further. Ellipses are classified using their center of mass computed as follows:

$$\overline{x} = \frac{1}{A} \sum_{i=1}^{n} \sum_{j=1}^{m} jB(i,j) \tag{2.7}$$

$$\overline{y} = \frac{1}{A} \sum_{i=1}^{n} \sum_{j=1}^{m} iB(i,j) \tag{2.8}$$

where B is an $n \times m$ image with area A in pixels. Elliptical contour fitting can be applied on images where faces are inclined. In order to improve the fitting accuracy, better results are obtained by first rotating the face prior to the fitting operation. The inclination angle is computed as follows:

$$\theta = \frac{1}{2} arctan(\frac{2\mu_{1,1}}{\mu_{2,0} - \mu_{0,2}})$$

(2.9)

where

$$\mu_{2,0} = \sum_{i=1}^{n} \sum_{j=1}^{m} (x'_{ij})^2 B(i,j)$$

(2.10)

$$\mu_{1,1} = \sum_{i=1}^{n} \sum_{j=1}^{m} x'_{ij} y'_{ij} B(i,j)$$

(2.11)

$$\mu_{0,2} = \sum_{i=1}^{n} \sum_{j=1}^{m} (y'_{ij})^2 B(i,j)$$

(2.12)

and

$$x' = x - \overline{x}$$

(2.13)

$$y' = y - \overline{y}$$

(2.14)

Also, the moment of inertia can be used to compute the length of the major and minor axis of the best-fitted ellipse.

$$I_{min} = \sum_{(x,y)\epsilon C} [(x - \overline{x})cos\theta - (y - \overline{y})sin\theta]^2$$

(2.15)

$$I_{max} = \sum_{(x,y)\epsilon C} [(x - \overline{x})sin\theta - (y - \overline{y})cos\theta]^2$$

(2.16)

where I_{min} and I_{max} are the least and the greatest moment of inertia of an ellipse with orientation θ. From this, the length of the major axis (a) and the length of the minor axis (b) are computed as follows:

$$a = (\frac{4}{\pi})^{1/4}[\frac{(I_{max})^3}{I_{min}}]^{1/8} \tag{2.17}$$

$$b = (\frac{4}{\pi})^{1/4}[\frac{(I_{min})^3}{I_{max}}]^{1/8} \tag{2.18}$$

2.7.1.5   Motion segmentation

Also known as "Background subtraction" method, motion segmentation is performed using a color change detector. This technique works assuming that a reference background image is available for the segmentation to succeed. Some motion segmentation methods use an adaptive background algorithm (Li *et al.* (2008)).

2.7.2 Learning-Based Classifiers

In this section, we review relevant learning-based (i.e. tracking cue) techniques used for face tracking.

2.7.2.1 Haar-like features

Learning-based techniques attempt to model the face pattern using distribution functions in a probabilistic framework. The Haar-like features, originally proposed by Papageorgiou *et al.* (1998), are used to represent face features. Three types of rectangular features exist that can be computed. For example, a rectangular feature can be computed by taking the difference between the sums of two rectangular blocks. A fast technique was proposed by Viola-Jones for computing these features used for face detection (Viola *et al.* (2001)). Scanning through the picture, their one-pass method uses an intermediate array to store a running sum of pixel above and to the left of the point (x, y):

$$I_{int}(x, y) = \sum_{x' \leq x, y' \leq y} I_{or}(x', y') \tag{2.19}$$

where $I_{int}(x, y)$ is the integral image, and $I_{or}(x, y)$ is the original image. Using expression (2.19), the Haar features are easily computed. For example, Figure 2.4 shows the rectangular region D that is computed by $I_{int}(4) - I_{int}(3) - I_{int}(2) + I_{int}(1)$ (Viola *et al.* (2001)).
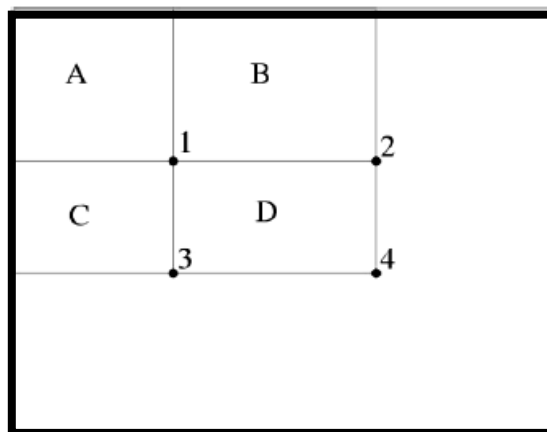
Figure 2.4: Integral image used to calculate the sum of pixels in a rectangle. For example, the value of the integral image at location 1 is the sum of the pixels in rectangle A. The value at location 2 is A+B, at location 3 is A+C, and at 4 is A+B+C+D. The sum within D is computed as (4+1)-(2+3).

2.7.3 Motion estimation

Motion estimation is another category of face tracking techniques, other than tracking cues (section 2.7.1), which deals with the major issues that occur in tracking algorithms. In face tracking, the main research problem is "Drifting". This issue is caused by the following: 1) rapid variation in appearance of the target; 2) abrupt movement and poor motion continuity. The first problem can be solved by creating proper tracking cue models while the second issue entirely depends on the robustness of the motion estimation algorithm. Dansheng (2009) classifies motion estimation algorithms as: 1) Kernel-based trackers and 2) Bayesian filter estimators. The latter is much more accurate and robust compared to the Kernel-based tracker and is considered the most suitable for low frame rate video where severe "drifting" occurs.

2.7.3.1 Mean shift tracking

The mean shift tracking algorithm is a nonparametric statistical method that seeks the nearest mode of a point sample distribution. In the mean shift tracking algorithms, a color histogram is used to describe the target region. The Kullback-Leibler divergence, Bhattacharyya coefficient and other theoretic similarity measures are commonly employed to measure the similarity between the template region and the current target region (Comaniciu *et al.* (2003)). Tracking is accomplished by iteratively finding the local minima of the distance measure functions using the mean shift algorithm.

In Dansheng (2009), a *kernel* is defined as a function $K : X \to R$ if there exists a function $k : [0, \infty] \to R$ called its *profile*, which is nonnegative, non-increasing, piecewise continuous and with, $\int_0^\infty k(r)dr < \infty$ such that $K(x) = k(||x||^2)$ where X is an n-dimensional Euclidean space.

Let $S \subset X$ be a finite set called the *sample data*, K a *kernel* and $W : S \to [0, \infty)$ a *weight* function. The *sample mean* with *kernel K* at a point $x \in X$ is defined as

$$m(x) = \frac{\sum_{s \in S} K(s - x)w(s)s}{\sum_{s \in S} K(s - x)w(s)} \tag{2.20}$$

From this, the *mean shift* is defined as $m(x) - x$ and the mean shift algorithm represents the repeated movement of data points to the *sample mean*. Let $T \in X$ be a finite set, and $m(T) = \{m(t) : t \in T\}$. The full *mean shift* procedure iterates and evolves T until it

finds a fixed point $T = m(T)$. After each iteration, the weights $w(s)$ can be either fixed or re-evaluated. In addition, T and S are usually different sets, with S a fixed set of samples. Here are the steps to compute the Mean Shift Algorithm (Dansheng (2009)):

    i.   Select a specific search window size.

    ii.   Select the initial location of the search window.

    iii.   Compute the mean location in the window.

    iv.   Center the search window at the mean location computed in step (iii).

    v.   Repeat steps (iii) and (iv) until the algorithm converges or until a predefined threshold is met.

One limitation of the mean shift algorithm is the fact that the original formulation of this method does not estimate the orientation of the tracked region. In addition, mean shift tracking uses fixed color distribution which can become an issue in some applications since color distribution can change due to rotation in depth. However, this issue is resolved used continuous adaptive mean shift (CAMSHIFT) (Bradski (1998)) which handles dynamically changing color distribution by searching the window size and computing color distribution for each search window.

2.8 Iris Recognition

Iris recognition is another highly studied and evolved technology in biometrics. The iris is known to contain a rich texture which means that unique information can be extracted from the iris to identify users. It has been shown that iris features have been used to

obtain high recognition accuracy for security applications (Bonney *et al.* (2005), Daugman (1993), Newton *et al.* (2007)). Even though iris recognition has shown to be extremely accurate for user identification, there are still some issues remaining for practical use of this biometric (Wayman *et al.* (2005)). For example, the fact that the human iris is about $1cm$ in diameter makes it very difficult to be imaged at high resolution without sophisticated camera systems. Traditional systems require user cooperation and interaction to capture the iris images. By observing the position of their iris on the camera system while being captured, users adjust their eye positions in order to localize the iris contour accurately (Newton *et al.* (2007), Wildes (1997)).

This step is crucial in iris recognition since iris features cannot be used for recognition unless the iris region is localized and segmented correctly. Many iris localization techniques exist and have been developed. Some of the classical methods for iris localization are Daugman's integro-differential operator (IDO) (Daugman (1993)) and Wildes' Hough transform (Wildes (1997)).

Figure 2.5 illustrates the major stages of an iris recognition system (Proenca (2006)). The initial stage involves segmenting accurately the iris area from an eye image. This process consists in localizing the iris inner and outer boundaries, assuming they have circular or elliptical shapes. This process also requires detecting and removing any eyelash noise from the image prior to segmentation. In order to compensate the variations in the pupil size and in the image capturing distances, the segmented iris region is mapped into a fixed length and dimensionless polar coordinate system (Daugman (2003)). In terms of feature extraction, iris recognition approaches can be divided into three major categories:

phase-based methods (Daugman (1993)), zero-crossing methods (Boles *et al.* (1998)) and texture analysis based methods (Wildes (1997)). Finally, the comparison between iris templates is made, and a metric is measured. If this value is higher than a threshold, the system outputs a non-match, meaning that each signature belongs to different irises. Otherwise, the system outputs a match, meaning that both templates were extracted from the same iris.
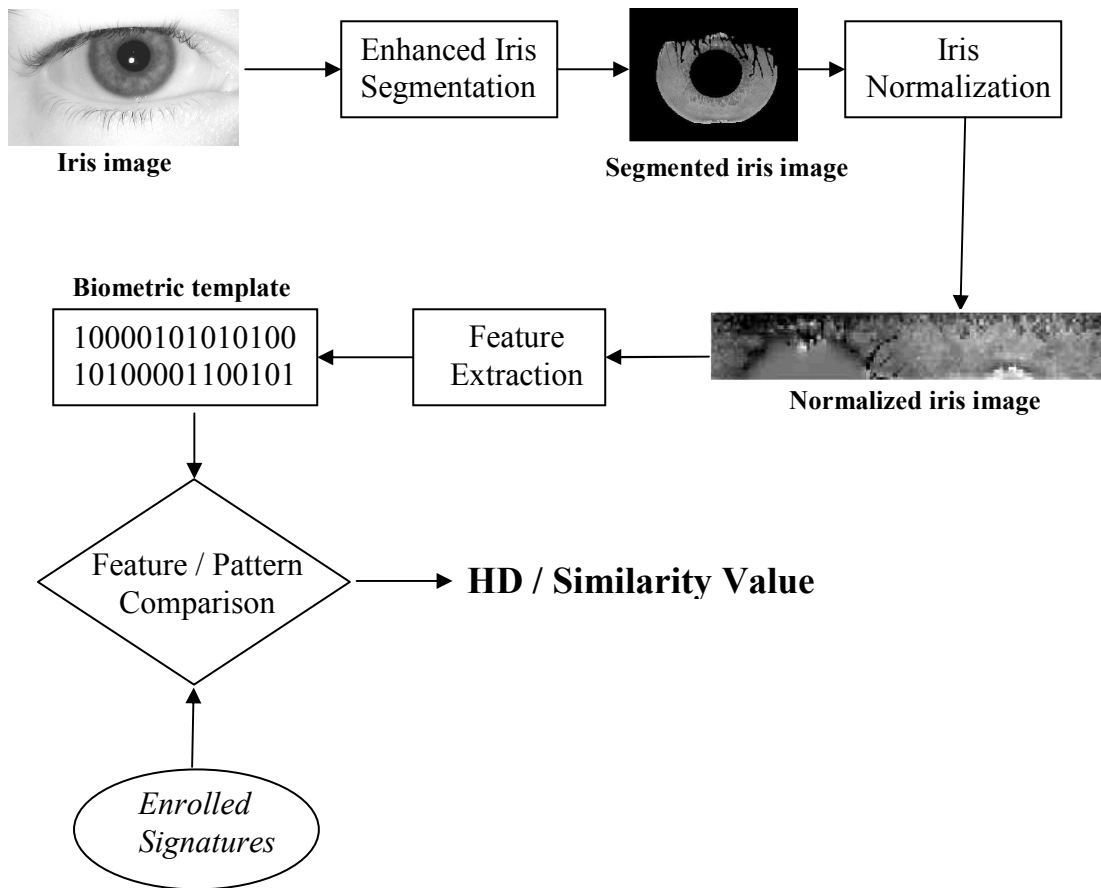
Figure 2.5: Different stages in an iris recognition system

2.8.1 Iris structure

The iris has a multi-layered structure where the most posterior layer is comprised of epithelial cells containing iris pigments and the anterior layer is comprised of two sets of muscles, the sphincter muscle and the dilator muscle. The sphincter muscle serves to contract the pupil and the dilator to open it. Further into the anterior side is the stromal layer composed of collageneous tissues which generates the most part of an iris image.

2.8.2 Iris texture pattern and colors

The iris texture features are composed of various components within the iris such as crypts, furrows, arching, collarette and rings of various shapes (Figure 2.6). In addition, the iris pattern comes in different color pigments, such as green, red and blue. The natural iris colors are generated mostly from a combination of melanin pigments, mostly in the anterior layer and stromal layer. Visible light goes through the iris, and the absorption and reflection of light depend on the wavelength. The iris color is further determined by the variation in the pigment density and the amount of reflected light.

In iris recognition, near infrared (NIR) cameras are usually used instead of visible light which tend to emphasize the texture pattern of the iris, especially for darker regions. The NIR camera uses a wavelength spectrum that ranges from $700\ nm$ to $900\ nm$ (Iridian Technology 2005). In addition, the fact that NIR illumination is a more comfortable imaging modality for subjects compared to regular light source makes NIR imaging widely used in the iris recognition field.

The iris contains a unique and rich texture which can be used in high security applications. The unique and abundant texture patterns in the iris images are "determined epigenetically by random events in the morphogenesis process" (Daugman *et al.* (2001)). Cross-comparisons were performed between genetically identical images, taken from the left and right eyes of the same persons and showed that the statistical distributions were the same for iris images coming from genetically related and genetically unrelated subjects. Nevertheless, in order for any emerging biometric technology to be accepted by the community, an independent party is required to perform the evaluations, design the protocols, collect the data sets, supervise the tests and analyze the results (Philips *et.* (2000)). There exist many accepted standards and frameworks for how to design a biometric testing protocol, how to collect data sets and minimize evaluation bias (Mansfield *et al.* (2002)). In general, the FNMR, FMR and the detection error rate curve (DET) are used as indicators of the level of accuracy of a typical iris recognition system. For this reason, the International Biometric Group (IBG), the Authenti-Corp and the National Institute of Standards and Technology (NIST) performed independent evaluations with various iris recognition systems to analyze its accuracy and performance levels.

Moreover, a project conducted by the University of Cambridge and the United Arab Emirates interior ministry showed that for 632500 iris images acquired in the Middle East and over 200 billion cross-comparisons generated between different eyes that a false match rate (FMR) of less than 1 in 200 billion was achieved using the Daugman algorithm (Daugman (2005)).

One experiment named *ITIRT* was funded by the US Department of Homeland Security for border control and security access consulting. The experiment was performed in July 2004 on several state-of-the-art iris recognition systems such as: "Iridian KnoWho OEM SDK", "LG IrisAccess 3000", "Oki IRISPASS-WG" and "Panasonic BM-ET300" (International Biometric Group (2005)). In this experiment, over 100,000 iris images were acquired at different times, with different devices. These images were taken from 1224 people of different ethnic cultures and age groups. The image templates were compared in order to generate the false accept rate, the false reject rate, the failure to enroll and the failure to acquire rates. For the feature extraction and matching algorithms, the generic version of the Daugman algorithm was implemented. The same algorithm is also used to test all of the four systems. As an indicator of error rates, the FNMR at FMR of 0.001 was used. The Panasonic BM-ET300 module achieved a FNMR of around 0.014. The Oki system achieved a FNMR of around 0.03 at an FMR of 0.001. The LG unit achieved a FNMR of around 0.038 (Newton *et al.* (2007)). This shows that all the tested iris recognition systems achieve very high identification rates, a strong inter-operability and repeatability.
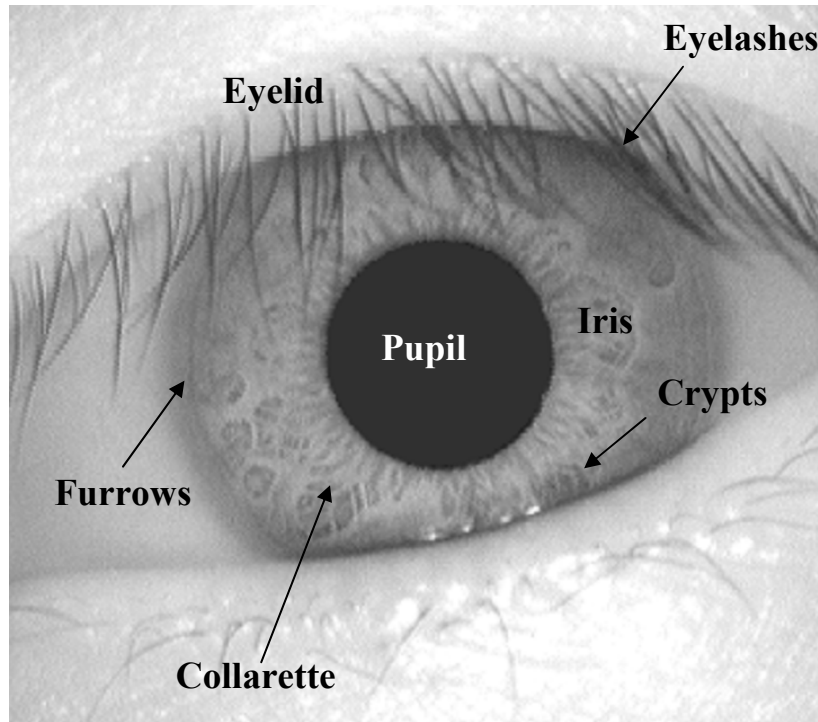
Figure 2.6: Example iris image taken from CASIA database.

2.8.3 Imaging Systems

Two well-known iris imaging algorithms developed by John Daugman and the Richard Wildes group are currently used (Daugman (2001), Masek (2003), Wildes (1996, 1997)). Both the Daugman and the Wildes techniques achieve good identification rates by using monochrome gray-scale images. The main difference between the two imaging systems is the lighting source implementation where the Daugman system implementation consists of a lateral light source, while the Wildes system applies a diffuser to illuminate the entire eye region (Figure 2.7, Figure 2.8).

The Daugman system is shown in Figure 2.7 which demonstrates the position of the light source to the side of the eye. The camera captures the reflected light after passing through a beam splitter. The resulting iris image has a diameter ranging from 100 to 200 pixels,

which gives enough information for iris recognition. On the other hand, the Wildes imaging system applies a series of light sources, illuminating the iris region through a diffuser and a circular polarizer (Figure 2.8). Using this system, the captured iris image has a diameter of around 256 pixels. The Wildes system generates iris images with reduced specular reflections compared to a single light source system since it uses an evenly distributed light illumination system (Wildes *et al.* (1996)).
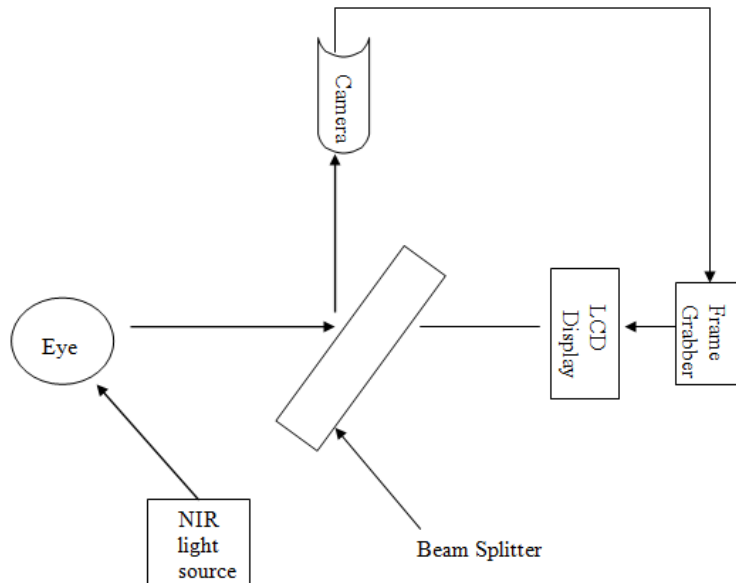
Figure 2.7: The Daugman iris imaging system

Diffuser to spread light beam

Point light source

Eye — Image to be captured → Lens — Camera — Frame Grabber

Point light source

Diffused light beam

Circular Polarizer
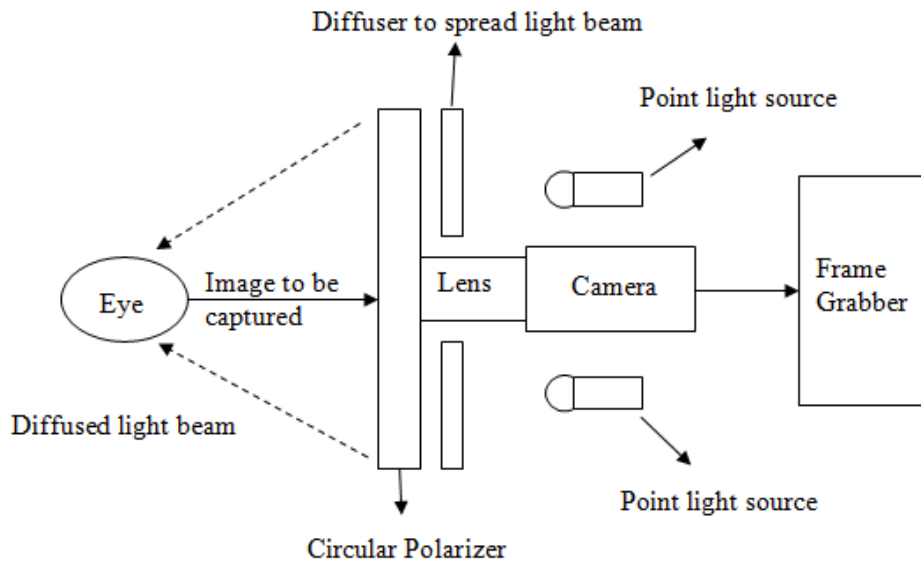
Figure 2.8: The Wildes iris imaging system

2.8.4 Iris Localization and Segmentation

Iris localization and segmentation is a crucial step in iris recognition since it severely affects the system's performance. This section of the algorithm consists in segmenting the specific iris region from an eye image by locating the exact iris boundary, the pupil region, and the upper and lower eyelids. In some cases, artifacts can be found in the resulting iris image which can be a combination of eyelash occlusion, eyelid occlusion and/or noise. Advanced algorithms are required for successful removal of these artifacts in order to generate a clean iris region for subsequent recognition. In fact, various methods have been proposed to identify and eliminate artifacts in iris images, particularly by detecting and removing eyelash occlusion and eliminating specular reflections. In general, most algorithms perform reasonably well except that they tend to overestimate

eyelash occlusion (Xie (2007)). The following section describes few iris-pupil segmentation techniques widely used in some iris recognition systems.

2.8.4.1 Pupil and Iris Localization

The integro-differential operator, proposed by Daugman, locates the pupil, the iris inner and outer boundaries as well as the upper and lower eyelid boundaries (Daugman (2004)).

$$max_{(r,x_0,y_0)} \left| G_\sigma(r) * \frac{\partial}{\partial r} \oint_{r,x_0,y_0} \frac{I(x,y)}{2\pi r} ds \right| \qquad (2.21)$$

$$G_\sigma(r) = \frac{1}{\sqrt{2\pi}\sigma} e^{-\frac{(r-r_0)^2}{2\sigma^2}} \qquad (2.22)$$

where $I(x,y)$ represents the eye image, (r, x_0, y_0) are parameters that correspond to a circle of radius r and center coordinates (x_0, y_0), respectively. $G_\sigma(r)$ is a radial smoothing Gaussian function with center r and standard deviation σ. One application of this function is that it searches the entire eye image for integrations along different circular contours with center coordinates (x_0, y_0) and an increasing radius r. The maximum contour integral derivative found will then be classified as the most likely circle tracing the iris. In a similar manner, the circular boundaries for the pupil and iris regions are localized by searching through the entire iris image for the maximum integration along various circular contours. In addition, Daugman approximates the upper and lower eyelids with two open curves that are part of two different circles. Finally, the iris region

surrounded by the upper and lower eyelids as well as the extracted circular pupil and iris boundaries are used for further feature extraction in the iris recognition process.

2.8.4.2   Hough transform

The circular Hough transform is a standard technique used in the machine vision field to locate circular contours in images. The Hough transform is applied directly on an intensity gradient edge map usually obtained through a gradient-based edge detector (Wildes (1997)). The latter method is used in many iris recognition algorithms such as the Wildes system (Wildes (1997)). First, the entire iris image $I(x, y)$ is smoothed with a Gaussian filter $G(x, y)$ with centers (x_0, y_0) and a standard deviation σ of $3/4$ (equation 2.24). Then, the intensity gradient image map $M(x, y)$ is generated from the smoothed image $F(x, y)$, as shown in equation (2.25) using the gradient operation defined in (2.26). Subsequently, the binary edge map is generated by setting a threshold on the intensity gradient image $M(x, y)$. The threshold is usually selected based on experimental data and depending on the application. Finally, using the binary image map, the Hough transform is performed to locate a circle with the largest number of edge points and with circular parameters $(x_0; y_0; r)$ calculated as shown in equation (2.27). $(x_0; y_0; r)$ represents a circle to be located within the iris image such that the circle is characterized by a radius r, and center coordinates (x_0, y_0) with possible edge point (x_i, y_i).

$$F(x, y) = G(x, y) * I(x, y) \tag{2.23}$$

$$G(x, y) = \frac{1}{2\pi\sigma^2} e^{-\frac{(x-x_0)^2 + (y-y_0)^2}{2\sigma^2}} \tag{2.24}$$

$$M(x, y) = |\bigtriangledown F(x, y)| \tag{2.25}$$

$$\bigtriangledown \equiv (\partial/\partial x, \partial/\partial y)) \tag{2.26}$$

$$(x_i - x_0)^2 + (y_i - y_0)^2 = r^2 \tag{2.27}$$

From this, the Hough transform is then performed through the entire collection of the edge points. Whenever equation (2.27) is satisfied, it means that the circular contour goes through $(x_0; y_0; r)$, and one extra vote is added to the histogram count for possible circular contours. Once the entire image is scanned for all possible contours, the contour that obtained the highest amount of votes represents the most likely circle in the edge map.

2.8.4.3   Discrete Circular Active Contour Model

The discrete circular active contour (DCAC) model can also be used to locate the pupil and iris boundaries in the iris image (Ritter *et al.* (1999)). First, in order to localize the pupil region in the iris image, the variance image must be computed from the original image and then, an active contour model with a starting point in the center of the pupil, is initiated and moved within the iris image under the influence of so called "internal and external forces". Along the active contour, the vertex v moves from time t to time $t + 1$ according to:

$$v_i(t + 1) = v_i(t) + F_i(t) + G_i(t) \tag{2.28}$$

where v_i represents the position of the vertex at a specific time t, F_i and G_i represent the internal and external forces, respectively.

The internal force is characterized by the continuity, and other prior knowledge about the iris (i.e. circular contour) while the external force is directly related to the gray-scale intensity values within and outside the vertex, which also includes the iris region. Finally, the iris contour is segmented after an extensive iterative contour searching operation which ends when equilibrium with minimum energy or minimum mean variance of the annulus is attained. DCAC has shown good results but do suffer from few limitations such that the performance of this method greatly depends on the iris image quality. For instance, if the image contains severe noise, specular reflections or distortions, the method will fail in locating the proper boundaries (Ritter *et al.* (2003)).

2.8.4.4   Noise and artifacts in iris images

In order to achieve higher system performance and better accuracy in the image processing steps within an iris recognition system, noise and artifacts in iris images must be reduced or if possible, completely eliminated. Such artifacts include the eyelash occlusion, the eyelid occlusion and specular reflections. As seen in Figure 2.6, the iris image includes severe eyelash and eyelid occlusion. Hence, a part of the iris is covered by the top eyelid and some eyelashes are spread across the iris area which will affect the system's performance.

In addition, specular reflections are mirror-like reflections that occur during the iris image acquisition procedure in such a way that the light source gets reflected and imaged by the camera. Figure 2.9 shows one example of specular reflection seen on the iris region as a "white spot" which results in high pixel values that deviate from the original iris patterns and that constitute a major source of distortion.

In order to address all these issues with image artifacts, a new method is developed in chapter 4 to detect and eliminate noise in iris images. This will then generate better results when properly segmented iris images are used for further processing in the iris recognition system.
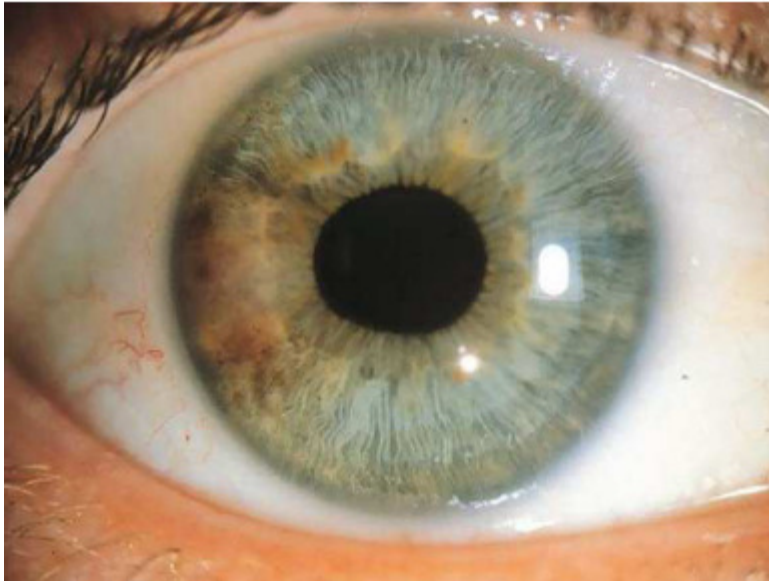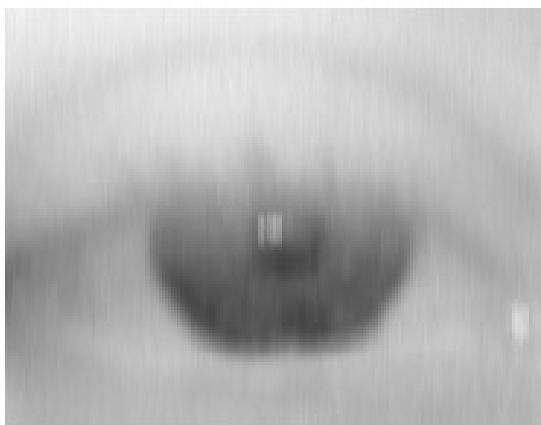
Figure 2.9: Iris image showing severe specular reflections taken from Montgomery (2007)

The following table shows few examples of iris noise images (Proenca (2006)).

Type of iris noise	Addressed in this thesis	Examples
Eyelid and eyelash occlusions	YES	
Lighting reflections	YES	
Out-of-focus	YES	

Off-angle iris	NO	
Out-of iris images	YES	
Motion blurred irises	NO	

2.8.5 Size-invariant Unwrapping and Representation

This section describes a method to normalize the iris region once it is properly segmented

in order to obtain a size-invariant rectangular representation of the original iris pixels.

This method, referred to as "Daugman's Rubber Sheet Model", is developed by Daugman

(2003) to map the sampled iris pixels from the Cartesian coordinates to the normalized

polar coordinates in order to accomplish a size-invariant sampling of the original iris points.
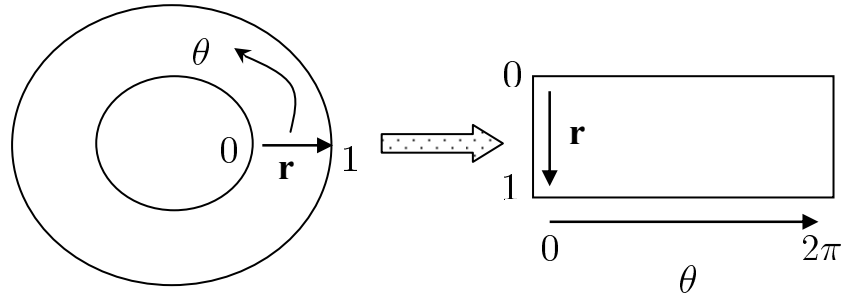
Figure 2.10: Unwrapping of the Iris using Daugman's Rubber Sheet Model

The Daugman's rubber sheet model finds for every pixel in the iris, an equivalent position on the polar axes (r, θ) where r is the radial distance and θ is the rotated angle at the corresponding radius. The radial resolution is described as the number of data points in the radial direction while the angular resolution is the number of radial lines generated around the iris region. Using equation (2.29), the iris region is transformed to a 2D array with horizontal dimensions corresponding to the angular resolution and the vertical dimension to radial resolution (Figure 2.10).

$$I[x(r, \theta), y(r, \theta)] \rightarrow I(r, \theta) \tag{2.29}$$

where $I(x, y)$ corresponds to the iris region, (x, y) and (r, θ) are the Cartesian and normalized polar coordinates, respectively. θ ranges from 0 to 2π and r from 0 to 1. $x(r, \theta)$ and $y(r, \theta)$ are defined as linear combinations of pupil boundary points. The following equations perform the transformation:

65

$$x(r,\theta) = (1-r)x_p(\theta) + x_i(\theta) \tag{2.30}$$

$$y(r,\theta) = (1-r)y_p(\theta) + y_i(\theta) \tag{2.31}$$

$$x_p(\theta) = x_{p0}(\theta) + r_p\ cos(\theta) \tag{2.32}$$

$$y_p(\theta) = y_{p0}(\theta) + r_p\ sin(\theta) \tag{2.33}$$

$$x_i(\theta) = x_{i0}(\theta) + r_i\ cos(\theta) \tag{2.34}$$

$$y_i(\theta) = y_{i0}(\theta) + r_i\ sin(\theta) \tag{2.35}$$

where (x_p, y_p) and (x_i, y_i) represent the pupil and iris coordinates along the θ direction, respectively. (x_{p0}, y_{p0}) and (x_{i0}, y_{i0}) correspond to the pupil and iris center coordinates. Two different cases can occur with the rubber sheet model after mapping the iris region from the circular Cartesian scale to the rectangular polar scale. First, if the pupil and iris boundary centers are located at the same pixel point, the sampled points are uniformly distributed across the iris region, as shown in Figure 2.11. On the other hand, if the center of the iris circular boundary and the center of the pupil circular boundary are different, the feature points are then sampled non-uniformly within the iris region. In order to deal with this situation, a series of sampling lines are emitted from the center of the pupil circle, and rotated along the circumferential direction for 360°. Afterwards, a fixed number of sampled points are taken inside the iris region along each sampling line, as shown in Figure 2.12.
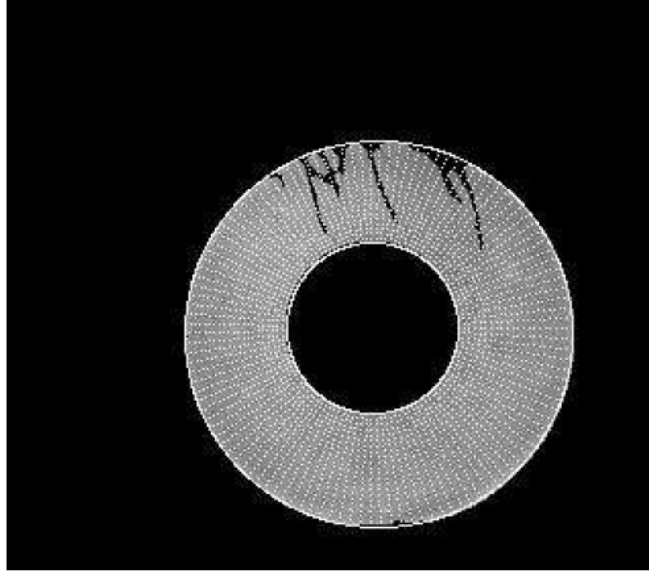
Figure 2.11: Uniform feature points sampling with the Daugman's rubber sheet model.
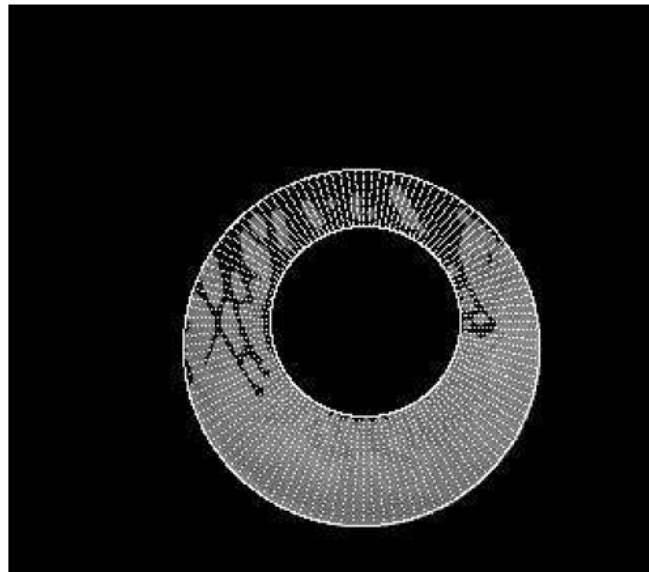
Figure 2.12: Feature points sampling with displaced pupil and iris centers.

2.8.6 Feature Extraction

The iris has a particularly interesting structure and provides abundant texture information.

Iris feature extraction is applied on the grayscale image intensity values after the iris

segmentation and noise removal steps. Feature extraction is a crucial part in any iris recognition system since good identification rates are directly related to the uniqueness and variability of the extracted features used to distinguish between different biometric templates.

2.8.6.1   2D Gabor features

Gabor filter based methods have been widely used in computer vision, especially for texture analysis. A Gabor filter is constructed by modulating a sine/cosine wave with a Gaussian (Daugman (2003)). These filters provide optimum conjoint representation of a signal in both space and spatial frequency since a sine wave is perfectly localized in frequency, but not in space. A quadrature pair of Gabor filters is used to decompose a signal, with a real part specified by a cosine modulated by a Gaussian, and an imaginary part specified by a sine modulated by a Gaussian. The real part of the filter is known as the even symmetric and the imaginary part as the odd symmetric components. The filter's centre frequency corresponds to the frequency of the sine/cosine wave, and the bandwidth of the filter is specified by the width of the Gaussian.

In the Daugman's iris recognition system, 2D versions of Gabor filters are used in order to encode the iris pattern data in the normalized polar coordinates (r, θ). The filter wavelet function can be described as follows:

$$H(r, \theta) = e^{-iw(\theta - \theta_0)} e^{-(r - r_0)^2/\alpha^2} e^{-i(\theta - \theta_0)^2/\beta^2} \tag{2.36}$$

where α and β are used to specify the multi-scale 2D wavelet size. w represents the wavelet angular frequency. (r_0, θ_0) are the center location of the frequency selective filter bank.

The feature encoding process begins by sampling a collection of feature points from the original iris image into the Cartesian coordinates. Afterwards, these feature points are unwrapped into a matrix representation in the normalized polar coordinates using the Daugman's rubber sheet model described in section (2.8.5). Once this is done, a set of Gabor filter banks is applied to the matrix which is then decomposed into a set of complex coefficients h at location (r_0, θ_0) as follows:

$$h = \int_r \int_\theta I(r, \theta) e^{-iw(\theta-\theta_0)} e^{-(r-r_0)^2/\alpha^2} e^{-(\theta-\theta_0)^2/\beta^2} r dr d\theta \tag{2.37}$$

where r and θ represent the dimensions along the radial and circumferential directions in the normalized polar coordinates, respectively. Once the complex coefficients are calculated using equation (2.37), the complex domain is divided into four phases or quadrants, and each phase is represented by two binary bits (Figure 2.13).

After the Gabor feature extraction, Daugman demodulates the output of the Gabor filters in order to compress the data. This is done through phase quantization into four levels, for each possible quadrant in the complex plane. In general, phase information provides more discriminating information compared to amplitude information since it discards redundant information such as illumination variation within the image. Therefore, a complex feature matrix is generated from the image and for each complex feature value h, two binary bits (h_R, h_I) are used to represent phase information at the pixel location in

the iris template. A compact 256-byte iris template is then created, which allows for efficient pattern comparison and decision making. The Hamming distance is calculated between two binary feature templates to evaluate their match probability (Daugman (2003)).
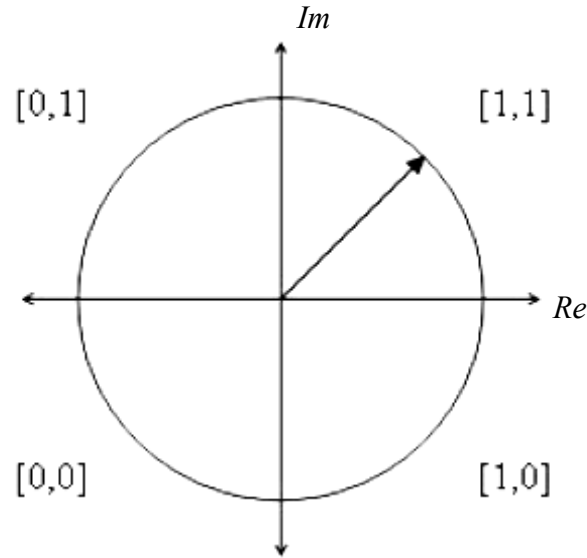
Figure 2.13: Phase quantization (taken from Masek (2003))

This process which includes Gabor feature extraction and phase encoding is repeated on the entire iris image. One set of Gabor filter banks will extract one pair of complex phasors for each feature point. For example, by applying *k* sets of Gabor filter banks on an unwrapped image template of size $M \times N$, a phase matrix of binary bits will be created with size $2\mathbf{k}M \times 2\mathbf{k}N$. This will be the binary iris template that is used for the Hamming distance calculation.

2.8.6.2 Log-Gabor filter

Brady *et al.* (2000) propose a model to explore the effectiveness for encoding the information in raw biometric images. The Log-Gabor filter is examined to encode the spatial, frequency and orientation information in an image. It was noticed that one weakness of the Gabor filter is that the even symmetric filter produces a DC component whenever the bandwidth is larger than one octave (Field (1987)). However, the use of a Gabor filter that is Gaussian on a logarithmic scale will eliminate the DC component. This is known as the Log-Gabor filter. The frequency response of a Log-Gabor filter is given by:

$$G(f) = exp\left(\frac{-(log(f/f_0))^2}{2(log(\sigma/f_0))^2}\right) \tag{2.38}$$

where f_0 and σ represent the centre frequency and the filter bandwidth, respectively.

To encode iris information when working with an unwrapped iris matrix representation, each row of pixel intensities corresponds to a ring of pixels centered at the pupil center. In order to extract the phase feature templates, the Log-Gabor filter is applied to the 1D image vectors. Since the normalization process involves unwrapping the iris region from the circular shape to a rectangular matrix (i.e. from the Cartesian coordinates to the normalized polar coordinates), the spatial relationship along the concentric sampling rings and the radius become independent. Knowing this, the 2D Gabor filter feature extraction mechanism will basically mix the relative spatial relationship when it multiplexes over the normalized polar scale. Therefore, the 2D Gabor filter applies a

symmetric Gaussian envelope to the normalized polar image representation that is not supposed to be treated evenly between radial and circumferential directions. On the other hand, the 1D Log-Gabor filter extracts the feature vector from each row of the normalized matrix representation, which avoids mixing the relative position information between the radial and the circumferential directions.

2.8.6.3 2D Hilbert transform

The 2D Hilbert transform can be used on the Daugman rubber sheet model representation in order to extract the features from the normalized rectangular iris images (Tisse *et al.* (2002)). The analytical signal $z_x(t)$ becomes:

$$z_x(t) = x(t) + jHx(t) \qquad\qquad (2.39)$$

where $z_x(t)$ represents the 1-D complex feature vector generated from original signal $x(t)$, and H stands for the Hilbert transform. In a similar fashion, the 2D version of the Hilbert transformed image is computed in order to calculate the instantaneous phase and frequency. From this, the complex phase information is taken as the iris feature template, in the same way as the Gabor transformed phase template in the Daugman system.

2.8.7 Matching Algorithms and Distance Measure

Using one of the previously described feature extraction schemes, an iris image is processed and transformed into a unique representation within the feature space. In order to see if two iris templates match (i.e. extracted from the same eye) which involves making an accept/reject decision, a distance measure is indeed necessary to measure the closeness of a match. For example, some widely used methods in the iris recognition field are the Hamming distance (HD), the normalized correlation (NC) and the weighted Euclidean distance (WED). Other distance measures have also recently been proposed, which aren't used in this thesis.

2.8.7.1 Hamming distance

In order to measure the statistical independence between two iris templates, the Daugman algorithm calculates the correlation between them. For instance, the Hamming distance is used to measure the difference between encoded binary phase feature vectors. The Hamming distance between two iris templates is defined as follows:

$$HD = \frac{||(template_A \cap mask_A) \otimes (template_B \cap mask_B)||}{||mask_A \cap mask_B||} \tag{2.40}$$

where $template_A$ and $template_B$ represent the two encoded iris feature matrices. $mask_A$ and $mask_B$ are two binary masks where the location of noise pixels is marked by "0" and the rest of the mask with binary "1". The operator $\otimes$ represents the logical XOR

operation where it compares bit by bit, and $\cap$ stands for the logical AND operator which takes the common area between the two matrices representing the valid iris regions. Hence, the Hamming distance calculates the pattern difference between iris templates by using a bit to bit comparison. For iris templates extracted from the same eye, the statistical independence and the Hamming distance tend to approach zero, while two different iris templates will have a Hamming distance close to 0.5. For this reason, it is important to set a proper threshold when computing the Hamming distance between two iris templates in order to decide if both templates come from the same eye, thus achieving accurate feature identification.

2.8.7.2   Normalized correlation

The normalized correlation method is implemented in the Wildes system in order to measure the closeness of match between two encoded iris images. The normalized correlation is defined as follows:

$$NC = \frac{\sum_{i=1}^{n}\sum_{j=1}^{m}(p_1[i,j] - u_1)(p_2[i,j] - u_2)}{nm\sigma_1\sigma_2} \tag{2.41}$$

where p_1 and p_2 represent the two encoded iris templates of size $n \times m$, u_1 and u_2 correspond to the mean of p_1 and p_2, respectively. σ_1 and σ_2 are the standard deviations of p_1 and p_2, respectively.

2.8.7.3   Weighted Euclidean distance

Similar to the Hamming distance, the weighted Euclidean distance (WED) is another distance metric that can be used in a biometric system. It defines the closeness of match between two iris feature templates. For the weighted Euclidean distance, the norm between two vectors is calculated. As described in (Zhu *et al.* (2000)), the weighted Euclidean distance measure computed for a known and an unknown iris template is calculated as follows:

$$WED = \sum_{i=1}^{N} \frac{(f_i - g_i)^2}{\delta_i{}^2} \tag{2.42}$$

where f_i and g_i represent the unknown and known (i.e. in database) iris templates, respectively. i denotes the index of the features in the templates, and δ_i is the standard deviation of the ith feature calculated from template g.

2.8.8 Evaluation Metrics

2.8.8.1   Genuine-Impostor distributions

From the biometric templates computed in an iris recognition system, the genuine $f(x)$ and impostor $g(x)$ distributions are plotted showing a normalized histogram of the distance measures (Figure 2.14). The histogram shows the matching measure according to whether or not the biometric feature templates belong to the same subject. For

instance, the genuine histogram reflects all the distances measured within the same class while the impostor histogram presents all the distances between different classes. Therefore, the genuine distance measurements should be smaller than the impostor distances since they represent the closeness of two iris templates extracted from the same eye. Generally speaking, in an ideal biometric system, the genuine and impostor distributions should be completely separated which signifies that all images are well classified since they either come from the same or a different class. Unfortunately, this doesn't occur in most practical systems and the underlying genuine and impostor distributions overlap at the tail (Figure 2.14). For this reason, a threshold must be selected in order to obtain a good separation between both distributions. The latter are also used to calculate the amount of overlap between the two curves which represent the false match and non-match rate.
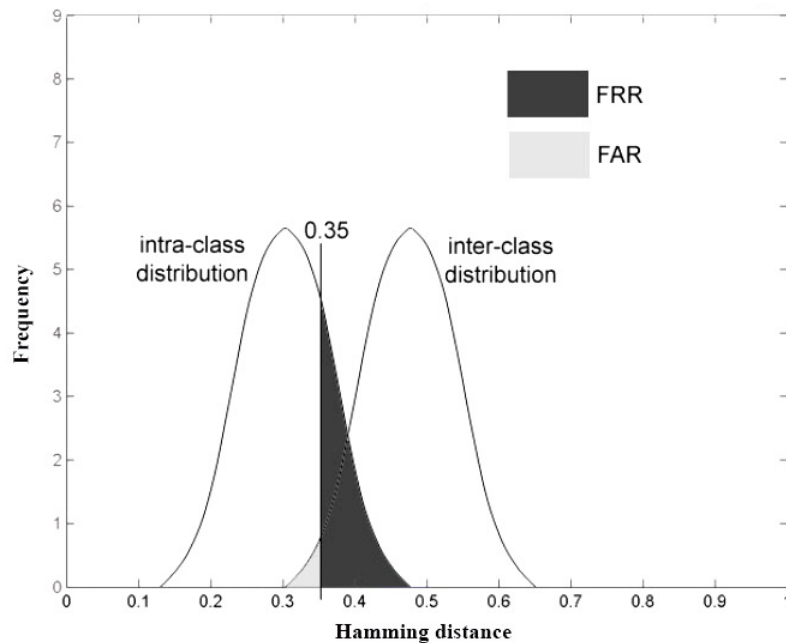
Figure 2.14: FAR and FRR seen from the overlap of the intra-class and inter-class distributions. Also, as an example, the separation Hamming distance in this figure is 0.35 (Masek (2003)).

2.8.8.2 False Match Rate and False Non-Match Rate

The main goal of an iris recognition system is to be able to identify users by achieving a good separation between the intra-class and inter-class Hamming distance distributions. When the Hamming distance between two templates is less than a selected threshold value, the processed templates are classified as coming from the same iris and a match is found. On the other hand, if the Hamming distance is greater than the chosen threshold, the templates are considered to come from different irises. The performance of the system can be evaluated using the variability among the iris feature templates. Such a measure also includes the *within* and the *between* subject variability where the *between* variability sets the limit for minimum false match rate (FMR) and the *within* variability measure sets the limit for minimum false non-match rate (FNMR) (Daugman (2004)). The intra-call and inter-class comparisons between the biometric feature templates can be represented using the genuine ($f(x)$) and imposter ($g(x)$) distributions. From this, the x-axis represents the direction along which the WED between the iris features are plotted and the y-axis shows the percentage of WED that fall into that range. Using this, the FMR and FNMR are calculated as follows (Wayman (1999)):

$$FMR(\tau) = \int_{\tau^-}^{\infty} f(x)dx = 1 - \int_{-\infty}^{\tau^+} f(x)dx \qquad (2.43)$$

$$FNMR(\tau) = \int_{-\infty}^{\tau^-} g(x)dx \qquad (2.44)$$

A series of FMR and FNMR values are calculated using equations (2.43 and 2.44) for different values of threshold τ. The match and non-match rate pairs are plotted in one

graph showing FNMR against FMR values. This graph is useful in a sense that it clearly illustrates the tradeoff between the false reject to false accept rates when varying the threshold τ during the identification process. Clearly the separation point or threshold will affect the false accept and false reject rates. For instance, a lower separation Hamming distance will decrease FMR while increasing FNMR, while a larger threshold will cause the opposite effect (Figure 2.14). For this reason, when choosing a separation point it is important to consider both the false accept rate and false reject rate. FNMR-FMR graphs have been used extensively to evaluate the performance of a biometric system, and it is termed as detection error tradeoff (DET) in other occasions. The DET curve has been used in this thesis to evaluate the performance of iris recognition algorithm.

Another measure is the decidability metric which determines the performance of a system. It helps determining the optimum parameters from which we can analyze the system's performance for optimal configuration (Masek (2003)). This metric is described in the next section.

2.8.8.3   Decidability measure

A good metric to measure the separation between the distributions is the "decidability", which takes into consideration the mean and standard deviation of the intra-class and inter-class distributions, respectively (Daugman (2002)). The decidability (d') is calculated as follows:

$$d' = \frac{|\mu_S - \mu_D|}{\sqrt{\frac{(\sigma_S^2 + \sigma_D^2)}{2}}} \tag{2.45}$$

where μ_S, μ_D represent the mean of the intra-class and inter-class distributions, respectively. In addition, σ_S, σ_D correspond to the standard deviation of the intra-class and inter-class distributions, respectively. The decidability d' corresponds to a distance measured in standard deviation and is a function of the magnitude of the difference between the means of the intra-class and inter-class distributions. Therefore, from equation (2.45), it is seen that higher the decidability, the greater the separation of intra-class and inter-class distributions, which allows for more accurate recognition. Thus, a system that has a higher decidability value tends to have a better intra and inter-class distribution separation.

2.8.8.4   Rank-1 Identification rate

The identification process in a biometric system requires distance measurement (i.e. Euclidean or Hamming distance) in order to determine the closeness of match between two iris biometric templates. From this, matches are sorted according to distance measures and the smallest distance obtained is considered to be the rank-1 match. Also, the percentage of all the correct matches among all comparisons is the rank-1 match score. In this work, the Hamming distance is used as a comparison metric.

2.8.8.5   Cumulative Match Curve

Another approach widely used to evaluate the performance of a biometric system is the cumulative match curve (CMC). It is a plot of the cumulative match score against the rank, which represents the percentage of images identified below the rank (Rukhin *et al.* (2005)). This is generated by comparing each feature template against all the other feature templates in the database. From this, a complete set of distance metrics is created among which the smallest one is taken as the closest match in that specific class. Also, among all the comparisons, the rank-1 match score would reflect the percentage of the correct matches using the smallest distance to determine a correct match.

In a similar way, the rank-2 match score would be the percentage of correct matches if using the second smallest distance as the correct match. Therefore, a series of match scores could be calculated against the ranks such that the rank-*n* match score would represent the percentage of correct matches when using the nth smallest distance as a match.

2.8.9 Image Database and Open Source Software

In this thesis, iris images from the CASIA database (*Institute of Automation of the Chinese Academy of Sciences*, (2003)) are used to test and evaluate our system's performance. The CASIA database includes 689 iris images that are taken from 108 subjects (i.e. different eyes) using near-infrared cameras. The iris images are grayscale bit-map with a resolution of 320×280. In this work, a specific class of iris images corresponds to one subject and each class consists of 6 or 7 iris images acquired from the

same eye. From the CASIA database, 327 low quality iris images, containing partial eyelash occlusions and noise, are selected for further testing. Therefore, eyelash detection, iris segmentation, circular localization, feature extraction, feature matching and distance measurements are conducted on these images. Afterwards, biometric information is calculated on the segmented iris region. Some of the code used in this thesis such as the normalization, the Gabor filter and the Hamming distance was taken from the open source Matlab code framework implemented by Masek (Masek *et al.* (2003)) that is based on the Daugman's iris recognition scheme. The rest of the newly developed scheme creates a new methodology in order to improve the iris recognition system's performance in low quality images as well as to improve the match score using enhanced segmentation.

2.9 Non-Cooperative Iris Recognition

One of the main objectives of this work is to develop new techniques that can be applied in the biometrics field for non-cooperative face and iris recognition in an uncontrolled environment. Non-cooperative iris recognition is the process of automatically recognizing individuals using their eye/iris images captured at a distance and without requiring any active participation. The problems that can occur in a non-cooperative environment are related to image acquisition challenges, image quality, noise, lighting, pose and many others. Figure 2.15 illustrates a non-cooperative face detection and iris recognition biometric system where initially, subject's face is captured in an uncontrolled environment, then pre-processed for further tracking. Afterwards, we propose an

algorithm to capture an eye image, eliminate noise in it and then, use the resulting image for further iris localization and automatic identification.

Some work exists related to non-cooperative iris recognition that attempts to solve this challenging issue. For example, Dorairaj *et al*. (2005) developed an iris recognition system that deals only with off-angle images. Their method consists in estimating the gaze direction, through the Hamming distance between the Independent Component Analysis of a frontal view image and the one that is actually captured. In addition, they applied a projective transformation in order to bring the captured iris image to frontal view. This then becomes similar to a standard frontal view iris recognition process. The authors used images of the CASIA database, as well as few other images captured in their institute.

Sung *et al*. (2002) addressed the challenges on non-cooperative iris recognition by roughly identifying some potential problems that should be resolved for accurate detection. They considered the problem of lighting conditions as being insoluble, unless special lighting methods are introduced. The problem of off-angle images, when the gaze of the subjects is not directed to the camera, motivated the development of a slightly uncommon segmentation method composed by the initial inner eye corner detection followed by a least square elliptical fit to the limbic edge pixels. The authors propose a method based on wavelet packet maximum Shannon entropy reconstruction for measuring the image information in order to identify the information degradation resultant from the non-cooperative image capturing, especially on the acquisition of

defocused images. Afterwards, the authors applied a bank of complex-valued 2D Gabor filters for the feature extraction. From this, the authors then concluded that the feature comparison by means of correlation and classification through the nearest neighbor outperforms the Hamming distance matching metric, although they used a small database to test their method.

Fancourt *et al.* (2005) claim that it is possible to achieve iris recognition at up to 10 meters distance by using an imaging framework composed from a telescope and an infrared camera. Images were captured at various distances, capture angles, environmental lighting and eyewear. The authors concluded that minor performance degradation was seen with an increasing distance, off-angle images and eyewear. They used a local correlation matching metric for the pattern comparison process. However, similarly to Du *et al.* (2005), their results were obtained using high quality images that do not contain a significant amount of noise.

All the above proposed methods claim the possibility of capturing iris images with enough quality in less cooperative biometric systems while achieving accurate human recognition. However, these methods do not deal with some major issues such as underexposed images, face occlusion, highly occluded iris regions, rapid head movement, and many more.
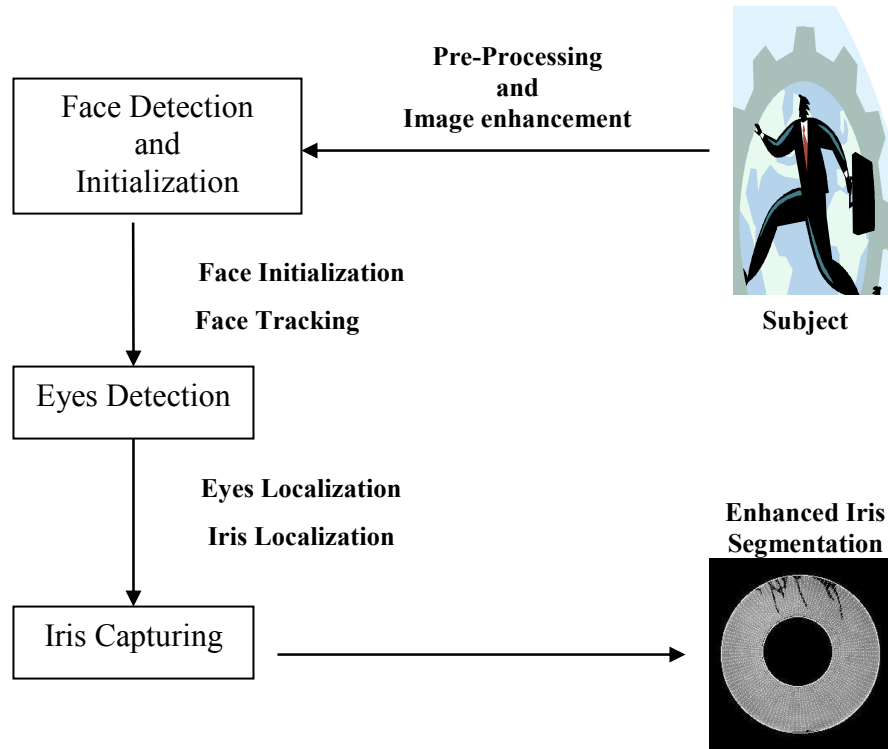
Figure 2.15: Possible non-cooperative face detection and iris recognition system.

2.10   Summary

In this thesis, new methods and solutions are developed in order to improve the iris recognition system's performance when using low quality images. As mentioned in Jain *et al.* (2000), an iris recognition system is a pattern recognition system which performs personal identification by using unique and rich texture information extracted from an iris image in order to establish the authenticity of a specific physiological characteristic possessed by the user. The iris recognition system applied in this thesis makes use of some of the existing techniques such as the log-Gabor filter for feature extraction, phase

quantization for template encoding and finally, the Hamming distance as a matching metric.

Since one of the main issues with low quality iris images is eyelash and eyelid occlusions, methods must be developed in order to eliminate this type of noise prior to matching. A typical example of an occluded image is shown previously in Figure 2.6. The upper eyelid and eyelashes have covered a significant portion of the iris, which falsifies some the of the iris texture information. If this problem is not resolved before proceeding with the feature extraction and matching steps, these erroneous pixel values will cause the matching between two genuine biometric templates to be inaccurate which might result in a false match.

For this reason, a new algorithm is developed in this thesis to detect most eyelash pixels in a low quality iris image. When noise is properly removed, additional valid iris pixels are then used and higher accuracy can then be achieved at the matching level. Further in this thesis, system's improvement due to proper eyelash detection and elimination is shown through the ROC curve which demonstrates improved error rates in most of the FMR range (Figure 4.20).

Chapter 3

Using infrared illumination to improve eye & face tracking in low quality video images

3.1 Introduction

Recently, biometrics has been a major field of research that is indispensable for authentication and identification of subjects and for increasing security. The use of biometrics as a way to authenticate user's identities has been a topic of research for years. Eye tracking and face detection and recognition are a major branch of biometrics that is employed in many areas, such as airport security and border management. The need of fully automated systems that analyze the information contained in face images is necessary and for this reason, robust and efficient face and eye detection algorithms are required. Given a single image or a sequence of images, the goal of face detection is to identify all image regions which contain a face regardless of its three-dimensional position, orientation and lighting conditions. Such a problem is challenging because faces and eyes are non-rigid and have a high degree of variability in size, shape, color, and texture. The ability to detect faces and eyes in a scene is critical to modern surveillance applications. While many image processing algorithms exist to detect faces in images,

their performance is not completely reliable, especially in situations with variable lighting, and when dealing with low resolution images (Fromherz *et al.* (1997)).

Many authors used different techniques to detect eyes in images obtained under active IR illumination. For example, appearance-based methods are developed in (Huang *et al.* (2000), Pentland *et al.* (1994)). These methods use the bright pupil effect and its motion characteristics to track the eye regions. However, these methods fail when eyes are closed or occluded and when subjects show rapid head movement. Another method based on the Hough transform is presented in (Nixon (1985)) to detect the eye region. This technique is time-consuming and requires high quality eye images with a good contrast to succeed in the detection process. Other papers developed methods using Kalman filtering and the mean shift tracker (Comaniciu *et al.* (2000), Zhu *et al.* (2005)) to detect and track eyes in an image. However, these methods might fail when applied on low quality images for eye tracking.

In this work, we develop a new robust system for eye and face tracking in low quality images using the bright pupil effect (Haro *et al.* (2000), Morimoto *et al.* (1998)). By using IR illumination, it is possible to get information from which the eye positions in the image can be calculated. Our system consists of three major parts: face localization, eye detection and eye tracking. This is accomplished using traditional image-based passive techniques such as shape information of the eye and active based methods which exploit the spectral properties of the pupil under IR illumination. A frame differential template-based technique (Ebisawa *et al.* (1993)) and a feature-based principal component analysis

method are used to search the image for valid eye regions. Afterwards, Kalman filtering is applied to locate the bright pupil candidate of interest. If the processed image contains weak reflections due to occlusion or eye closure, the algorithm uses the contour and shape information of the eye to approximate the pupil location. This is achieved by using adaptive thresholding techniques to extract the eye contour (Niblack (1986)). The developed method shows promising results in tracking subject eyes and face in low quality images under variable illumination and different head orientations. The algorithm is also tested on underexposed images where the subject shows large head movements.

3.2 Algorithm design

This section develops a system designed in the goal to automate the detection of faces and eyes in images taken under low illumination with ON and OFF IR. The proposed algorithm is designed to detect and track the subject's eyes under challenging conditions. Using the computed eyes location, face detection in the subsequent frames can be easily accomplished. The developed algorithm consists of several steps in order to pre-process the low quality and underexposed face images. For instance, our method uses some existing image processing techniques with the objective of increasing the system's robustness and performance when dealing with challenging situations such as low and non-uniform illumination, rapid head movement, occlusions, out-of-plane and in-plane head rotations and many more.

3.3 Face detection

This section elaborates on eye and face detection using image enhancement, frame differencing and adaptive template correlation techniques. The initialization step is accomplished by using geometric and shape constraints of the eye to find the pupil regions in the enhanced difference image. Some of the applied constraints are: the eye separation distance, angle measurement, pupil size and eyes location within the face boundary.

3.3.1 Experimental setup

Underexposed low quality images are taken using a single black and white camera, sensitive to infrared light, with zoom lens of $2.5 - 75\ mm$ and a NTSC output to the frame grabber. In order to adjust the overall illumination of the area where images are taken, a standard 60W bulb with variable illuminations was installed. IR illumination is produced with IR diodes strobed by a frequency generator, allowing the acquisition of experimental data with ON and OFF IR. The complete setup can be found in (Asfaw *et al*. (2002)). The data are captured for different users under various experimental conditions to simulate real life scenarios. Each volunteer is placed $1.5\ m$ away from the camera. 24 test samples (5 seconds each) per volunteer are acquired with a combination of ON and OFF IR. The pupil is then detected using the subtraction method (Zhu *et al*. (2005)) using the dark and bright pupil images.

3.3.2 Non-linear image enhancement and denoising

This step is crucial for low quality images taken in low illumination (Figure 3.2). The original image is low pass filtered with a 5×5 Gaussian filter with $N = 4$ iterations, using the non-linear edge and contrast enhancement algorithm described in (Deng *et al.* (1993, 1994)). We consider the image gray level digital representation in the $[0, M)$ range, where $M = 255$ for an 8-bit image. In order to avoid "clipping" (i.e. losing information), arithmetic operations on image pixel values are defined in a logarithmical mapped space where the forward mapping function between the image pixel space (F) and the real number space (ψ) is: $\psi(F) = log((M - F)/F)$. Since vector addition, subtraction and multiplication are bounded operations and well defined in the log space, it is possible to derive non-linear equations that overcome the "clipping" problem caused by linear methods (Bovik (2000)). The iterative technique shown in Figure 3.1 overcomes the limitations of linear methods by performing a non-linear weighting operation on the input pixels of the image. This requires the selection of parameters s_i to control the amount of high frequencies introduced in the solution. If $s_i < 1$, the solution will be smoothed; otherwise it amplifies edges. The output of this system results in an enhanced image with reduced high-frequency content and better contrast.
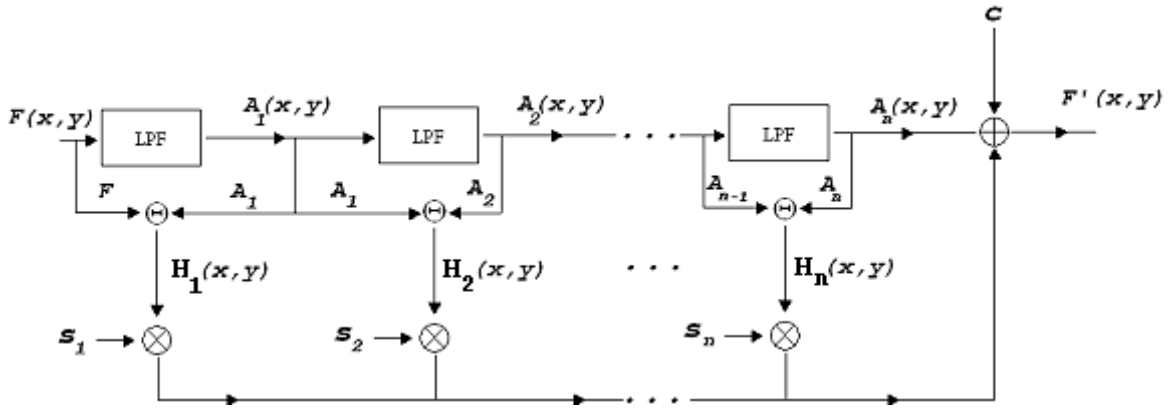
Figure 3.1: Multistage Algorithm block diagram showing three stages. At each stage, the input image *(F or A)* is filtered using a Gaussian [5×5] low-pass filter. An image containing only high-frequencies *H(x,y)* is obtained by subtracting the smoothed output from the input. The edge amplification parameter s_i is selected at each stage, *i*, based on the level of high frequency noise in *$H_i(x,y)$*. *c* is a scalar controlling the contrast level in the enhanced image.

3.3.3 Histogram stretch

The histogram in Figure 3.2b is stretched in order to fill the entire available gray-scale range. Lower and upper histogram threshold values t_L and t_H are calculated corresponding to 15% and 95% of the total number of pixels in the histogram. This results in a more visually distinctive image (Figure 3.2c) with a broad histogram (Figure 3.2d). Also, this operation provides better edge delineation, which facilitates the extraction of the face contour from the background in the initialization step.
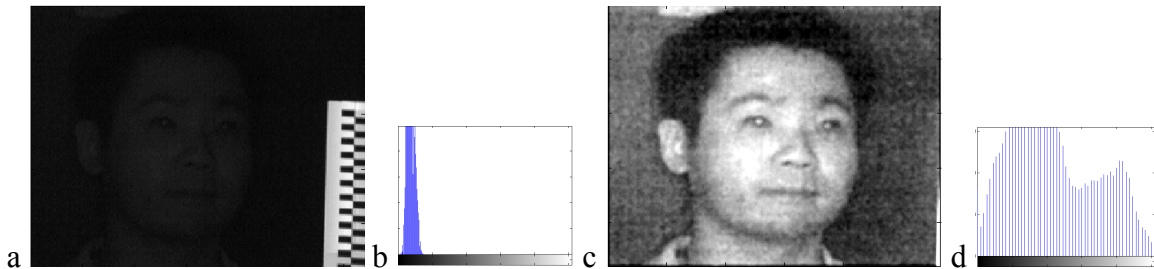
Figure 3.2: (a) Low quality underexposed IR image showing shows that most pixels have low intensity values due to poor illumination, (b) its corresponding histogram, (c) Noise reduction and contrast enhancement using the log-ratio approach. The histogram stretch operation (d) presents better edge delineation around the face region. Image a) shows that the pupil classification problem is very challenging since subject's eyes show very weak reflections.

3.3.4 Non-linear coarse edge enhancement

The image obtained in section (3.3.3) is low pass filtered with a 9×9 Gaussian filter with $N = 8$ iterations, using the non-linear image enhancement algorithm described in section (3.3.2). The output of this system results in a coarsely enhanced image with a well-defined face boundary (Figure 3.3b).

(a)   (b)
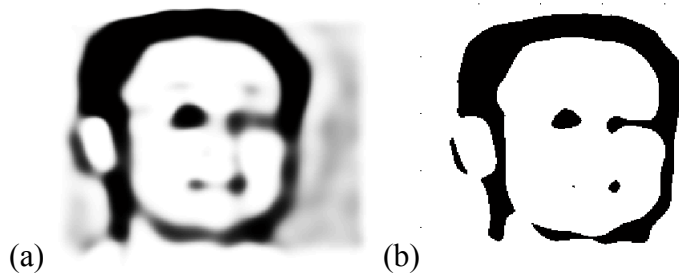
Figure 3.3: (a) Coarsely enhanced image using non-linear enhancement algorithm, (b) binary image using t_H as threshold

3.3.5 Morphological image erosion operation and Edge detection

Morphological erosion is applied on the binary image in Figure 3.3b to reduce region expansion caused by the blur effect from the non-linear edge enhancement operation in section (3.3.4). A 3×3 disk-shaped structuring element is used for the morphological image erosion operation. Using the eroded binary image, a Sobel operator is constructed to perform a 2D spatial gradient measurement on an image and gives more emphasis to high-frequency regions that correspond to edges (Figure 3.4a). The Sobel operator consists of a pair of 3×3 convolution kernels, which are designed to find horizontal and vertical edges in an image (Bovik (2005)).

3.3.6 Initial face contour extraction

Initial face contour extraction is performed as follows:

- Compute all points on the contour in the image of Figure 3.4a obtained from section (3.3.5).

- Find an arbitrary point located in the face region by scanning the image row-wise and by taking the mean of all computed edge points on the contour.

- Starting at the approximated face location found in the previous step, search for all points located on the inner face boundary that are not black (iteratively).

- Create an intensity vector by summing all intensity values in Figure 3.4a column-wise. The intensity values corresponding to both maxima on the graph in Figure 3.4b and that are located on the inner contour are chosen as face proximities.

(a) (b)
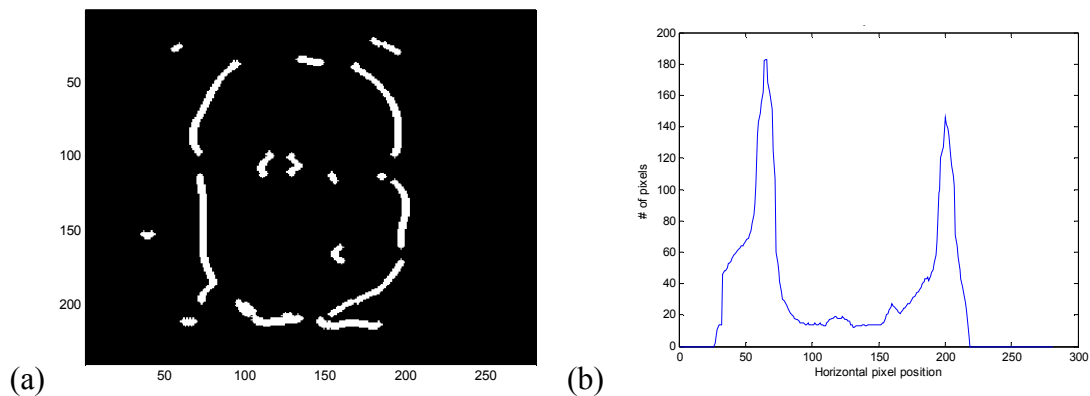
Figure 3.4: (a) Inner face contour extracted using a Sobel operator and connected component analysis, (b) plot of pixel intensity summation in the vertical direction.

3.4 Initial eye detection

The first step is to locate the eye position in the initial bright (i.e. image taken under IR illumination where pupil show reflections) and dark eye images sequence. This is achieved by first subtracting the dark eye image from the bright eye image. Also, an image obtained using the morphological opening operator (a disk structuring element of size 2) is also subtracted from the bright pupil image. The resulting difference images are then thresholded using a weak threshold in order to account for all the reflections in the image. In order to reduce the background noise caused by non-uniform illumination, we apply a logical AND operator to both images in order to keep the reflections common and present in the binary images. The process is presented in Figure 3.5 as a block diagram and the resulting images are shown in Figure 3.6. Afterwards, in order to locate the right pupil region, the binary image (Figure 3.6h) is then processed using shape and geometric information of the eye. Some of the measures that are used to segment the true pupil regions are: the within-eye distance, angle measurement, pupil size and eyes location within the face boundary. For example, any blob with area greater than 50 pixels is neglected since it cannot correspond to eye reflections. The remaining blobs are processed using distance and angle constraints as follows:

- Compute a matrix (Λ) of size $i \times j$ as all possible distances in the vertical direction between all eye regions such as

$$\Lambda(i, j) = |y_i - y_j| \text{ if } i \neq j, \text{ and } 0 \text{ otherwise.}$$

- Repeat the process by computing a matrix (Θ) of Euclidean distances between all possible candidate regions as

$$\Theta(i, j) = \sqrt{(x_i - x_j)^2 + (y_i - y_j)^2}$$

where *x* and *y* are image coordinates in the horizontal and vertical direction, respectively.

- Search through Λ and Θ for two candidate regions that have the smallest distance (greater than zero) in the vertical direction and which have an Euclidean distance "d_{euc}" located within 25% and 75% of the face width $(0.25d_{sides} < d_{euc} < 0.75d_{sides})$. d_{sides} is computed from section (3.3.6).
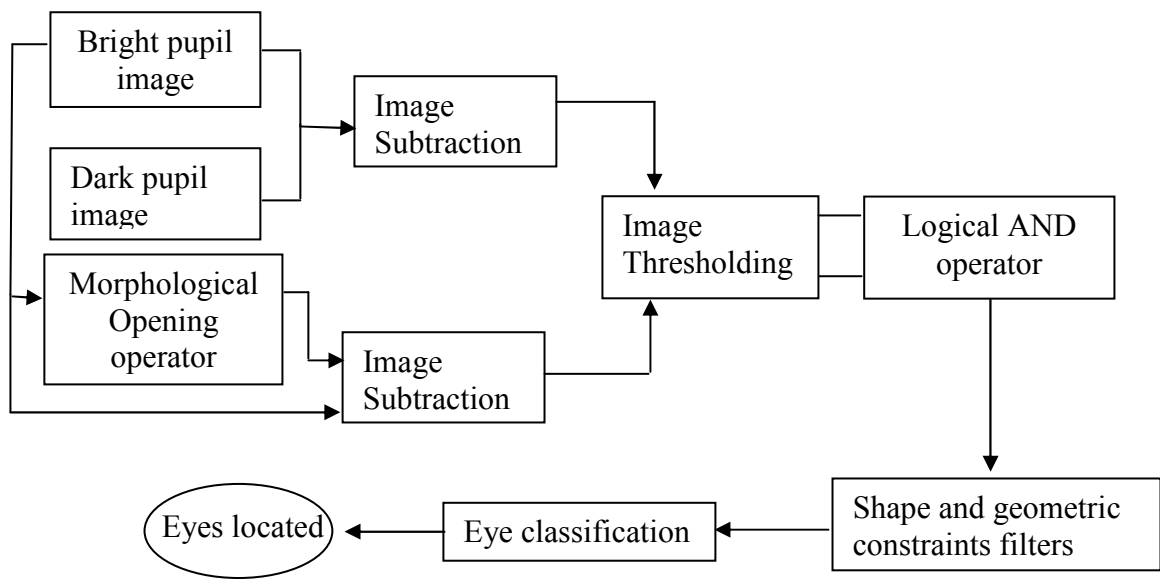
Figure 3.5: Initial Eye detection block diagram

(a)

(b)

(c)

(d)

(e)

(f)

(g)   (h)
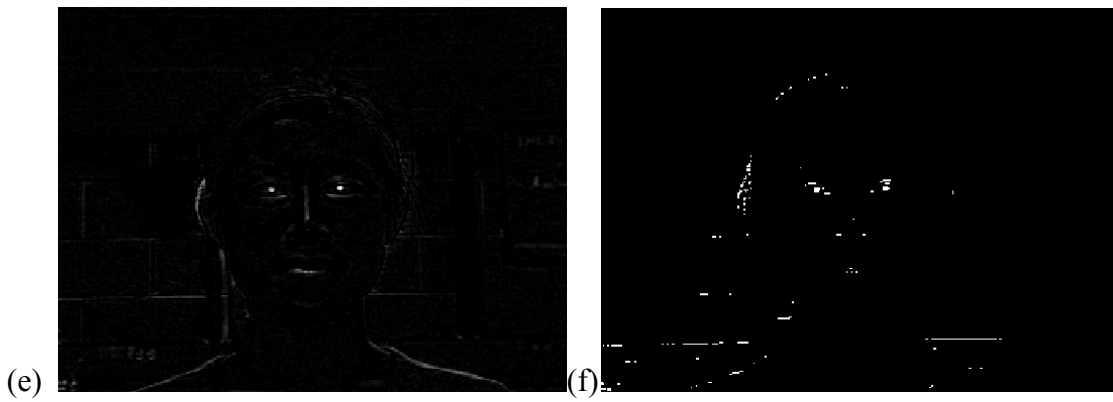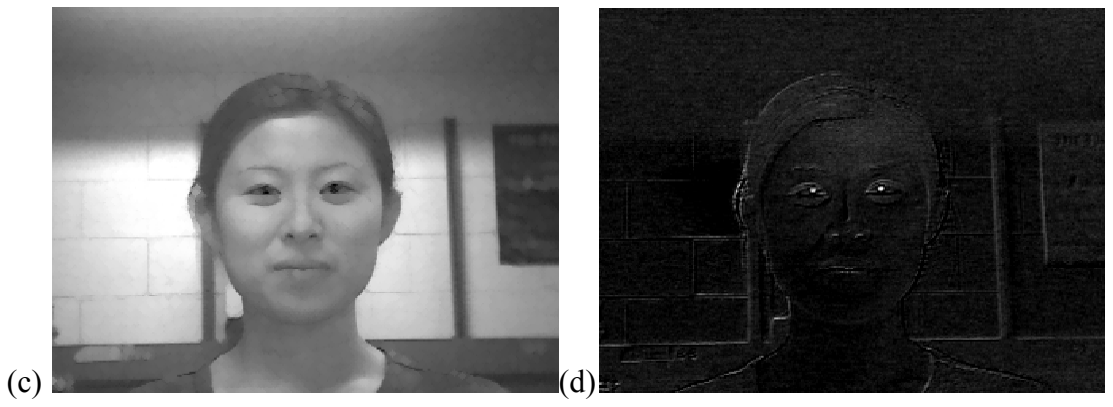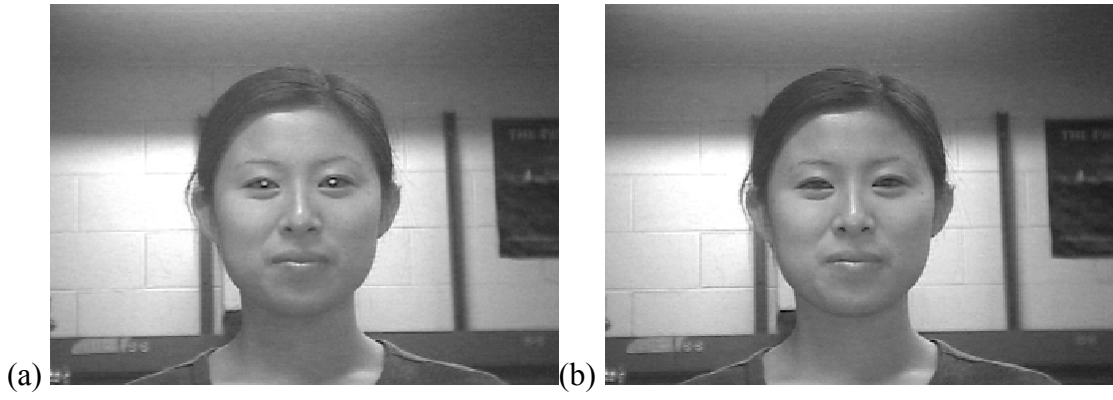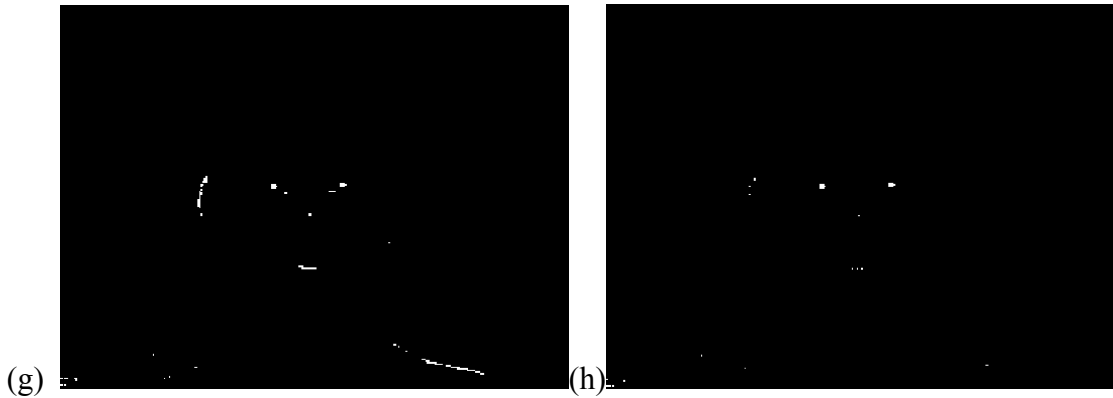
Figure 3.6: Image differencing process: (a) The original bright pupil image, (b) dark pupil image, (c) image obtained after morphological opening with a disk structure of size 2, (d) Subtraction result of images: [a-b], (e) Subtraction result of: [a-c], (f) Thresholded image (d) using a very small threshold to account for most reflections in the image, (g) Thresholded image (e) using the same small threshold, (h) Image obtained using the logical AND operator which keeps the bright regions which appear in both thresholded images.

3.5 Eye and Face tracking

After computing the initial eye position in section (3.4), an eye and face detection algorithm is initiated for eye tracking. A Kalman filter is activated in order to track bright pupils in subsequent frames. In case the images contain weak reflections or if the subject exhibits rapid head movement, the Kalman filter might fail in tracking the exact location of the pupil which is then approximated using the extracted eye contour.

3.5.1 Template correlation

Using the initial eyes location computed in section (3.4), two eye templates are created for further matching. The template size is chosen to be 40×40 in our experiment, which has shown to provide accurate tracking and correlation scores. Templates are updated after each frame using the previously computed pupil positions. The correlation scores

are then calculated for every frame using the normalized correlation coefficient (Chau *et al.* (2005)):

$$C = \frac{\sum_{x,y}[f(x,y) - \overline{f}_{u,v}][t(x-u, y-v) - \overline{t}]}{\sqrt{\sum_{x,y}[f(x,y) - \overline{f}_{u,v}]^2 \sum_{x,y}[t(x-u, y-v) - \overline{t}]^2}} \qquad (3.1)$$

where $f(x,y)$ is the intensity value of the video frame at point (x,y), $\overline{f}_{u,v}$ is the average value in the current search window, $t(x,y)$ is the intensity value in the template image at location (x,y), $\overline{t}$ is the mean value of the template image. In order to reduce computation time, this operation is not performed on the entire image, but instead only on the extracted face region found in the frame at time $t-1$. This computation gives correlation scores between -1 and 1 where 1 indicates a probable match between the search region of interest and the correlation template. This similarity measure has the advantage that it is insensitive to changes in lighting conditions which can then be used for images taken in low illumination.

3.6 Eigen-eyes

In case the template matching method does not provide high correlation scores, a principal component analysis technique (Turk *et al.* (1991)) is used to search for possible eye regions. The previously computed eye templates T_{eye} of size 40×40 are normalized with centers located at (x_{t-i}, y_{t-i}). Using T_{eye}, the principal component analysis is performed as follows:

- Represent T_{eye} in a vector format Γ_i

- Compute the mean Ψ of the previous templates

$$\Psi = \frac{1}{M} \sum_1^M \Gamma_i \tag{3.2}$$

- Subtract the mean ϕ_i from the data (eye templates)

$$\phi_i = \Gamma_i - \Psi \tag{3.3}$$

- Compute the covariance matrix C as

$$C = \frac{1}{M} \sum_{n=1}^M \phi_n \phi_n^T = AA^T \tag{3.4}$$

where $A = [\phi_1 \phi_2 ... \phi_M]$

- Compute the eigenvectors and eigenvalues of the covariance matrix

$$A^T A v_i = \mu_i v_i \tag{3.5}$$

- Determine the most dominant K eigenvalues with their eigenvectors.

- The template eye image can be represented as a linear combination of the K eigen-basis vectors such that:

$$\hat{\phi}_i - \Psi = \sum_{j=1}^K w_j \mu_j \tag{3.6}$$

where $w_j = \mu_j \phi_i$ and μ_j represent the eigen-eyes

The normalized eye template can be represented in the developed basis by the following vector:

$$\Omega_i = \begin{bmatrix} w_1^i \\ ... \\ w_k^i \end{bmatrix}, i = 1, 2, ... M \tag{3.7}$$

Eye region detection:

- Each candidate eye image Γ in the extracted face region is projected into the corresponding eigen-space

- Compute $\phi = \Gamma - \Psi$

- Compute $\hat{\phi} = \sum_{i=1}^{K} w_i \mu_i, \ w_i = \mu_i^T \phi$

- Compute $e_d = \| \phi - \hat{\phi} \|$

If $e_d < Threshold$, where e_d measures the distance from the eye space, then the selected region is possibly an eye. $Threshold$ is selected based on the image database that is used and it is chosen through experimentation.

3.7 Face detection using the previous face template

In case eye regions are not detected possibly due to occlusions or head rotation, the algorithm must keep track of the face region. This is achieved by using previous face template extracted using preceding eye location. The intensity distribution of face region around the eyes is calculated in order to locate the exact contour of the face in the succeeding frames. Using the previously calculated face template at time $t - 1$ and the current dark pupil image, both images are downsampled prior to correlation in order to reduce the processing time. Afterwards, correlation scores are computed using equation (3.1). The sub-region with the highest correlation score (close to 1) is assumed to contain face information. This process is illustrated in Figure 3.7.
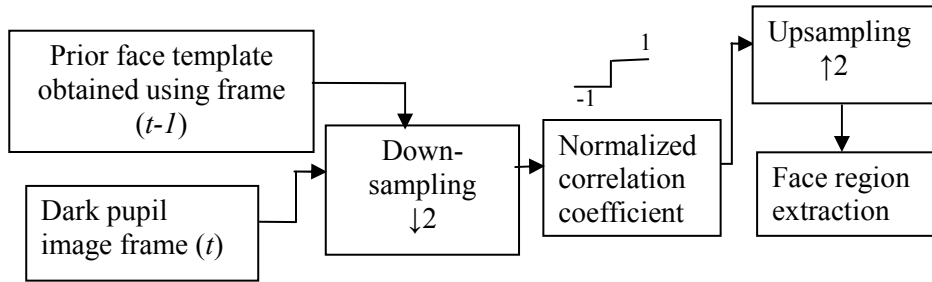
Figure 3.7: Block diagram showing face detection using prior face template. This algorithm is activated when the processed image does not contain valid eye regions possibly due to out-of-plane head rotation or occlusions.

3.8 Pupil candidate regions computation and eye tracking

Once the eye and face regions are approximately located, the current bright and dark pupil images are preprocessed as described in section (3.4), and all possible eye candidate regions computed. The elimination of non-eye blobs is achieved by first imposing the same geometric and shape constraints in the selection process and then activating a multi-stage eye tracking module based on Kalman filtering and eye contour segmentation. The classification and tracking process is described as follows:

- Compute the centroid of all the remaining blobs in the binary image obtained using connected component analysis and mark them all as possible pupil candidates (Bovik (2005)).

- Eliminate all regions with centroids located outside the face contour computed in section (3.3.6).

- Eliminate all regions with centroids located outside the eye regions computed through template matching. If all blobs in the binary image are eliminated, go back to the previous step and skip this one. This might happen if the subject shows rapid head movement in which case all candidate regions will be located far from the prior eye location, outside the estimated boundary.

- Find the region that minimizes the following equation which calculates the closest centroid to the prior eye location computed in images at instance $t - 1$.

$$d_i = min_i \sqrt{(x_{t-1} - x_t^i)^2 (y_{t-1} - y_t^i)^2} \qquad (3.8)$$

where (x_{t-1}, y_{t-1}) represent the prior pupil location and (x_t^i, y_t^i) are the centroid position of blob i. (This operation is done for the left and the right eye separately).

- After detecting possible pupil candidates, the Kalman filter (section (3.9)) is then used to compute the exact location of the bright pupil in the difference image. In case none of the binary regions are classified as possible pupil candidates, go to the next step.

- If none of the blobs are classified as possible pupil candidates (probably because of weak reflection, eye closure or occlusion), an eye contour extractor (section (3.10)) is then activated to give a more accurate approximation of the pupil location.

- After computing the pupil coordinates, update the eye and face templates to process the successive frames.

The entire process is shown in Figure 3.8 as a block diagram.
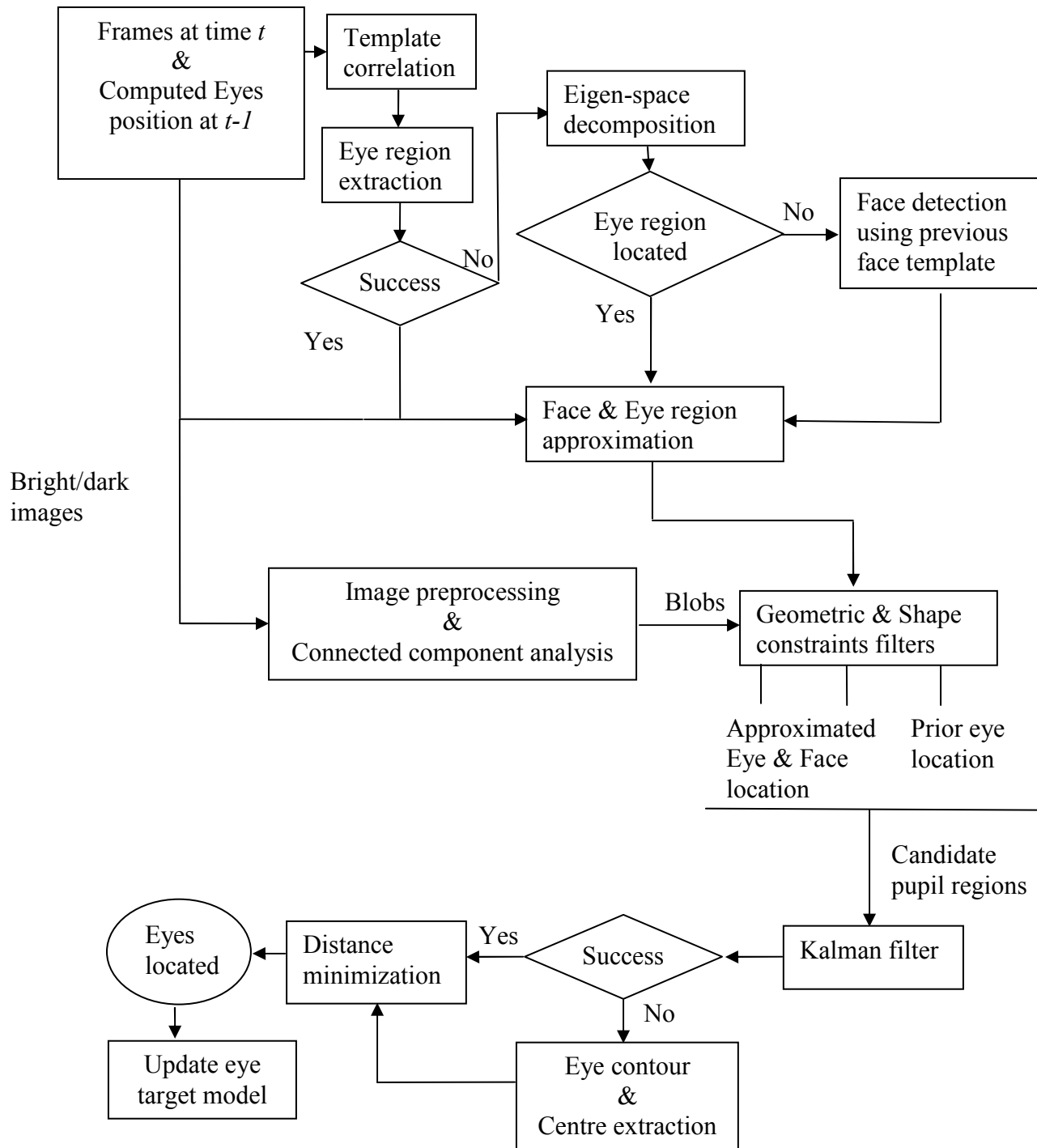
Figure 3.8: Block diagram showing eye and face tracking algorithm. The algorithm is initialized with the previously computed eyes and face location at time *t-1*. Subsequent frames are then processed using a Kalman-based and adaptive thresholding techniques to successfully track eyes in low quality images.

3.9 Kalman filtering

Kalman filtering is applied on the thresholded difference image obtained using the dark and bright pupil images. The Kalman tracker has proven to work well when the pupil shows bright reflections and when the subject's head is slowly moving (Zhu *et al.* (2005)). We start by characterizing the motion of the pupil in the eye image at each time instance by its position and velocity. The pixel position or centroid in the binary image is represented by (x_t, y_t) at time t. (u_t, v_t) represent the pixel velocity in the x and y directions, respectively. The system model (*predictor*) can then be written as follows:

$$\mathbf{x_{t+1}} = \varphi \mathbf{x_t} + \mathbf{w_t} \tag{3.9}$$

where the state vector at time *t* is $\mathbf{x_t} = [\mathbf{x_t} \ \mathbf{y_t} \ \mathbf{u_t} \ \mathbf{v_t}]^{\mathbf{T}}$, φ is the state transition matrix and $\mathbf{w_t}$ is the system perturbation. $\mathbf{w_t}$ is normally distributed as $p(\mathbf{w}_t) \sim N(0, Q)$ where Q represents the process noise covariance.

Using our feature extractor estimates $\mathbf{z_t}$ of the pupil position in each frame, the measurement model (*updater*) can be written as follows:

$$\mathbf{z_t} = \mathrm{H}\mathbf{x}_t + \mathbf{r}_t \tag{3.10}$$

where H is a matrix relating the current state information to the current measurement and r_t represents the measurement uncertainty and is normally distributed as $p(\mathbf{r}_t) \sim N(0, R)$

where R is the measurement noise covariance. The system and measurement models are used to provide an estimate of the state and its covariance matrix at time $t + 1$. In this experiment $H = \begin{bmatrix} 1 & 0 & 0 & 0 \\ 0 & 1 & 0 & 0 \end{bmatrix}$ since z_t deals with the pupil position information only.

Assuming a bright pupil effect, the estimate of the pupil position obtained using the geometric and shape constraints filters is combined with the Kalman estimate to provide us with the final pupil position.

3.10   Eye contour extractor

In a situation where the subject's eyes show weak reflections or are occluded, the Kalman filter will not predict the correct pupil location in the difference image. For this reason, an alternative way of approximating the pupil location should be developed to complement the first approach. The selected method processes the possible eye regions computed in section (3.4) and automatically detects the eyelids using an adaptive thresholding technique described in (Niblack (1996)). Global thresholding methods fail in extracting the eye contour since the eye template does not necessarily have a bi-modal distribution where an optimal threshold can be easily selected to separate the desired region and the foreground. For this reason, we use a local adaptive thresholding technique that selects a unique threshold based on the local neighborhood of each sub-region in the image where illumination is assumed to be uniform (Niblack (1996)). Local thresholds are chosen using the following equation:

$$T(i, j) = m(i, j) + k\sigma(i, j) \tag{3.11}$$

where $m(i,j)$ and $\sigma(i,j)$ are the local mean and variance of the corresponding local region. In this experiment, a 10×10 window size is chosen with $k = -0.2$ based on our experiment. This operation allows thresholding images that do not have an intensity histogram with two major peaks and that might contain strong and non-uniform illumination.

This method shows good contour extraction in complex eye images where the eyes are closing or in the presence of rotation and head movement. Once the eyelids are extracted, the pupil position is then assumed to be located at the center of this region. A distance minimization method is then applied to select the candidate blob with its centroid located the closest to the estimated pupil location using the eye contour and that is nearby the prior pupil location computed in frame at time $t - 1$. Once these conditions are satisfied, the binary blob is then marked as the possible pupil location in order to update the eye template model in the subsequent frame. The entire process is described in Figure 3.8.

3.11   Experimental Results

The algorithm is tested on two different eye image databases where images are taken for moving subjects (males and females of different ethnicity) under low and variable illumination where subjects show rapid head movement, eye closure, various facial expressions and in-plane/out-of-plane head rotation. The first set is composed of the low quality images of section (3.3.1) and the other is the RPI ISL IR Eye Database (Wang *et al.* (2005)). The image sequences are taken with IR cameras. Each image sequence is

decomposed into dark pupil image sequence and its corresponding bright pupil image sequence. We processed 1200 image sequences taken from the ISL database and 600 images from the low quality image set. The selected frames display various facial expressions, and show small and large head movements and long eye closure.

For the initialization part, the s_i parameters were set to $[0.1, 0.1, 1.0, 1.0]$ in section (3.3.2) and to $[0.1, 0.1, 0.1, 0.1, 1.0, 5.0, 5.0, 5.0]$ in section (3.3.4). These choices were motivated by the requirement in section (3.3.2), to reduce noise and to slightly brighten the image by shifting the histogram of the image towards higher pixel intensity values. When the images show bright pupil reflection, the Kalman filter succeeds in tracking the pupil location in the difference image. However, when the subject shows significant head movement and out-of-plane head rotations, the bright pupil effect disappears causing the Kalman filter to fail. This will then activate the eyelid extractor in order to get a better approximation of the pupil location. A 10×10 window size is chosen for the local adaptive thresholding technique of section (3.10) with $k = -0.2$.

Figure 3.9 and Figure 3.10 show eye detection results in weak and strong reflection scenarios, respectively. By treating the human-identified parameters as ground truth, we estimated the pixel and standard deviation results for eye detection in the horizontal and vertical directions. Table (3.1) shows the detection and tracking results for the two sets of images. From this, we can conclude that the proposed approach detects and tracks the eyes accurately. The detection rate is 100% using the ISL database and 98.5% using the low quality images. It is worth mentioning that 6 images in the low quality image data set

contained only one eye due to a 90 degree out-of-plane head rotation. For this reason, the algorithm does not detect the eye region which is not appearing on the image. However, the proposed method is able to re-locate the eye target region once it re-appears in the subsequent frames. The average and standard deviation pixel offset error in the horizontal and vertical direction are shown in table (3.2). This illustrates the efficiency and accuracy of our method since in general, an average pixel offset error <5 pixels means that the detected pixel position is still located within the pupil region that has a diameter of approximately 5 pixels in both the ISL and the low quality images databases.
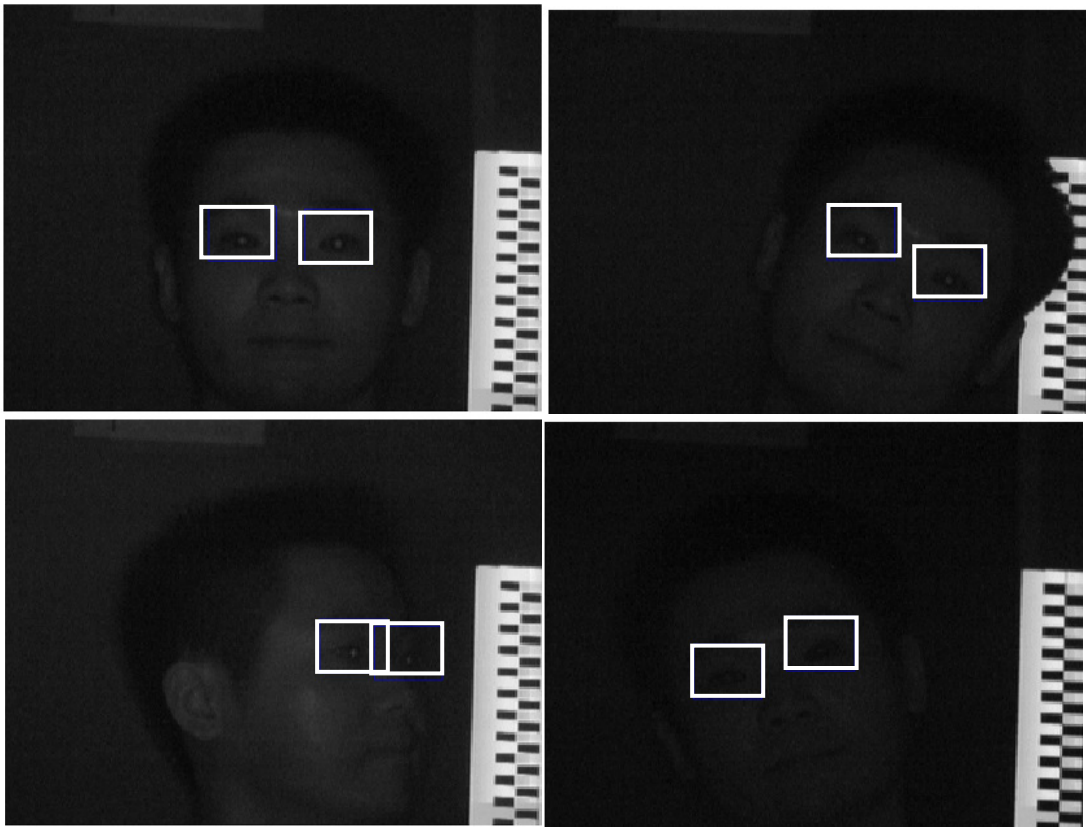
Figure 3.9: Eye detection results obtained using low quality images taken in very low illumination conditions.
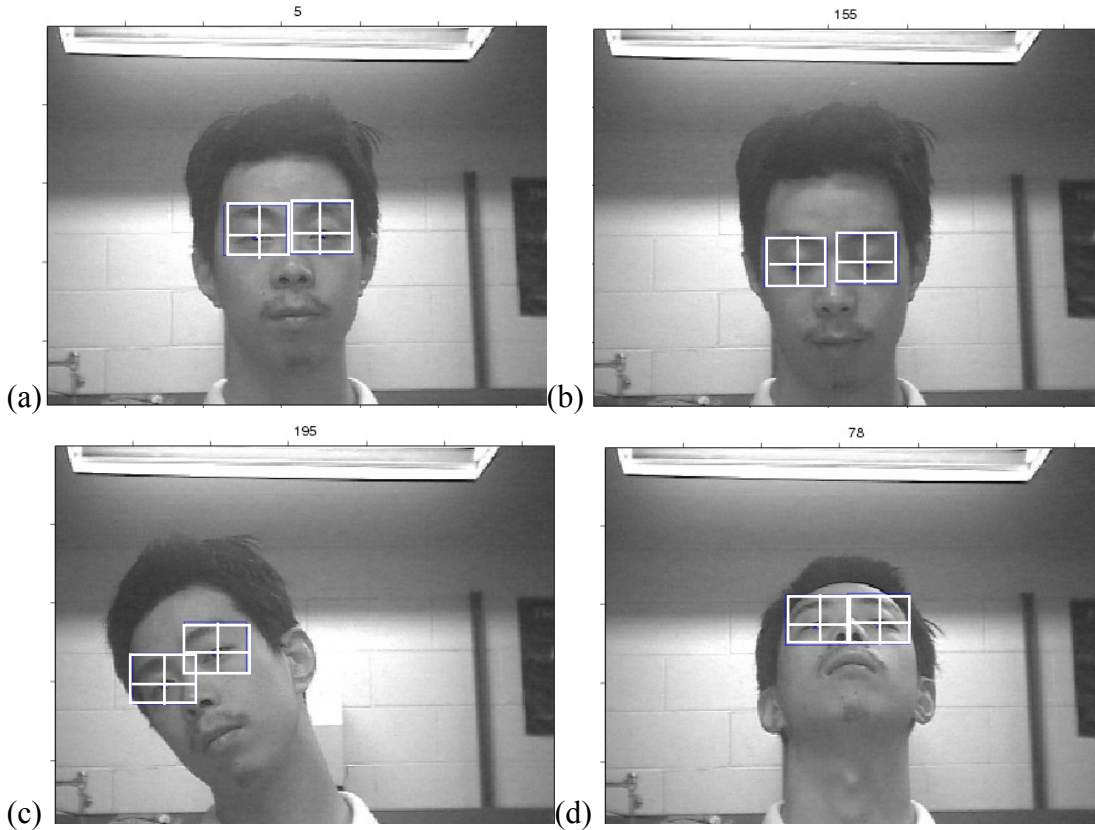
Figure 3.10: Eye detection results obtained using images from the ISL IR EYE database. Frames (b,d) show eye detection under challenging conditions where the subject has his eyes closed.

Database	Subjects	# of images per subject	Total processed images	Detection and tracking results
ISL EYE IR	4	300	1200	1200/1200
Underexposed low quality images	3	200	600	591/600

Table 3.1: Table showing eye detection and tracking results. 1800 images are processed in total using two different databases. A pupil detection rate of 100% and 98.5% were achieved using 1200 images of the ISL database and 600 underexposed images, respectively. A pupil is located successfully in an image when the estimated pupil position is contained within the pupil area that has a 5 pixels diameter.

Database	μ_{error} in pixels (x-direction)	σ_{error} in pixels (x-direction)	μ_{error} in pixels (y-direction)	σ_{error} in pixels (y-direction)
ISL: 1200 frames	1.0976	0.9090	2.2352	1.9794
Low quality: 600 frames	1.4402	1.3297	3.0829	1.9628

Table 3.2: Table showing average pixel offset error and standard deviation results for eye detection in the horizontal and vertical directions. μ_{error} is average pixel offset error and σ_{error} is the standard deviation of the offset error, respectively. x and y are the horizontal and vertical directions, respectively. It is worthwhile mentioning that the pupil diameter is approximately 5 pixels in both image databases.

3.12   Discussion

This work presents a new face and eye detection system that combines several image processing techniques in the goal to extract and track face and eye positions from surveillance type images with IR strobe taken under poor illumination. For example, in the case where many reflections (blobs) occur, the algorithm will find all possible eye locations and presents the best solution using multi-stage classification techniques. In order to reduce the set of possible eye region candidates, shape and geometric constraints are imposed in the classification process. A Kalman tracker is used to approximate eye location in bright pupil images. If the image contains weak reflections, a local adaptive thresholding technique is used to extract the eye contour in order to estimate the pupil location. This improves the performance and accuracy of the system when dealing with faces at different orientation and with eye closure. The algorithm achieves a pupil detection rate of 100% and 98.5% using 1200 images of the ISL database and 600 underexposed images, respectively. A pupil is located successfully in an image when the estimated pupil position is contained within the pupil area that has a 5 pixels diameter.

As a comparison, Zhu *et al*. (2005) developed an eye tracking technique that locates pupils using IR illumination. Their technique achieved a 96.7% detection rate when tested on 1600 frames taken from the ISL EYE IR database. However, their method does not address the challenge of tracking eyes in underexposed images.

Our developed algorithm consists of several steps in order to pre-process the low quality and underexposed face images. For instance, this multi-stage algorithm uses some existing image processing techniques with the objective of increasing the system's robustness and performance when dealing with challenging situations such as low and non-uniform illumination, rapid head movement, occlusions, out-of-plane and in-plane head rotations and many more. This algorithm is able to adapt to different situations, can track eyes and faces in challenging situations using advanced image enhancement techniques when dealing with low quality images.

3.13   Summary

This work proposes an algorithm to automatically detect and track faces and eye locations in IR images taken under poor illumination. The algorithm detects face region in the image, extracts the face contour and tracks eye location in subsequent frames using a Kalman filter. In case the images show weak reflections, a local adaptive thresholding technique is used to approximate the eye location. Tested on 1800 IR images, the proposed system achieves a 99.5% detection rate.

Chapter 4

Improved Identification of Iris and Eyelash Features

4.1 Introduction

Proper Iris segmentation is essential for various security applications using iris recognition technology for personal identification (Wang *et al*. (2002)). Irises are occluded by the eyelid and eyelashes as well as from specular reflections from the (typically infra-red) illumination system. In order to accurately process the image, it is important to identify such occluded regions in order to remove them from further processing. There exist some algorithms that try to bypass the eyelash occlusion by selecting an iris boundary within the real iris region, such as the one presented by Poursaberil *et al*. (2006). This method is not very efficient since it avoids eyelashes by eliminating both the eyelashes and certain iris regions, therefore, it underestimates the iris region. Furthermore, it changes the relative sampling distribution of the feature points. For this reason, inaccurate detection of these occlusions considerably reduces the performance of an iris-based identification system when subject cooperation is not possible. Cooperative users can be asked to stand still for multiple image acquisitions, while for Iris On the Move (*http://www.sarnoff.com/)* or covert surveillance applications (i.e. in airport security) such cooperation is not available. This will greatly affect the localization of the iris inner and outer boundaries as well as it will degrade the iris feature extraction process. For this reason, exact eyelash detection and segmentation is required

to improve the entire biometrics system's accuracy and improve the recognition performance. In this work, we develop an algorithm for accurate iris segmentation in images where the major portion of the iris is occluded. Our algorithm detects separable and multiple eyelashes, respectively. Separable eyelashes are first detected using a local intensity variation based algorithm while multiple eyelashes are found using the block mean and variance approach. Various methods have been proposed for eyelash detection (Kong *et al*. (2001), Huang *et al*. (2004), Yuan *et al*. (2004), Kovesi (1999)) which uses 1-D Gabor filter, intensity variance, phase congruency, template mean and standard deviation for multiple eyelash detection and a local intensity minimum method for separable eyelash detection. All these methods perform generally quite well but do suffer from some limitations such as computational complexity, inexact iris boundary segmentation, false eyelash detection and improper eyelash segmentation over the iris region. Specifically, all previous approaches tend to overestimate the occluded regions, and thus lose iris information that could be used for identification. In this chapter, a new algorithm is developed that improves the iris segmentation process by providing a detailed iris image area while eliminating distortion as much as possible. This enhanced iris segmentation approach results in iris images with fewer artifacts and distortion leaving more iris pixels for the recognition process. The masked images are normalized and encoded by the Log-Gabor filter described in section (2.8.6.2). This is followed by encoding the extracted iris features using phase quantization and then classifying them using the Hamming distance measure previously implemented in the Daugman's system (Daugman (2004), Xie (2007)). The proposed method addresses most of the noise and distortion issues within the iris images using a collection of image processing techniques

such as: logarithmic (i.e. non-linear) image enhancement, edge detection, morphological operators, Hough transform, intensity gradient based algorithm and a block mean and variance method using region's local statistics. Finally, our results show that the enhanced segmentation decreases the genuine distances and the error rates, which effectively increases the robustness of the recognition system. Our main algorithm is presented in section (4.2) and some experimental results are presented in section (4.3). Finally, section (4.4) concludes this work.

4.2 Enhanced Segmentation

The following section develops an algorithm to automate the detection and segmentation of eyelash features in an eye image. The design criterion is to determine the detailed eyelash regions without overestimation (falsely detecting iris regions in the image as eyelash). In performing this calculation, it localizes and segments the pupil-iris region using the Hough transform technique (Gonzalez (2002), Ballard (1981), Xie (2007)) and the non-linear image enhancement algorithm applied on the iris region in order to facilitate eyelash detection.

4.2.1 Pupil-Iris region localization and boundary extraction

Assuming that the pupil and iris regions have circular shapes, the Hough transform, combined with standard edge detection techniques, is used to detect the circular boundaries in iris images. This section describes an algorithm for accurate iris boundary

detection and contour extraction (Figure 4.1) based on a combination of image processing techniques.

4.2.1.1   Non-linear image enhancement

This recursive filtering technique overcomes the limitations of linear methods by performing a non-linear weighting operation on the input pixels of the image. This requires the selection of parameters s_i to control the amount of high frequency content introduced in the solution. If $s_i < 1$, the solution will be smoothed otherwise, it amplifies edges. The output of this system results in a binary enhanced image with sharper edges and better contrast (Figure 4.14c). Since this method attempts to remove distortions in the images, it makes the subsequent localization of the circular boundaries in iris images easier.The original eye image $F(x, y)$ goes through a recursive smoothing operation (Figure 3.1). At each iteration, $F(x, y)$ is low pass filtered with a 5×5 Gaussian filter using the non-linear edge and contrast enhancement algorithm described in (Deng *et al*. (1993), Deng *et al*. (1994)). In each step, the output image, obtained from the previous iteration, becomes the input to the next Gaussian low-pass filter (LPF). $A_n(x, y)$ represents the smoothed image at step n, $H_n(x, y)$ represents the subtraction of the images before and after the smoothing operation and s is a scalar that controls the contrast level in the final enhanced image $F'(x, y)$. The whole process is repeated until the following condition $A_{n-1}(x, y) \ominus A_n(x, y) \approx 0$ is met.

In order to avoid "clipping", arithmetic operations on image pixel values are defined in a logarithmical mapped space where the forward mapping function between the image pixel space (F) and the real number space (ψ) is

$$\psi(F(x,y)) = log\left(\frac{255 - F(x,y)}{F(x,y)}\right) \qquad (4.1)$$

Using equation (4.1), the addition, subtraction and multiplication operations in the logarithmic space are defined as follows:

$$A \oplus H = \psi^{-1}(\psi(A) + \psi(H)) \qquad (4.2)$$

$$A \ominus H = \psi^{-1}(\psi(A) - \psi(H)) \qquad (4.3)$$

$$s \otimes A = \psi^{-1}(s \; \psi(H)) \qquad (4.4)$$

where A, H and s represent the two grayscale images and a scalar, respectively. The Gaussian filtering is computed in the grayscale intensity space while the addition $\oplus$, subtraction $\ominus$ and multiplication $\otimes$ are defined in the logarithmic mapping space. The images are first mapped into the logarithmic space before the addition, subtraction and multiplication operations and then inversely mapped back into the grayscale intensity space after these operations (equations 4.2 to 4.4). These images are used for the segmentation, the feature extraction and the pattern comparison. In this case, $F'(x,y)$ is used to search for the circular boundaries of iris and pupil regions. Once the parameters of these boundaries are located, the original iris image is used for the feature extraction and subsequent processing.

4.2.1.2   Edge detection

The edge and contrast enhanced image $F'(x, y)$ obtained from the previous section is used to identify the spatial gradient map with the Sobel edge detector. The Sobel operator performs a 2D spatial gradient measurement on an image and gives more emphasis to high-frequency regions that correspond to edges. The Sobel operator consists of a pair of 3×3 convolution kernels, which are designed to find lines in an image. The edge map is shown in Figure 4.15b.

4.2.1.3   Hough transform

The Hough transform is a technique which can be used to isolate features of a particular shape within an image. In this section, it is used to locate the iris outer boundary. The Hough transform is applied directly on an edge map (calculated in section (4.2.1.2)) to reduce processing time. The Hough transform represents an image in terms of a three-dimensional accumulator array. For example, circles correspond to the equation $(x - a)^2 + (y - b)^2 = r^2$ which defines a circle of center (a, b) and radius r in the (x, y) space. For this specific feature, the accumulator array will contain the (a, b, r) parameters which are updated for each edge pixel (x, y). After updating the parameters for all pixels in the edge map, peaks in the accumulator array indicate the location of the desired feature (i.e. circle). From this information, the iris boundary is located (Figure 4.15c) and the iris-pupil region is segmented for further processing.

4.2.1.4   Enhanced iris segmentation

The iris contour given using the Hough transform technique in section (2.8.4.2) is an approximation of the proper iris boundary which is not always circular. To correct the offset on the iris contour, we recalculate a new contour using the edge map obtained in section (4.2.1.2). Starting at the center position of the approximated contour, scan outwards for the first set of pixels, different from black, that form a closed contour near the boundary computed in section (4.2.1.2). This process is shown in Figure 4.15b. The exact pupil-iris segmented region is shown in Figure 4.15d.

4.2.2 Eyelash detection

In this section, separable and multiple eyelashes are detected using an intensity gradient based algorithm and a block mean and variance method (Figure 4.3). The iris and non-iris images (Figure 4.15 (d, f)) are processed independently for improved image enhancement (Figure 4.15(e, g)) and precise eyelash detection based on the local region statistics and finally, the computed eyelash points are combined for exact iris region extraction.
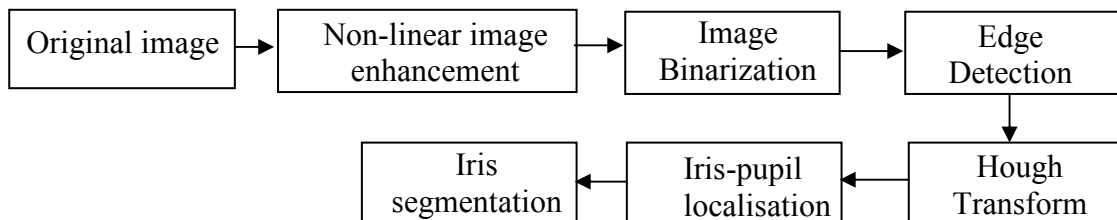
Figure 4.1: Iris segmentation algorithm based on local image enhancement

119

4.2.2.1 Local image enhancement

The iris region (Figure 4.15(d)) and the non-iris image (Figure 4.15(f)) are enhanced separately using the method described in section (4.2.1.1). This will improve eyelash detection since it depends on the local image statistics. The iris region tends to contain higher intensity variation than the overall eye image. The enhancement results are shown in Figure 4.15(e, g), respectively.

4.2.2.2 Separable eyelashes

In order to detect separable eyelashes in the horizontal, vertical and diagonal direction, the enhanced iris image obtained in section (4.2.2.1) is convoluted with the developed masks (Figure 4.2) as shown in equation (4.5). An image with all possible eyelash points is created. A possible eyelash candidate point is set to "0" when the mask response R_i is negative and to "1", otherwise.

A final eyelash map is created by selecting strong eyelash candidates only. This is obtained by taking $R_i < T$ where T is a threshold selected to be -200 in our experiment. The following operation is used in order to locate the eyelash pixels:

$$R_i(x, y) = \sum_{m=-N}^{N} \sum_{n=-N}^{N} I(x - m, y - n)M(m, n) \qquad (4.5)$$

where $I(x, y)$ is the original image, $R_i(x, y)$ is the mask response at position (x, y) and M is a $\left[(2N + 1) \times (2N + 1)\right]$ convolution mask. This condition also satisfies the connective

criterion (Huang *et al.* (2004)) which states that the eyelash is a continuous line instead of unconnected points. If a detected eyelash point is singled out as independent with no connection to another eyelash or eyelid pixel, then this point is removed from the candidates of potential eyelash pixels.

Using the masks shown in Figure 4.2, a negative mask response is obtained if and only if the center pixel is located between two adjacent eyelash points which satisfy the following connectivity criterion: if the center pixel is surrounded by non-eyelash points, the convolution operation will result in a value greater than the selected threshold which indicates that the pixel is not an eyelash point.

-1	-1	-1
2	2	2
-1	-1	-1

-1	2	-1
-1	2	-1
-1	2	-1

2	-1	-1
-1	2	-1
-1	-1	2

-1	-1	2
-1	2	-1
2	-1	-1
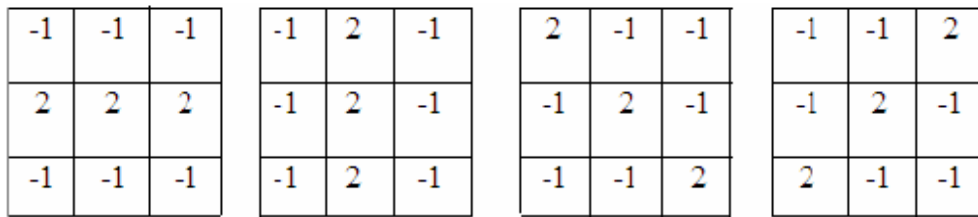
Figure 4.2: Four different masks for detecting horizontal, vertical and diagonal edges, respectively.

4.2.2.3   Multiple eyelashes

For regions containing multiple eyelashes, the mean and variance of an $n \times n$ region is taken to detect eyelash candidates. These regions are generally composed of lower intensity pixels with a higher variance. In order to find eyelash candidates in these regions, the computed block mean u_{bi} (equation 4.6) and variance v_{bi} (equation 4.7) are compared to different thresholds. If $u_{bi} < T_1$ or $v_{bi} > T_2$ then the center pixel in block i is considered to be an eyelash point. In our implementation, the block size used is 5×5.

$$u_{bi}(x,y) = \frac{1}{n^2} \sum_{i=-n}^{n} \sum_{j=-n}^{n} f(x+i, y+j) \qquad (4.6)$$

$$v_{bi}(x,y) = \frac{1}{n^2} \sum_{i=-n}^{n} \sum_{j=-n}^{n} (f(x+i, y+j) - u_{bi}(x,y))^2 \qquad (4.7)$$
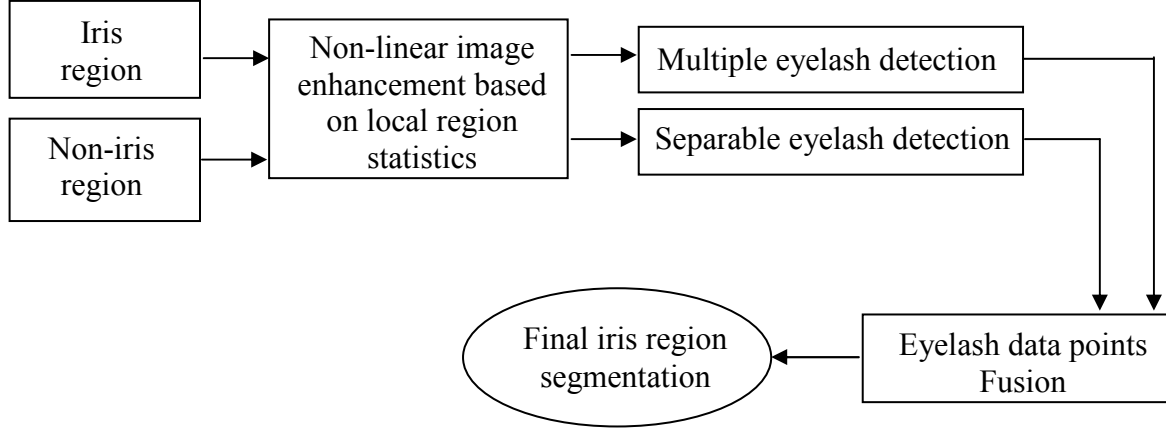
Figure 4.3: Eyelash detection algorithm and ideal iris region segmentation.

4.2.2.4 Specular Reflection

One way to locate the specular reflection points is by setting a threshold T_{spec} on the iris pixel values.

$$f(x,y) < T_{spec} \qquad (4.8)$$

For the transition area from the strong reflection to the surrounding iris region, the reflection intensities are relatively weaker, and they are still considered as noise instead

of genuine iris pixels. The detected area is considered noise and will not be used for further processing.

4.2.3 Enhanced Iris Recognition

This section describes the iris recognition scheme developed and used on the enhanced iris images where most of the eyelash and eyelid occlusions are eliminated. This section also describes the feature extraction method applied on the clean iris area followed by the phase quantization and pattern comparison using the Hamming distance matching metric. First of all, the enhanced iris image is unwrapped into a normalized polar scale template, according to the Daugman rubber sheet model described in section (2.8). Using the method developed in section (2.8.7), a mask indicating the location of unwanted artifact pixels is created in order to locate only the good iris pixels. This mask is also mapped from the Cartesian coordinates to normalized polar coordinates. Finally, the performance of our developed technique is evaluated and compared to the Masek's approach, which does not perform any eyelash detection prior to iris recognition (Masek (2003), Xie (2007)).

4.2.3.1   Enhanced Segmentation

First of all, it is important to mention that the traditional way of segmenting the iris image consists of locating the iris and pupil boundary circles, and the parabola of the upper and lower eyelids, using the Hough transform. For example, Figure 4.4 shows an image taken

from the CASIA database where the iris region is segmented using the Masek's algorithm (Masek *et al.* (2003)). Clearly, the image shows that the iris region is not well segmented since eyelash occlusions are overestimated, hence losing major iris information. This is shown in Figure 4.5 where the shaded regions covering the top and bottom of the iris image discard valid underlying iris pixels, classifying them as noise. The discarded pixels are replaced by the average pixel intensity value of the valid iris region for subsequent feature extraction.

On the other hand, the proposed method accurately detects the eyelash occlusions and classifies them as noise. It aims on improving the result of Figure 4.5 by eliminating the eyelashes outside the mask, and identifying all the valid iris pixels that were discarded as noise in the Masek's method. Using the proposed eyelash detection technique, iris segmentation results with enhanced eyelash detection are shown in Figure 4.6. The eyelashes are accurately detected, and the iris pixel locations occluded by the eyelashes are discarded as noise. In addition, valid iris pixels located between the eyelashes are kept for the subsequent feature extraction and the pattern matching. Hence, eyelash occlusion is not overestimated in our proposed technique since it reduces unwanted iris artifacts while revealing the iris pixels previously ignored in the Masek's segmentation.
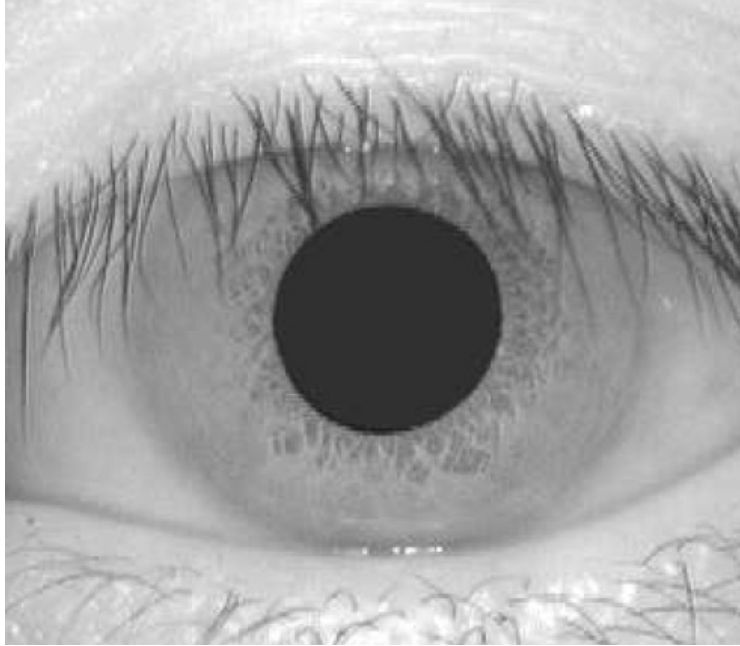
Figure 4.4: Iris image taken from the CASIA database.
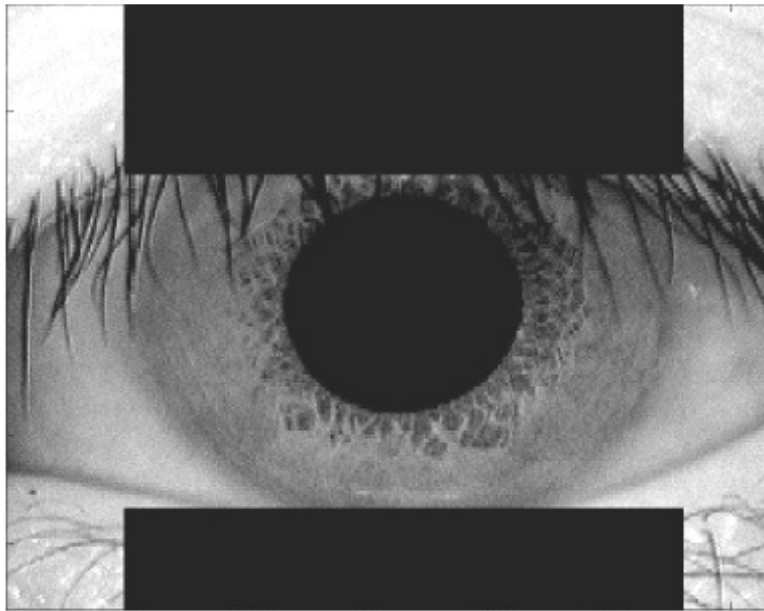
Figure 4.5: Iris segmentation using the Masek's algorithm. As seen in the image, the iris region includes some eyelash occlusion. In addition, some of the valid iris pixels are discarded as noise.
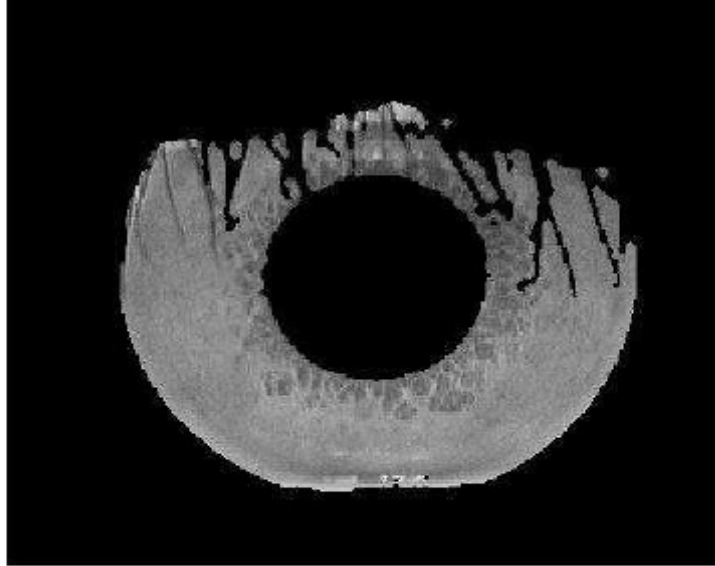
Figure 4.6: Iris segmentation using the developed enhanced eyelash detection algorithm.

4.2.4 Iris Unwrapping

Once the eyelashes are detected and iris area accurately segmented, it is necessary to unwrap the iris region using the rubber sheet model from the image space to the rectangular polar space matrix described in section (2.8). The unwrapping operation maps each point in the Cartesian coordinates (x, y) to the polar coordinates (r, θ) where r represents the radial distance from the center of pupil, and θ describes the angular shifting from 0 to 2π. The feature points are selected from the iris image with a specified sampling resolution of 20×120 where 20 feature points are selected along the radial direction and 120 along the circumferential direction. The rubber sheet model representation makes it easier to use the Gabor filter in order to create the iris feature templates for pattern comparison. The mapping function, described in (Masek (2003)), can be written as follows:

126

$$x(r,\theta) = (1-r)x_p(\theta) + rx_i(\theta) \tag{4.9}$$

$$y(r,\theta) = (1-r)y_p(\theta) + ry_i(\theta) \tag{4.10}$$

where (x,y) and (r,θ) represent the Cartesian and polar coordinates, respectively. (x_p, y_p) and (x_i, y_i) correspond to the Cartesian coordinates of the two iris radius end points. An example of iris unwrapping is shown in Figure 4.7. Each row in the unwrapped iris template corresponds to one circle in the iris region in the Cartesian scale. The unwrapped and normalized polar iris representation is robust since it compensates for pupil-iris center displacement and iris size. It provides uniform sampling of the feature points across the iris region where 20 points are taken along the radial direction and 120 points along the circumferential direction. This is shown as white dots in Figure 4.8 and Figure 4.9 where the sampling process was completed using the Masek and the enhanced iris segmentation techniques, respectively. The iris feature points covered by eyelids, eyelashes, and other artifacts are assigned an interpolated value before encoding. This corresponds to an average pixel value that corresponds to the average of all other valid iris pixel values within the segmented iris image (Masek (2003)). Some examples of unwrapped iris images are shown in Figure 4.10 and Figure 4.11. Once the iris region is unwrapped using the rubber sheet model, the rectangular template is then convolved, row by row, with a 1D Log-Gabor filter in order to extract iris feature vectors. The output of the convolution produces a complex value for each pixel point that is located in one of the four complex phase domains. In order to create a binary template, at each pixel location, phase quantization is applied as described in section (2.8). This will generate a binary pair for each complex number (i.e. every pixel). In a similar way, all the iris Log-

Gabor feature complex values are encoded with a binary pair in order to create the feature template that is used afterwards for pattern matching using the Hamming distance. However, before proceeding with the pattern comparison operation, the noise pixels are discarded using a binary mask template that is of the same size as the iris features template. In the binary mask, calculated in section (4.2.3.1), a binary '0' (i.e. black pixel) indicates the location of an unwanted pixel (i.e. noise) in the iris template (Figure 4.12 and Figure 4.13). Therefore, the quadrature phase information for each pixel is given by two binary values. Hence, for each iris template of size $M \times N$, a complex feature template of the same size is generated, which is then represented by a binary phase template of size $2M \times 2N$. The phase quantization process is repeated for all the pixels in the complex iris template in order to discard all the feature points related to noise and/or eyelash occlusions during the Hamming distance calculation.
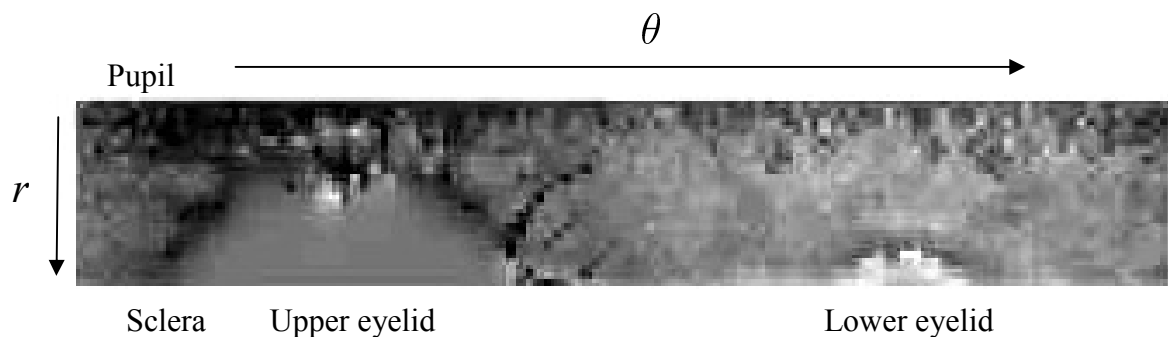
Figure 4.7: Example of the iris region unwrapping using the rubber sheet model described in Xie (2007).
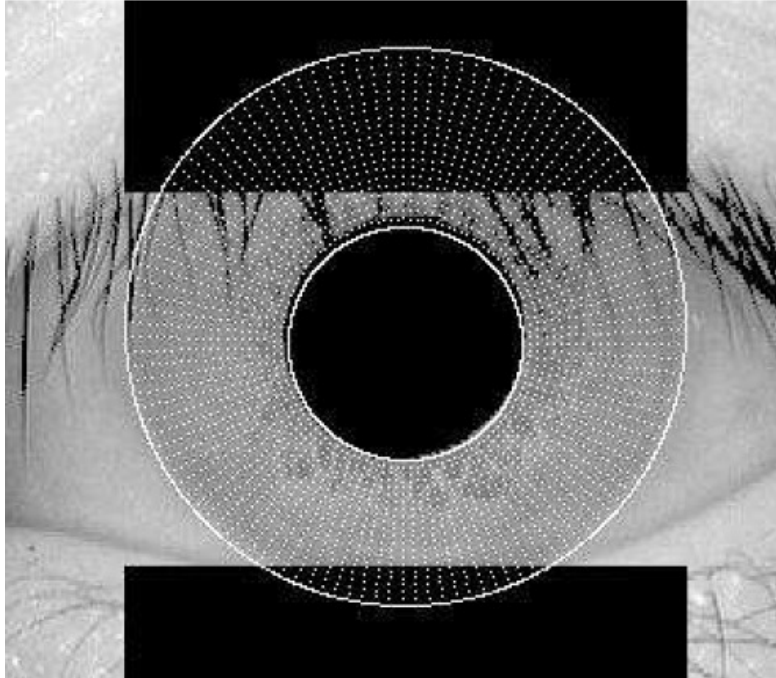
Figure 4.8: Iris feature sampling points using the Masek's iris segmentation scheme.
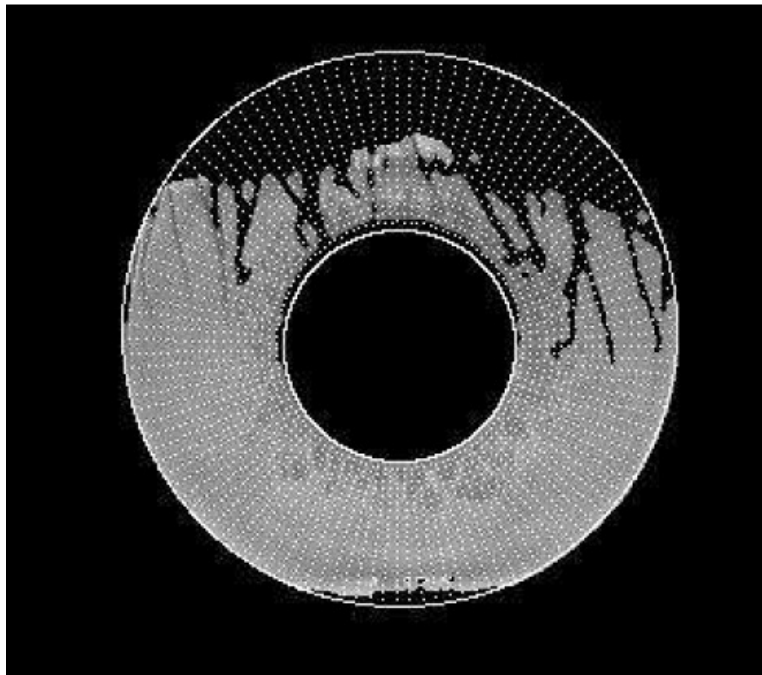
Figure 4.9: Iris feature sampling points using the enhanced iris segmentation scheme.
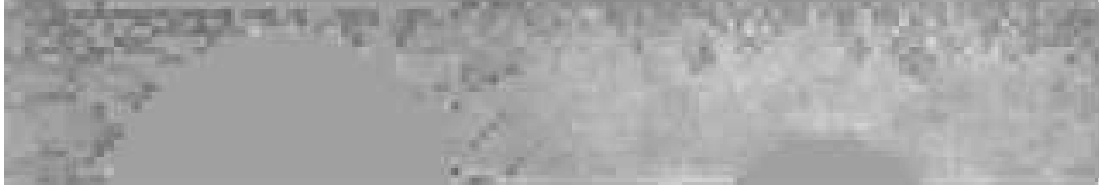
Figure 4.10: Iris region unwrapping using the Masek's technique.
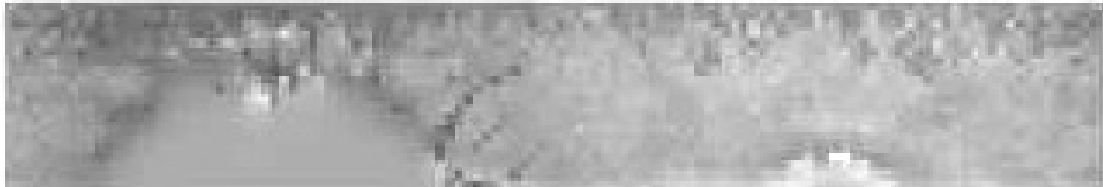
Figure 4.11: Iris region unwrapping using the enhanced technique.

Figure 4.12: Example of a binary mask applied on the unwrapped iris image in the Masek's segmentation technique. The binary 0s (black pixels) indicate noise and are used to discard the underlying pixel values in the iris template. The pixel value corresponding to 1s (white) are used for the Hamming distance calculation.

Figure 4.13: Example of a binary mask applied on the unwrapped iris image in the enhanced segmentation technique. The mask shows accurate eyelash and noise detection.

130

4.2.5 Pattern Matching

Pattern matching is crucial in order to determine if two biometric iris templates correspond to the same eye (i.e. intra-class comparison) or if they come from two different eyes (i.e. inter-class comparison). Pattern matching involves the selection of a distance measure and a decision threshold. Since intra-class comparison involves distance calculation between two iris templates taken from the same subject, it generally results in smaller distances compared to the inter-class comparisons. In this work, the Hamming distance is used as a matching metric (section (2.8.7.1)) which measures the closeness of match between the intra-class and inter-class. The Hamming distance uses the binary iris template and its corresponding binary mask in the distance calculation. Once all the noise pixels are identified by the binary "0" in the mask, the rest of the binary pixels are used in the XOR operation between the two valid iris feature templates. The Hamming distance is then computed as the average of the XOR resulting operation. After computing all the Hamming distances between the iris templates, the smallest distance is used to determine a match and to select the right class for which that subject belongs. In order to obtain smaller Hamming distances, circular shifting between the encoded iris templates is required. This will compensate for rotation invariance by row-wise circularly shifting (left and right) the encoded templates. This operation will compensate for circular rotation of the iris in the original Cartesian coordinates since each row in the binary iris template corresponds to one circular contour in the original iris region (Masek (2003)).

4.3 Results

The algorithm was tested on iris images taken from the CASIA database which comprised 689 gray-scale iris images in bit-map format. From the entire database, 327 iris images, partially occluded by eyelashes, were used to test the developed algorithm. Figure 4.16(d,e,f) show accurate detection of eyelashes in different images. Figure 4.16(g,h,i) illustrates an accurate segmentation of the iris region using the enhanced segmentation method proposed in this thesis. The following parameter values were chosen in this process: $s_1 = 0.1, s_2 = 0.1, s_3 = 2, s_4 = 5, s_5 = 150, T_1 = 20$, and T_2 was set to the variance of the entire region. These values were selected after running few tests with the algorithm in order to determine the sensitivity of the results to the parameter choices, and results did not vary significantly for a wide range of parameter choices near the values used. Figure 4.17 shows normalized iris regions for (a) an iris image without segmentation, (b) an iris with eyelash segmentation using Masek's technique and (c) an iris image obtained with our enhanced segmentation algorithm. In the normalized iris region obtained using the enhanced technique, fewer iris noise and eyelash occlusion is present in the image compared to the other two. From this, Figure 4.18 shows the genuine-impostor distributions computed using 327 iris images for (a) the Masek's algorithms and (b) the enhanced algorithm. This graph is obtained by plotting the intra-class and inter-class distributions. An overlap exists at the tail from which the FAR and FRR can be calculated. In order to quantify the improvement that the enhanced method brought to the developed system, the decidability measure described in section (2.8.8.3) is calculated. The latter method measures the separation between the intra-class and inter-class Hamming distance distributions (Figure 4.19). It is seen that a higher

decidability measure is obtained for the enhanced algorithm which implies that the iris recognition system implementing the enhanced eyelash detection scheme tends to have a better intra and inter-class distribution separation (Masek (2003)). This also implies a lower false accept rate and false reject rate since it is easier to select a threshold that provides a good genuine-impostor distribution separation.

Figure 4.20 shows the detection error trade-off curve (DET) plotting the false non-match rate against the false match rate. The red curve represents the DET curve of the Masek's segmentation and the green curve represents the DET curve of the enhanced segmentation using the enhanced eyelash detection technique. From this curve, it is noticed that the enhanced segmentation technique outperforms the Masek's method for most of the cases except in the very low FMR range where it becomes very close. Therefore, the match score using the enhanced technique is better within the entire comparison range since it uses more of the valid iris region in the matching operation by discarding most of the eyelash occlusions and other iris distortions. Masek's code neglects some valid iris pixels since it overestimates eyelash occlusion and noise pixels. This will result in a loss of valid iris pixels which will eventually decrease the system's performance. Thus, the enhanced algorithm can be applied when the iris images are acquired in a more challenging or uncontrolled environment (i.e. at a distance) where more noise and distortion can occur in the images as a result of camera tilting or lack of client cooperation.

In addition, it is also shown that the identification rate is improved from 93.67% (Masek) to 95.25% as illustrated in the cumulative match curve in Figure 4.21. The green curve

represents the cumulative match curve without any eyelash detection and the red curve represents the one with eyelash detection. It is clearly shown that the Rank-1 identification rate is improved.

(a)

(b)
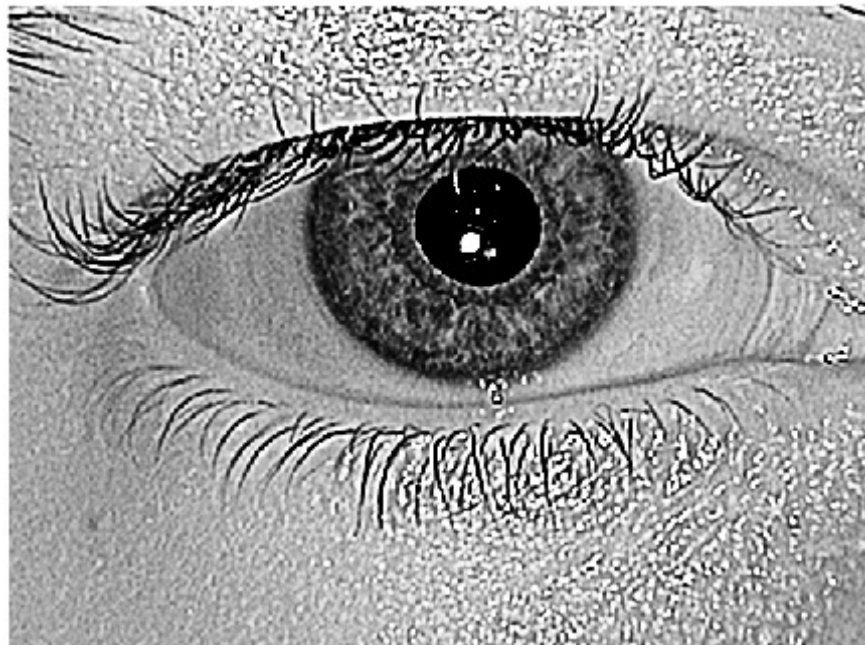
(c)
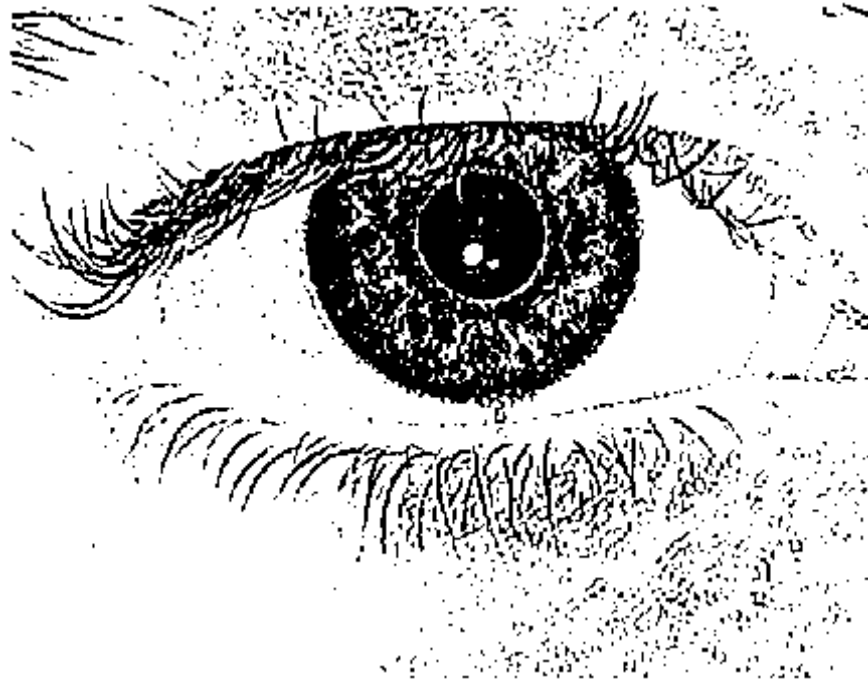
Figure 4.14: Image enhancement result: (a) Original image of the eye, (b) Non-linear image enhancement, (c) Binarized image

(a)

(b)

(c)   (d)

(e)
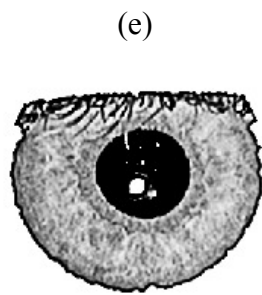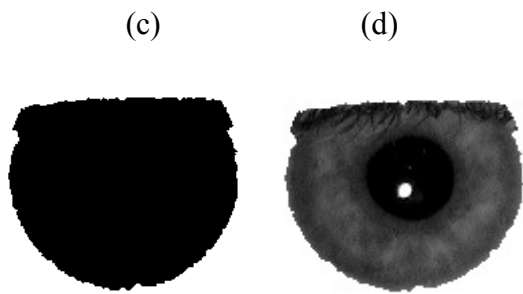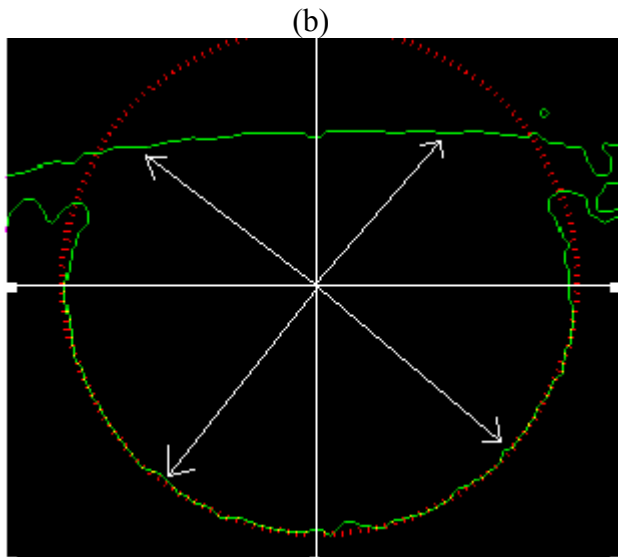
(f)
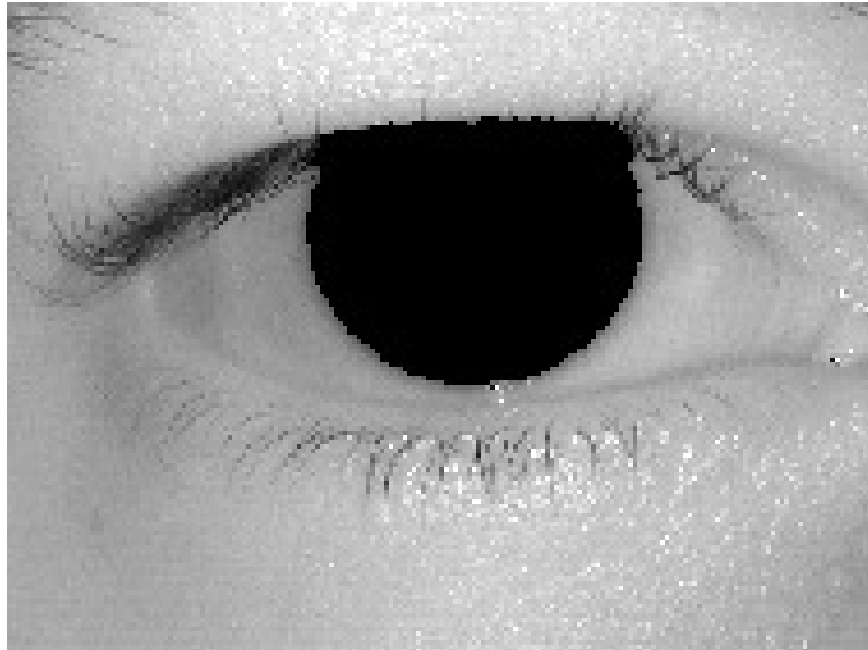
(g)
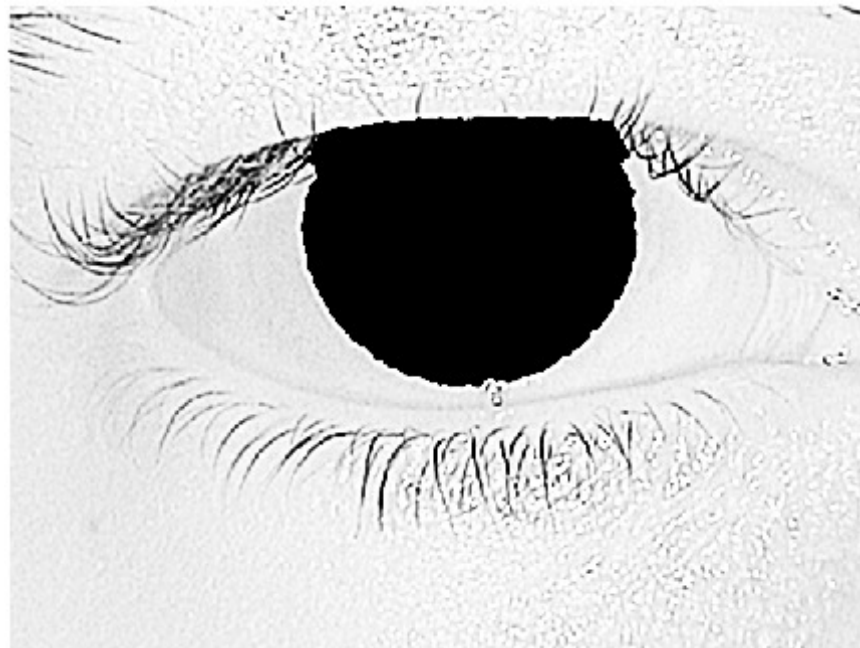
Figure 4.15: Accurate iris boundary extraction and enhancement: (a) Approximated location of the iris outer boundary using the Hough transform, (b) Edge map and accurate iris boundary calculation, (c) Accurate pupil-iris boundary extraction, (d) Exact Pupil-iris region segmentation, (e) Pupil-iris local region enhancement, (f)Non-iris eye image, (g) Non-iris local image enhancement.

(a)　　　　　　　　(b)　　　　　　　　(c)

(d)　　　　　　　　(e)　　　　　　　　(f)

(g)　　　　　　　　(h)　　　　　　　　(i)
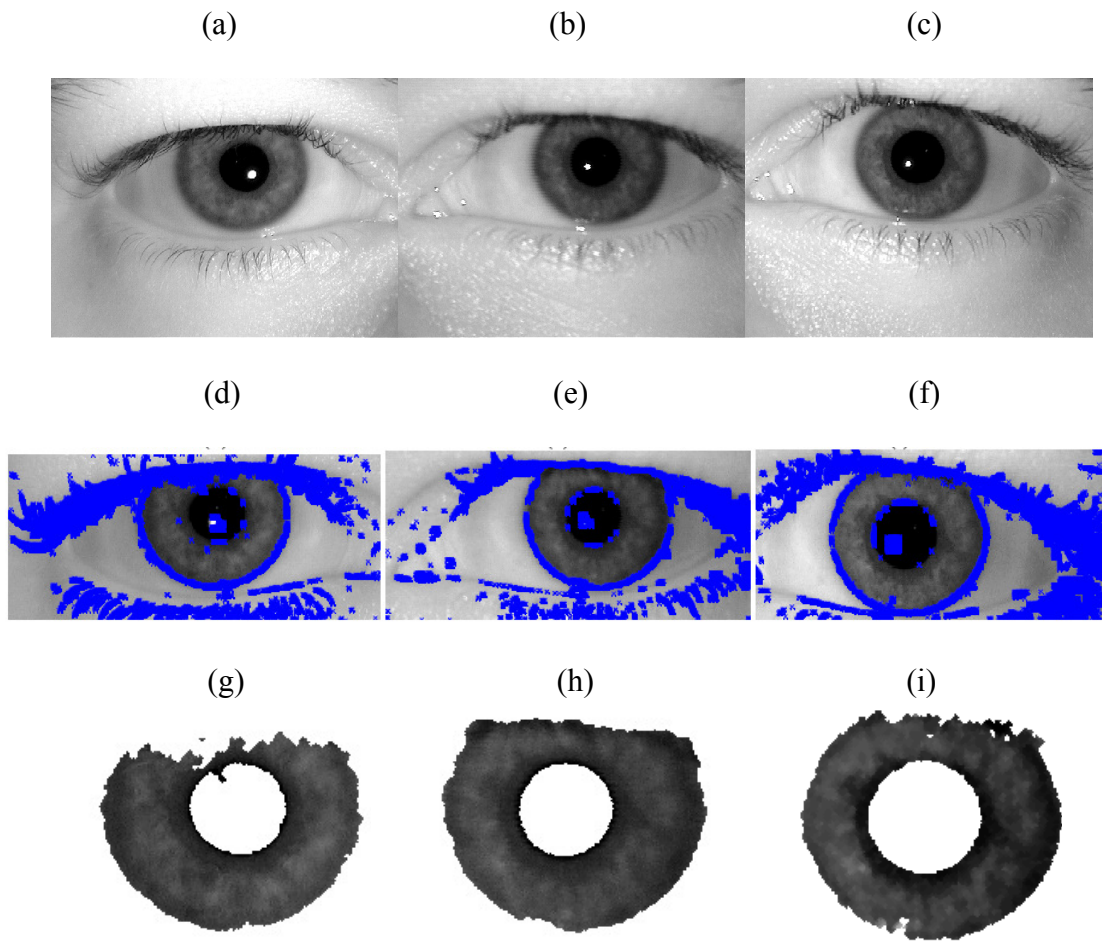
Figure 4.16: Eyelash detection and iris segmentation examples: (a, b, c) Original eye images, (d, e, f) Computed candidate eyelash points using our algorithm, (g, h, i) Accurate segmentation of the iris regions without eyelash occlusions.
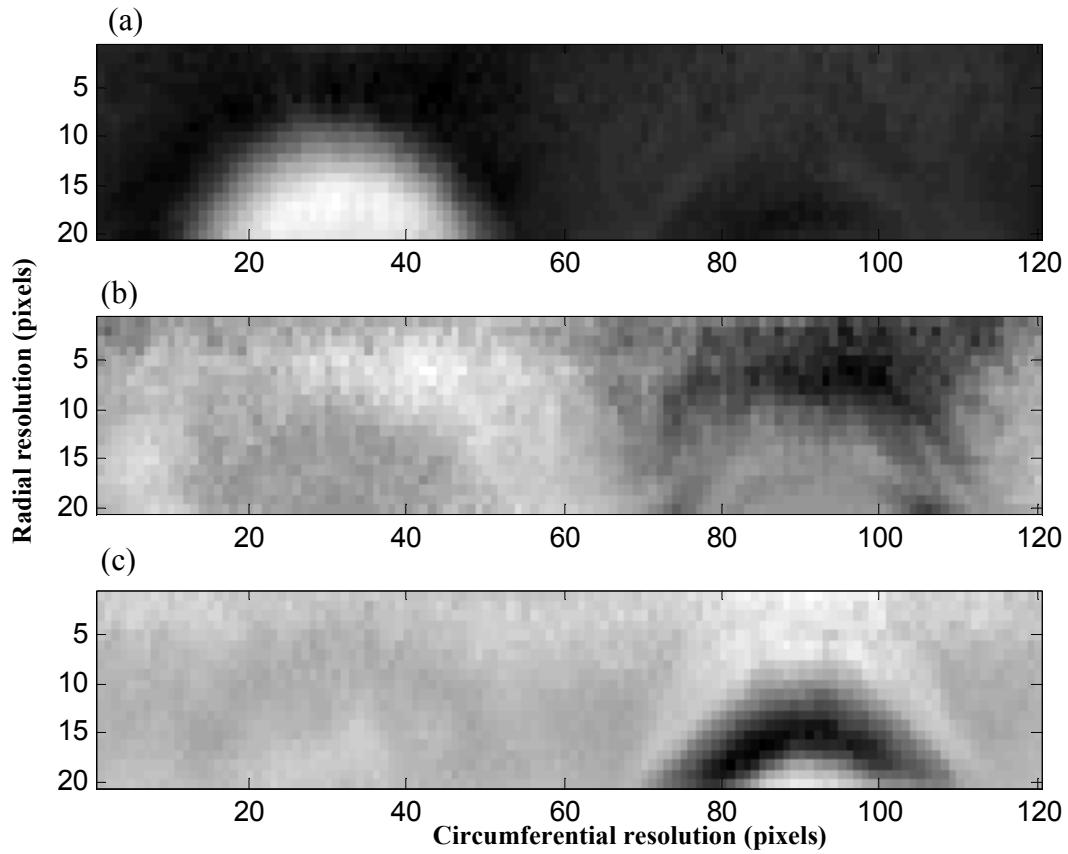
Figure 4.17: Normalized iris images in the polar space. (a) shows a normalized iris region without eyelash detection, (b) shows the result of iris normalization using the Masek's algorithm and (c) represents normalization using the enhanced segmentation algorithm. The y-axis represents the radial resolution and the x-axis corresponds to the circumferential (circular) resolution.

(a)

(b)
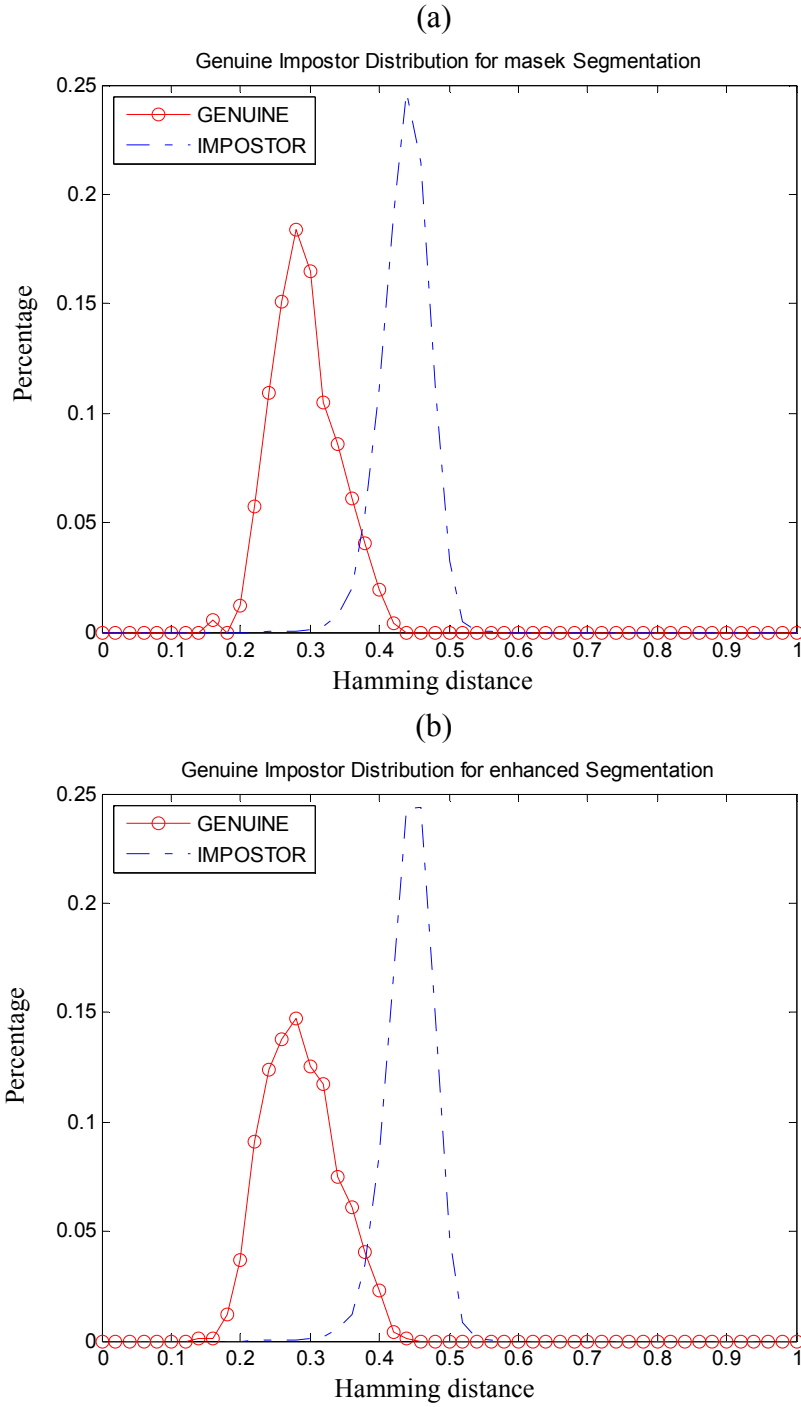
Figure 4.18: (a) Plot of the intra-class and inter-class distribution using the Masek's segmentation algorithm, (b) Genuine-impostor distributions using the enhanced segmentation algorithm.
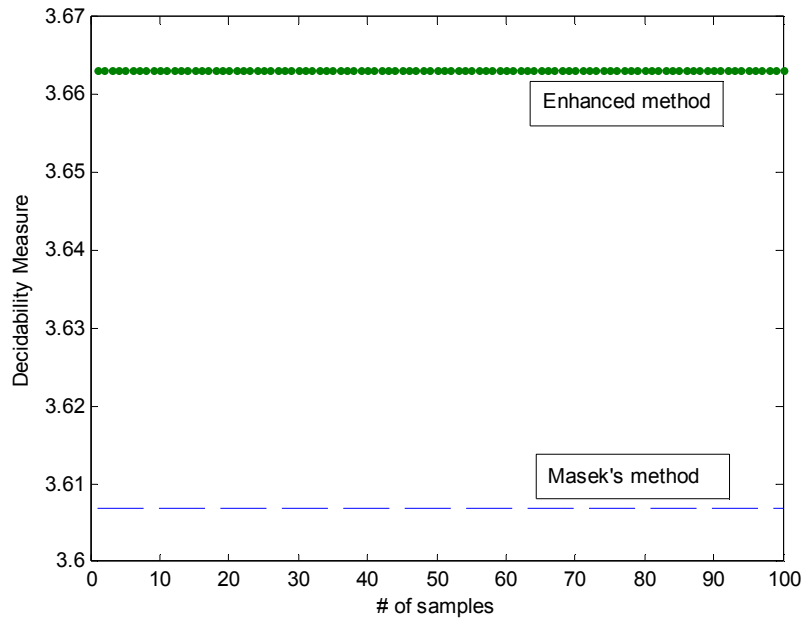
Figure 4.19: The decidability (d') measure showing a higher decidability measure for the enhanced algorithm.

(a)

(b)
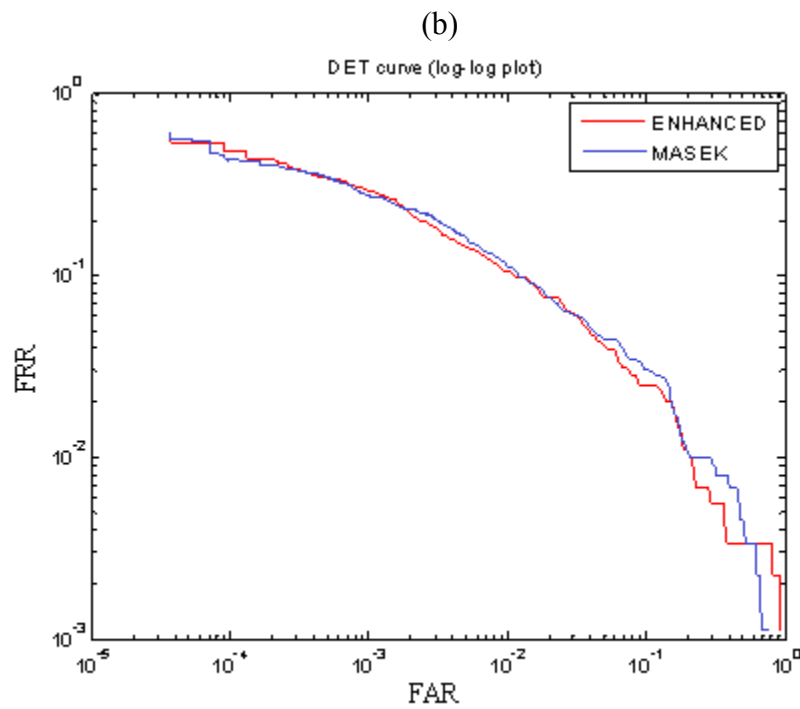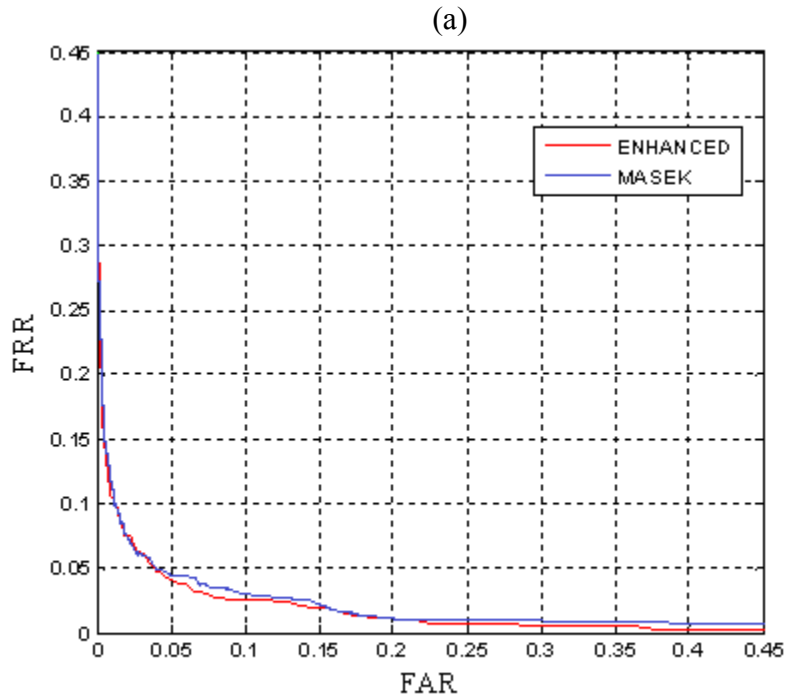
Figure 4.20: (a) DET curve and (b) log-log plot showing the FRR vs FAR for the Masek's and the enhanced segmentation methods, respectively. An incremental improvement is seen when using the enhanced segmentation technique which results in a smaller EER.

142
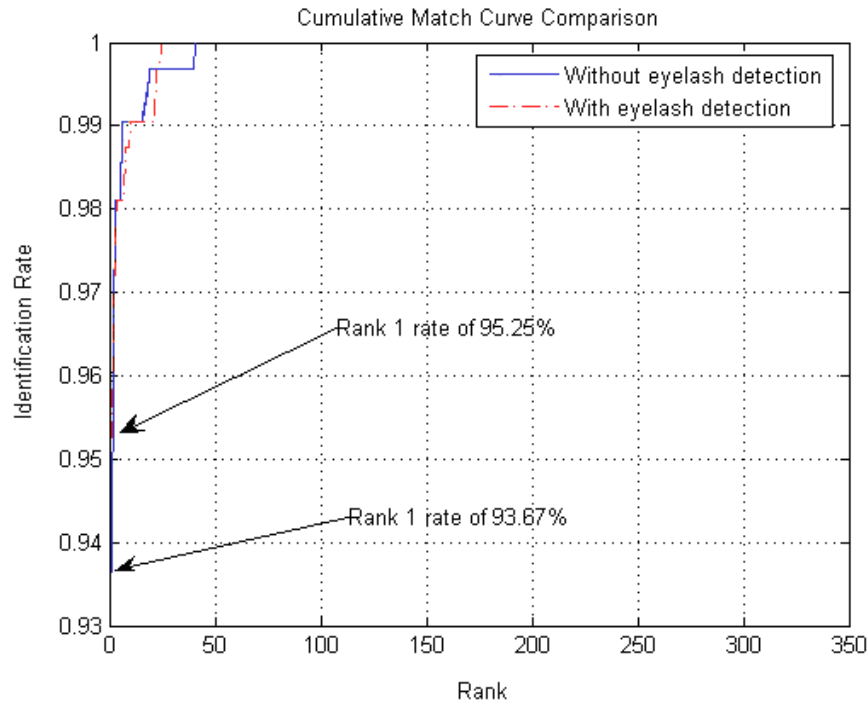
Figure 4.21: Cumulative Match Curve comparison. A 95.25% rank-1 identification rate is obtained using our proposed method while 93.67% is calculated using Masek's technique.

4.4 Discussion

The proposed algorithm shows promising results for eyelash noise detection, accurate iris boundary extraction and ideal iris segmentation. The results obtained using the enhanced algorithm do not show particularly large increases in performance compared to the existing iris segmentation schemes since the latter existing segmentation/identification algorithm is already extracting enough iris information to achieve high recognition rates. This explains the small increase in our enhanced identification rate but still shows an important improvement. The proposed algorithm locates the iris region using logarithmic image enhancement and the Hough transform techniques, locates the iris boundary, extracts the exact iris contour, detects eyelash based on the local image statistics and

block intensity and finally, proposes an iris model for accurate iris recognition. The developed method overcomes the limitations encountered in other iris segmentation and eyelash detection techniques such that our method detects accurately separable and multiple eyelashes, extracts the exact iris contour and is illumination invariant. In addition, the developed method does not overestimate the eyelash noise in the eye image, maximizing iris information. Using our technique, fewer iris noise and eyelash occlusions are found in the normalized iris region compared to the Masek approach. Also, the decidability metric is calculated for both methods in order to measure the separation between the intra-class and inter-class Hamming distance distributions. It is seen that a higher decidability measure is obtained for the enhanced algorithm which implies that the iris recognition system implementing the enhanced eyelash detection scheme tends to have a better intra and inter-class distribution separation. In addition, this will result in lower false accept rate and false reject rate since it is easier to select the decision threshold that provides a good genuine-impostor distribution separation. Furthermore, the match score using the enhanced technique is better within the entire comparison range since it uses the most of the iris region in the pattern matching process. Masek's code neglects some valid iris pixels since it overestimates eyelash occlusion and noise pixels. This will result in a loss of valid iris pixels which will probably decrease the system's performance.

4.5 Summary

This work proposes a new system for eyelash noise detection, accurate iris boundary extraction and ideal iris segmentation. The results obtained using the enhanced algorithm show incremental but important improvement in performance compared to the existing iris segmentation schemes. The proposed algorithm locates the iris region using logarithmic image enhancement and the Hough transform techniques, locates the iris boundary, extracts the exact iris contour, detects eyelash based on the local image statistics and block intensity and finally, proposes an iris model for accurate iris recognition. Using our technique, fewer iris noise and eyelash occlusions are found in the normalized iris region compared to the Masek approach. In addition, a higher decidability measure is obtained for the enhanced algorithm which implies that the iris recognition system implementing the enhanced eyelash detection scheme tends to have a better genuine-impostor distributions separation. Finally, it is also shown that the rank-1 identification rate improved from 93.67% (Masek) to 95.25% (enhanced method) as illustrated in the cumulative match curve in Figure 4.21.

Chapter 5

Measuring Information Content in Biometric Features

5.1 Introduction

How much information is there in a face, or a fingerprint? This question is related to many issues in biometric technology. For example, one of the most common biometric questions is that of uniqueness, e.g. to what extent are fingerprints unique? From the point of view of identifiability, one may be interested in how much identifying information is available from a given technology, such as video surveillance. In the context of biometric fusion (Ross *et al.* (2003)) one would like to be able to quantify the biometric information in each system individually, and the potential gain from fusing the systems. Additionally, such a measure is relevant to biometric cryptosystems and privacy measures. Several authors have presented approaches relevant to this question. For example, Wayman (2004) introduced a set of statistical approaches to measure the separability of Gaussian feature distributions using a "cotton ball model". Another approach is developed by (Daugman (2003)) to measure the information content of iris images based on the discrimination entropy (Cover *et al.*(1991)), which is calculated directly from the match score distributions. Also, Golfarelli *et al.* (1997) showed that the most commonly used feature representations of hand geometry and face biometrics have a limited number of distinguishable patterns, on the order of 105 and 103, respectively, as

measured by a theoretical estimate of the equal error rate. In this work, we elaborate an approach to address this question based on definitions from information theory. We define the term "biometric information" as follows:

Biometric information (BI): the decrease in uncertainty about the identity of a person due to a set of biometric features measurements.

In order to interpret this definition, we refer to two instants: 1) before a biometric measurement, t_0, at which time we only know a person p is part of a population q, which may be the whole planet; and 2) after receiving a set of measurements, t_1, we have more information and less uncertainty about the person's identity. BI may be used to answer two different types of questions. First, given a set of measurements from a specific person, we want to know how identifiable that individual is in a population. This is the individual biometric information (IBI). Second, given a system which makes biometric measurements, such as fingerprint minutiae or eigenfaces, we want to know, on average, how distinguishable people are in the population, using those biometric features. This is the system biometric information (SBI). The difference is that IBI is the information of an individual's features and SBI is the average information over the population. In order to motivate our approach, we initially consider the properties that such a measure should have. Consider a soft biometric system which measures height and weight; furthermore, assume all humans are uniformly and independently distributed in height between 100-200 cm and weight between 100-200 lb. If a person's features were completely stable and could be measured with infinite accuracy, people could be uniquely identified from these

measurements, and the biometric features could be considered to yield infinite information. However, in reality, repeated biometric measurements give different results due to measurement inaccuracies and to short- and long-term changes in the biometric features themselves. If this variability results in an uncertainty of ± 5 cm and ±5 lb, one simple model would be to round each measure to 105, 115, ..., 195. In this case, there are 10×10 equiprobable outcomes, and an information content of $log_2(100) = 6.6 bits$. Such an analysis is intrinsically tied to a choice of biometric features. Thus, our approach does not allow us to answer "how much information is in a fingerprint?", but only "how much information is in the position and angle data of fingerprint minutiae?". Furthermore, for many biometrics, it is not clear what the underlying features are. Face images, for example, can be described by image basis features or landmark based features (Zhao *et al.* (2003)). To overcome this, we may choose to calculate the information in all possible features. For example, we may provide height in inches as well as cm; however, in this case, a good measure of information must not increase with such redundant data.

This work also develops a new approach to measuring Biometric image quality. Biometric sample quality is a measure of the usefulness of a biometric image (ISO JTC1 SC37 (2007)). One recent development is the significant level of interest in standards for measurement of biometric quality. For example, ISO has recently established a biometric sample quality draft standard (ISO JTC1 SC37 (2007)). According to (ISO JTC1 SC37 (2007)), biometric sample quality may be considered from the point of view of character (inherent features), fidelity (accuracy of features), or utility (predicted biometrics performance). A general consensus has developed that the most important measure of a quality metric is its utility – images evaluated as higher quality must be those that result

in better identification of individuals, as measured by an increased separation of genuine and impostor match score distributions. The nature of biometric sample fidelity has seen little investigation, although for specific biometric modalities, algorithms to measure biometric quality have been proposed. For example, the NFIQ algorithm (Tabassi *et al.* (2004)) is a widely used measure for fingerprint image quality.

One current difficulty is that there is no consensus as to what a measure of biometric sample fidelity should give. In this work, we propose a new approach to measure this quantity, based on an information theoretic framework. We begin with the intuitive observation that a high quality biometric image is more useful to identify the individual than a low quality image. This suggests that the quantity of identifiable information decreases with a reduction in quality. Given a way to measure the decrease in information caused by a given image degradation, one can measure the associated decrease in biometric information. In this chapter, we develop a mathematical framework to measure biometric feature information in a given system for a set of biometric features. We address ill-conditioning in the measurements using distribution modeling and regularization. We then use this algorithm to analyze the biometric information content of two different face recognition algorithms and then define the information loss due to degradation in image quality.

In addition, this chapter presents a new method to calculate the iris biometric feature information using the system described in section (2.8) and the relative entropy measure. The developed algorithm is divided into the following sections: i. distribution modeling of iris biometric features, ii. relative entropy calculations, iii. ICA iris feature extraction and biometric information calculation. The iris regions used in the entropy calculation are

obtained using the Masek and the enhanced iris segmentation techniques described in section (4.2).

5.2 Theoretical framework

In this section we develop an algorithm to calculate biometric information based on a set of features, using the relative entropy measure (Cover *et al.* 1991). We then measure the effect of an image degradation model on biometric image quality. We explain our method in the following steps: 1) measure requirements, 2) relative entropy of biometric features, 3) Gaussian models for biometric features and relative entropy calculations, 4) regularization methods for degenerate features, 5) regularization methods for insufficient data, 6) information loss due to degradation.

5.2.1 Requirements for biometric feature information

In order to elaborate the requirements that a good measure of biometric feature information must have, we consider the system that measures height and weight. These values differ within the global population, but also vary for a given individual, both due to variations in the features themselves and to measurement inaccuracies. We now wish to consider the properties a measure of biometric feature information should have:

1. If an intra-person distribution p is exactly equal to the inter-person q distribution, then there is no information to distinguish a person, and biometric feature information is zero.

2. As the feature measurement becomes more accurate (less variability), then it is easier to distinguish someone in the population and the biometric information increases.

3. If a person has unusual feature values (i.e. far from the population mean), they become more distinguishable, and their biometric feature information will be larger.

4. The biometric information of uncorrelated features should be the sum of the biometric information of each individual feature.

5. Features that are unrelated to identity should not increase biometric information. For example, if a biometric system accurately measured the direction a person was facing, information on identity would be unchanged.

6. Correlated features such as height and weight are less informative. In an extreme example consider the height in inches and in cm. Clearly, these two features are no more informative than a single value (except perhaps a reduction in noise from the averaging of repeated measurements).

Based on this definition, the most appropriate information theoretic measure for the biometric feature information is the relative entropy ($D(p\|q)$) (Cover *et al.* (1991)) between the intra- ($p(\mathbf{x})$) and inter-person ($q(\mathbf{x})$) biometric feature distributions. $D(p\|q)$, or the Kullback-Leibler distance, is defined as the measure of the information gain in moving from a prior distribution $q(\mathbf{x})$ to a posterior distribution $p(\mathbf{x})$, or to be the "extra bits" of information needed to represent $p(\mathbf{x})$ with respect to $q(\mathbf{x})$. $D(p\|q)$ is defined to be

$$D(p\|q) = \int\limits_{\mathbf{x}} p(\mathbf{x}) log_2 \frac{p(\mathbf{x})}{q(\mathbf{x})} d\mathbf{x} \qquad (5.1)$$

where the integral is over all feature dimensions, $\mathbf{x}$. $p(\mathbf{x})$ is the probability mass function or distribution of features of an individual and $q(\mathbf{x})$ is the overall population distribution. A comment on notation: we use p to refer to both an individual person, and the distribution of the person's features, while q represents the population and the distribution of its features. This measure can be motivated as follows: the relative entropy, $D(p\|q)$, is the extra information required to describe a distribution $p(\mathbf{x})$ based on an assumed distribution $q(\mathbf{x})$ (Cover *et al.* (1991)). $D(p\|q)$ differs from the entropy, $H(p)$, which is the information required, on average, to describe features $\mathbf{x}$ distributed as $p(\mathbf{x})$. H is not in itself an appropriate measure for biometric feature information, since it does not account for the extent to which each feature can identify a person p in a population q. An example of a feature unrelated to identity is the direction a person is facing. Measuring this quantity will increase H of a feature set, but not increase its ability to identify a person. The measure $D(p\|q)$ corresponds to the requirements: given knowledge of the population feature distribution q, the information in a biometric feature set allows us to describe a particular person p.

5.2.2 Distribution modeling

In a generic biometric system, S biometric features are measured, to create a biometric feature vector $\mathbf{x}$ $(S \times 1)$ for each person. For person p, we have N_p features samples,

while we have N_q samples for the population. For convenience of notation, we sort p's measurements to be the first grouping of the population. Defining **x** as an instance of random variable X, we calculate the population feature mean μ_q

$$\mu_q = \underset{q}{E}[X] = \frac{1}{N_q} \sum_{i=1}^{N_q} \mathbf{x}_i \qquad (5.2)$$

where the feature mean of person p, μ_p, is defined analogously, replacing q by p. The population feature covariance Σ_q is

$$\Sigma_q = \underset{q}{E}\left[(X - \mu_q)^t(X - \mu_q)\right] = \frac{1}{N_q - 1} \sum_{i=1}^{N_q} (\mathbf{x}_i - \mu_q)^t(\mathbf{x}_i - \mu_q) \qquad (5.3)$$

The individuals feature covariance,Σ_p, is again defined analogously. One important general difficulty with direct information theoretic measures is that of data availability. Distributions are difficult to estimate accurately, especially at the tails; and yet $log_2\left(p(\mathbf{x})/q(\mathbf{x})\right)$ will give large absolute values for small $p(\mathbf{x})$ or $q(\mathbf{x})$. Instead, it is typical to fit data to a model with a small number of parameters. The Gaussian distribution is the most common model; it is often a good reflection of the real world distributions, and is analytically convenient in entropy integrals. Another important property of the Gaussian is that it gives the maximum entropy for a given standard deviation, allowing such models to be used to give an upper bound to entropy values. Based on the Gaussian model, which seems to be the simplest and appropriate for p and q, we write:

$$p(\mathbf{x}) = \frac{1}{\sqrt{|2\pi\Sigma_p|}} exp\left(-\frac{1}{2} \left(\mathbf{x} - \mu_p \right)^t \Sigma_p^{-1} \left(\mathbf{x} - \mu_p \right) \right) \tag{5.4}$$

$$q(\mathbf{x}) = \frac{1}{\sqrt{|2\pi\Sigma_q|}} exp\left(-\frac{1}{2} \left(\mathbf{x} - \mu_q \right)^t \Sigma_q^{-1} \left(\mathbf{x} - \mu_q \right) \right) \tag{5.5}$$

From which we can calculate $D(p\|q)$ as:

$$D(p\|q) = \int p(\mathbf{x}) \left(log_2 p(\mathbf{x}) - log_2 q(\mathbf{x}) \right) d\mathbf{x}$$

$$= -k \left(ln|2\pi\Sigma_p| - ln|2\pi\Sigma_q| + 1 - \underset{p}{E} \left[\left(\mathbf{x} - \mu_q \right)^t \Sigma_q^{-1} \left(\mathbf{x} - \mu_q \right) \right] \right) \tag{5.6}$$

$$= k \left(ln\frac{|2\pi\Sigma_q|}{|2\pi\Sigma_p|} + trace\left((\Sigma_p + \mathbf{T})\Sigma_q^{-1} - \mathbf{I} \right) \right)$$

where $\mathbf{T} = (\mu_p - \mu_q)^t(\mu_p - \mu_q)$ and $k = log_2\sqrt{e}$.

This expression calculates the relative entropy in bits for Gaussian distributions $p(\mathbf{x})$ and $q(\mathbf{x})$. This expression corresponds to most of the desired requirements for a biometric feature information measure introduced in the previous section:

1. If person's feature distribution matches the population, $p = q$; this yields $D(p\|q) = 0$, as required.

2. As feature measurements improve, the covariance values, Σ_p, will decrease, resulting in a reduction in $|\Sigma_p|$, and an increase in $D(p\|q)$.

3. If a person has feature values far from the population mean, $\mathbf{T}$ will be larger, resulting in an larger value of $D(p\|q)$.

4. Combinations of uncorrelated feature vectors yield the sum of the individual $D(p\|q)$ measures. Thus, for uncorrelated features s_1 and s_2, where $\{s_1, s_2\}$ represents concatenation of the feature vectors,

$$D(p(s_1)\|q(s_1)) + D(p(s_2)\|q(s_2)) = D(p(\{s_1, s_2\})\|q(\{s_1, s_2\}))$$

5. Addition of features uncorrelated to identity will not change $D(p\|q)$. Such a feature will have an identical distribution in p and q. If U is the set of such uncorrelated features, $[\Sigma_p]_{ij} = [\Sigma_q]_{ij} = 0$ for i or $j \in U$ and $i \neq j$ while $[\Sigma_p]_{ii} = [\Sigma_q]_{ii}$ and $[\mu_q]_i = [\mu_p]_i$. Under these conditions, $D(p\|q)$ will be identical to its value when excluding the features in U. One way to understand this criterion is that if the distributions for q and p differ for features in U, then those features can be used as a biometric to help identify a person.

6. Correlated features are less informative than uncorrelated ones. Such features will decrease the condition number (and thus the determinant) of both Σ_p and Σ_q. This will decrease the accuracy of the measure $D(p\|q)$. In the extreme case of perfectly correlated features, Σ_p becomes singular with a zero determinant and $D(p\|q)$ is undefined. Thus, our measure is inadequate in this case.

In the next section, we develop an algorithm to deal with this effect.

5.2.3 Regularization Methods for degenerate features

In order to guard against numerical instability in our measures, we wish to extract a mutually independent set of W "important" features ($W \leq S$). To do this, we use the principal component analysis (PCA) (Draper *et al.*(2003)) (Grother (2000)) to generate a mapping ($\mathbf{U}^t : X \rightarrow Y$), from the original biometric features $X(S \times 1)$ to a new feature space Y of size $W \times 1$. The PCA may be calculated from a Singular Value Decomposition (SVD) (Alter *et al.* (2000)) of the feature covariance matrix, such that

$$\mathbf{U}\mathbf{S}_q\mathbf{U}^t = svd(cov(X)) = svd(\Sigma_q)$$

Since Σ_q is positive definite, $\mathbf{U}$ is orthonormal and $\mathbf{S}_q$ is diagonal. We choose to perform the PCA on the population distribution q, rather than p, since q is based on far more data, and is therefore likely to be a more reliable estimate. The values of $\mathbf{S}_q$ indicate the significance of each feature in PCA space. A feature j, with small $[\mathbf{S}_q]_{j,j}$ will have very little effect on the overall biometric feature information. We use this analysis, in order to regularize Σ_q, and to reject degenerate features by truncating the SVD. We select a truncation threshold of j where $[\mathbf{S}_q]_{j,j} < 10^{-10}[\mathbf{S}_q]_{1,1}$. Based on this threshold, $\mathbf{S}_q$ is truncated to be $W \times W$, and $\mathbf{U}$ is truncated to $S \times W$. Using the basis $\mathbf{U}$ calculated from the population, we decompose the individual's covariance into feature space Y:

$$\mathbf{S}_p = \mathbf{U}^t\Sigma_p\mathbf{U} \tag{5.7}$$

where $\mathbf{S}_p$ is not necessarily a diagonal matrix. However, since p and q describe somewhat similar data, we expect $\mathbf{S}_p$ to have a strong diagonal component comparable to $\mathbf{S}_q$, as seen in Figure 5.4.

Based on this regularization scheme, equation (5.6) may be rewritten in the PCA space as:

$$D(p\|q) = k \left(\beta + trace \; \mathbf{U} \left((\mathbf{S}_p + \mathbf{S}_t) \mathbf{S}_q^{-1} - \mathbf{I} \right) \mathbf{U}^t \right) \tag{5.8}$$

where $\beta = ln \frac{|\mathbf{S}_q|}{|\mathbf{S}_p|}$ and $\mathbf{S}_t = \mathbf{U}^t \mathbf{T} \mathbf{U}$

5.2.4 Regularization Methods for insufficient data

The expression developed in the previous section solves the ill-posed nature of Σ_q. However, Σ_p may still be singular in the common circumstance in which only a small number of samples of each individual are available. Given N_p images of an individual from which W features are calculated, Σ_p will be singular if $W \geq N_p$, which will result in $D(p\|q)$ diverging to ∞. In practice, this is a common occurrence, since most biometric systems calculate many hundreds of features, and most biometric databases contain far less samples for each person. In order to address this issue, we develop an estimate which may act as a lower bound. In order to do this, we make the following assumptions:

1. Estimates of feature variances are valid $[\mathbf{S}_p]_{i,i}$ for all i.

2. Estimates of feature covariances $[\mathbf{S}_p]_{j,j}$ for $i \neq j$ are only valid for the most important L features, where $L < N_p$. Features which are not considered valid based on these assumptions, are set to zero by multiplying $\mathbf{S}_q$ by a mask M, where

$$M = \begin{cases} 1, & \text{if } i = j \text{ or } (i < L \text{ and } j < L); \\ 0, & \text{otherwise} \end{cases} \tag{5.9}$$

This expression regularizes the intra-person covariance, Σ_p, and assures that $D(p\|q)$ does not diverge. To clarify the effect of this regularization on $D(p\|q)$, we note that intra-feature covariance will decrease $|\Sigma_p|$ toward zero, leading a differential entropy estimate diverging to ∞. We thus consider this regularization strategy to generate a lower bound on the biometric feature information. The selection of L is a compromise between using all available measurements (by using large L) and avoiding numerical instability when $\mathbf{S}_p$ is close to singular (by using small L).

5.2.5 Average information of a biometric system

This section has developed a measure of biometric feature information content of a biometric feature representation of a single individual with respect to the feature distribution of the population. As discussed, the biometric feature information will vary between people; those with feature values further from the mean have larger biometric feature information. In order to use this approach to measure the biometric feature information content of a biometric system, we calculate the average biometric feature information for each individual in the population (weighted by the probability of needing to identify that person, if appropriate). This is a measure of the system biometric information (SBI) which can be calculated by the average IBI over the population q.

$$SBI = \underset{q}{E}\left[D(p||q)\right]$$

$$= \frac{1}{2}log_2|\Sigma_q\Sigma_p^{-1}| + tr(\Sigma_p\Sigma_q^{-1} - I) + \underset{q}{E}[t^T\Sigma_q t]$$

$$= \frac{1}{2}log_2|\Sigma_q\Sigma_p^{-1}| + tr(\Sigma_p\Sigma_q^{-1})$$

$$(5.10)$$

5.2.6 Information loss due to degradation

In this section, we explore the effect of image degradation and the resulting decrease in biometric quality on the relative entropy measure. Intuitively, it is expected that image degradation changes the intra and inter person distribution of the face features resulting in a loss of biometric information. Given a degradation process, we wish to measure how much BI is lost in the degraded images, G, versus the original images, F. This allows us to measure the severity of a degradation process. Features g are then extracted from the degraded images G using three feature extraction methods given. We then compute the biometric information for the non-degraded distributions $(D(p(f)||q(f)))$ and for the degraded distributions $(D(p(g)||q(g)))$ using equation (5.8). Here $(D(p(f)||q(f)))$ represents the relative entropy between the individual and population distribution prior to degradation while $(D(p(g)||q(g)))$ is the relative entropy measure between the degraded individual and population distributions, respectively. From this, we calculate the normalized mean square distance characterizing the loss of information caused by the degradation model on the underlying features as:

$$\Delta BI = \frac{1}{N_f} \sum_{i=1}^{N_f} \frac{|D(p(f_i)||q(f_i)) - D(p(g_i)||q(g_i))|^2}{\sigma_{D_f}^2} \tag{5.11}$$

where $\sigma_{D_f}^2$ is the variance of $D(p(fi)||q(fi))$. ΔBI measures the relative distance offset between the original and degraded distributions. ΔBI is a unitless measure, and may be interpreted as the fractional loss in BI due to a given image degradation. In order to motivate this calculation, we initially considered calculating $D(p(g)||q(f))$ as a function of degradation. Surprisingly, this measure increases with decreasing quality. The reasoning behind this stems from the fact that when a person's (p) feature distribution is degraded and compared to a high quality population feature distribution, the algorithm seems to be saying: Aha! I can recognize p. He always has a blurry face!. Therefore, it is necessary to compare a degraded person's image to the degraded population $(D(p(g)||q(g)))$ in order to compensate for this effect.

5.3 Face recognition

Information in a feature representation of faces is calculated using our described method for different individuals. In order to test our algorithm, it is necessary to have multiple images of the same individual. Using the Aberdeen face database (Belhumeur *et al.* (1997)), we chose 18 frontal images of 16 persons, from which we calculate the PCA (eigenface) features using the algorithm of (Grother (2000)) and the FLD face features components using the algorithm described in (Xiang *et al.* (2004)). Initially, all face images were registered by rotation and scaling to have eye positions at $(50, 90)$ and

$(100, 90)$. Images were then cropped to 150×200 pixels and histogram equalized to cover the intensity range 0–255. The same set of operations is applied to all images using the same thresholds. This results with the same effect on all images when computing the biometric feature information. Features are calculated from a set of N_q images using different component analysis methods such as Principal Component Analysis (PCA, also referred to as Eigenface features) (Grother (2000)) (Turk & Pentland (1991)) and Fisher linear discriminant (FLD) (Li *et al.* (2005)). μ_p and μ_q are $S \times 1$ vectors of the population and individual mean distributions, while Σ_p and Σ_q are $S \times S$ matrices of the individual and population covariance matrices.

The feature decomposition process was conducted on 18 images of each of 16 persons, giving 288 total images. For PCA and Fisher feature decompositions, 288 separate vectors were computed, and the most significant 100 features per image used for subsequent analysis. Figure 5.1 and Figure 5.2 illustrate PCA and FLD features, respectively. From this, $D(p\|q)$ is computed for each of 16 persons using equation (5.8), which assumes that p and q have Gaussian distributions. In order to test the validity of the Gaussian model for our data, we use the following normality tests:

• Kolmogorov-Smirnov test: compares the distributions of values in the two data vectors X_1 and X_2, where X_1 represents random samples from the underlying distribution and X_2 follows an ideal Gaussian with zero mean and variance. The null hypothesis is that X_1 and X_2 are drawn from the same continuous normal distribution. We reject the null hypothesis at $\alpha = 0.01$.

• The Lilliefors test (Conover (1980)): evaluates the hypothesis that $\mathbf{x}$ has a normal distribution with unspecified mean and variance, against the alternative that $\mathbf{x}$ does not have a normal distribution. This test compares the empirical distribution of X with a normal distribution having the same mean and variance as X. We reject the null hypothesis at $\alpha = 0.01$.

Figure 5.1: An example of PCA (Eigenface) face features. From left to right, PCA features number 3, 15, 35, 55 are shown. The PCA features are othonormal and fit the data in a least squares sense.

Figure 5.2: An example of FLD face features. From left to right, FLD features number 7, 10, 30, 50 are shown. FLD attempts to maximize class separation while minimizing the within class scatter.

Using these tests, an average of 88% and 89% for the FLD and PCA features marginal distributions are normally distributed.

5.3.1 Biometric information calculations

After fitting the distributions of $p(\mathbf{x})$ and $q(\mathbf{x})$ to a Gaussian model, we initially analyze the biometric feature information in each PCA and FLD feature separately. PCA features are shown in Figure 5.3, and show a gradual decrease from an initial peak at feature 2. The form of the curve can be understood from the nature of the PCA decomposition, which tends to place higher frequency details in higher number features. Since noise tends to increase with frequency, the biometric information in these higher numbered PCA features will be less. A sum of biometric feature information over the first 100 PCA features for one individual gives 40.5 bits. This does not assume statistical independence nor uncorrelatedness of PCA coefficients. Biometric feature information calculated using FLD features seems to be similar to PCA features such that most biometric feature information is computed for the most dominant fisherfaces. In order to calculate $D(p\|q)$ for all features, we are limited by the available information. Since $N_p = 18$ images are used to calculate the covariances, attempts to calculate $D(p\|q)$ for more than 17 features will fail, because Σ_p is singular. This effect is seen in the condition number (ratio of the largest to the smallest singular value) which was 4.82×10^3 for $\mathbf{S}_q$ and 1.32×10^{20} for $\mathbf{S}_p$. The relatively small condition number of $\mathbf{S}_q$ indicates that no features are degenerate for PCA and FLD face recognition features. However, $\mathbf{S}_p$ is severely ill-conditioned. To overcome this ill-conditioning, we introduced a regularization scheme based on a mask (equation 5.9) with a cut-off point L. This scheme is motivated by the diagonal structure of $\mathbf{S}_p$, as shown in Figure 5.4. To ensure convergence, the mask size L is set to a value smaller than N_p.

We solve this singularity of equation (5.8) using a mask for $\mathbf{S}_p$ based on a parameter L. To further explore the effect of parameters L and N_p, we artificially reduce the N_p by randomly eliminating some images from individuals. Results for $D(p\|q)$ for PCA features for each person as a function of L are shown in Figure 5.5 for $N_p = 8, 12, 16$ and 18. In these curves, we observe a "hockey stick" shape. The relative entropy measure remains stable when $L < N_p$, but if $L \geq N_p$, we observe a dramatic increase in $D(p\|q)$ as the algorithm approaches a singularity of Σ_p and the ill-conditioning of Σ_q. $L < N_p$, $D(p\|q)$ is stable with a lower and upper bounds between 35 to 50 bits. However, when $L \geq N_p$, $D(p\|q)$ estimates start diverging and reach very large values. Clearly, points for L greater than the knee in the hockey stick do not represent accurate estimates of $D(p\|q)$. We also argue that when L approaches N_p, the inherent ill-conditioning of Σ_p makes the our algorithm over-estimate $D(p\|q)$. On the other hand, small values of L will under-estimate $D(p\|q)$, since these values will mask inter-feature correlations. This effect increases $|\mathbf{S}_p|$ as L decreases. However, the results suggest that this effect is minor, especially in Figure 5.5a and Figure 5.5b, where the "base" of the hockey stick is more flat. In order to produce an unique and stable estimate for $D(p\|q)$, it is necessary to choose a compromise between these effects. We recommend choosing $L = \frac{3}{4}N_p$, since a larger value of L puts the estimate in an unstable region of Figure 5.4. Using this algorithm and value of L, we calculate the overall biometric feature information for different face recognition algorithms. For PCA features, the average $D(p\|q)$ is 45.0 bits, and for FLD features $D(p\|q)$ is 37.0 bits. If PCA and FLD features are combined (making 200 features in all), average $D(p\|q)$ is 55.6 bits (Figure 5.6). This combination

of features illustrates that a biometric fusion of similar features may offer very little information above that of the individual underlying features. It is initially somewhat surprising that FLD feature information is measured to be lower than that from PCA. This result may be understood because PCA features retain unwanted information due to variations in facial expression and lighting, which are measured to contain useful information, while FLD "projects away" variations in lighting and facial expression while maintaining the discriminant features. In order to understand the difference in the discriminating effect between PCA and FLD features, the DET curves (Figure 5.7) showing the FRR as a function of FAR are shown for PCA, FLD and PCA+FLD features, respectively. Results show a smaller EER is obtained by fusing PCA and FLD features. This effect is consistent with the calculation of the highest BI (55.6 bits) compared to PCA (45.0 bits) and FLD (37.0 bits) in Figure 5.6. Similarly, better system performance was obtained when using PCA features compared to FLD which is also seen in the DET curves plot of Figure 5.7. Therefore, the increase in BI calculation for a specific set of features is reflected in a DET curve as a relative decrease in the EER. Higher biometric feature information indicates that the feature set used in the biometrics system under test contains additional discriminating information which should reduce the FAR and FRR which is shown in Figure 5.7.

Moreover, feature decomposition using independent component analysis (ICA) (Golfarelli *et al.* (1997)) was also conducted on the same set of faces. ICA has the advantage that it does not only decorrelate the signals but also reduces higher-order statistical dependencies in order to make the signals as statistically independent as possible (Lee (1999)). Since ICA maximizes non-Gaussianity, it fits less well to the

assumptions of our model. For ICA features, an average of 39.0 bits was computed for $D(p\|q)$.
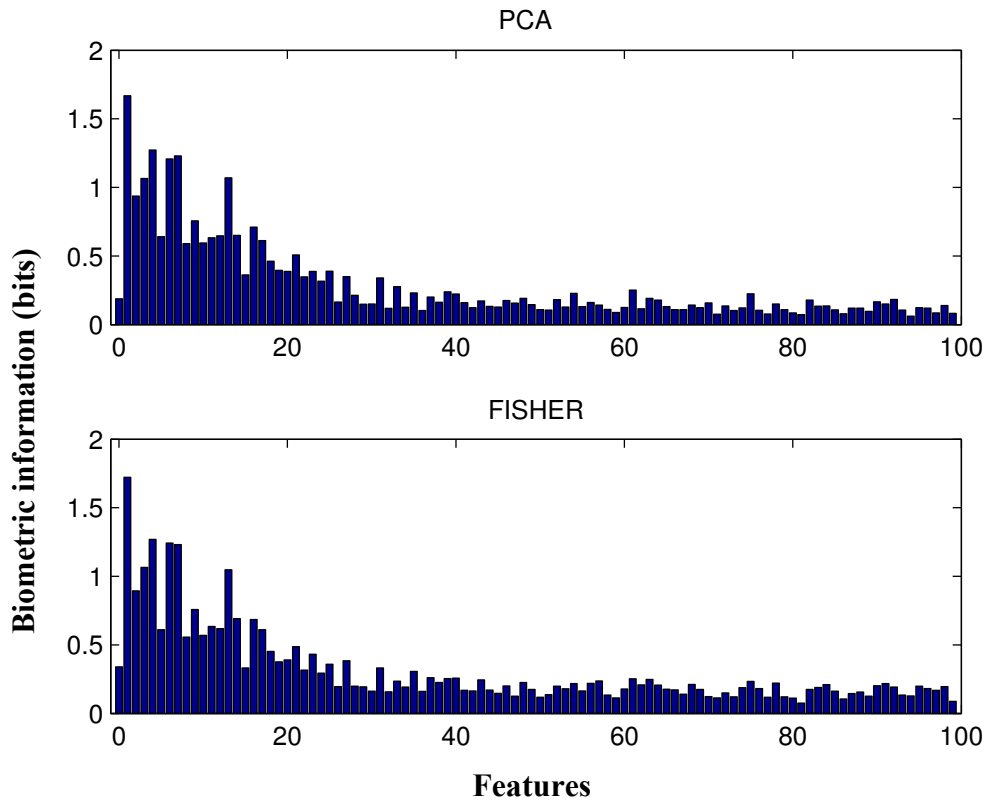
Figure 5.3: Biometric information (bits) as a function of number of features for (A) PCA (Eigenface) and (B) FLD (bottom) face feature decomposition.

Figure 5.4: The regularized intra-person covariance matrix Sp showing dominant components along its diagonal. Since Σp represents similar information to Σq it is reasonable to expect the matrices have similar eigenvectors, resulting in strong diagonal components in Σp.
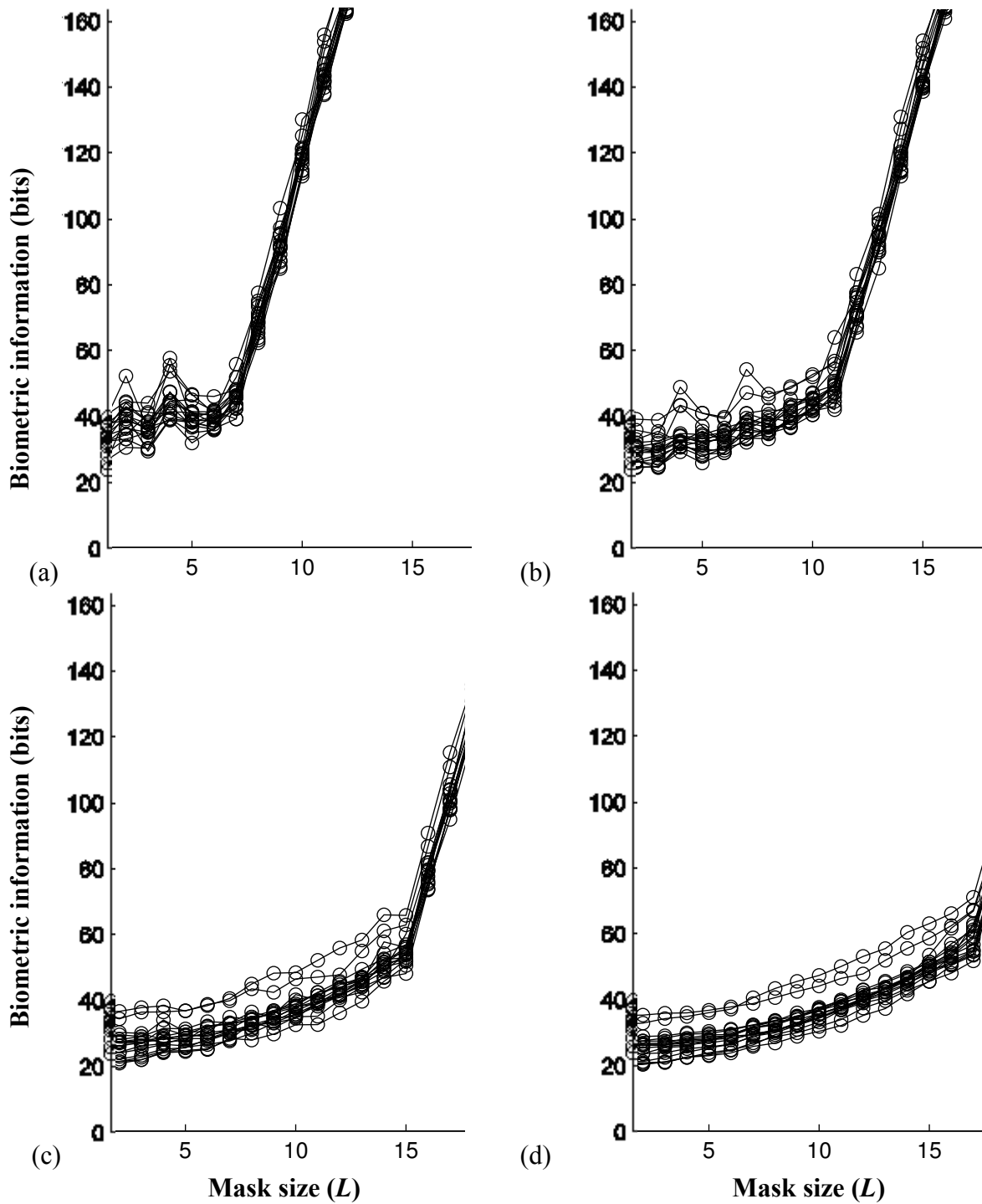
Figure 5.5: Biometric information (in bits) (y-axis) vs. the mask size (L) (x-axis) for each person. Each subfigure represents a different value of Np (images of the same person): (A) 8, (B) 12, (C) 16 and (D) 18. The curves show that $D(p\|q)$ diverges as Σ_p becomes singular ($L \geq$ Np). The relative entropy increases with the size of the mask.
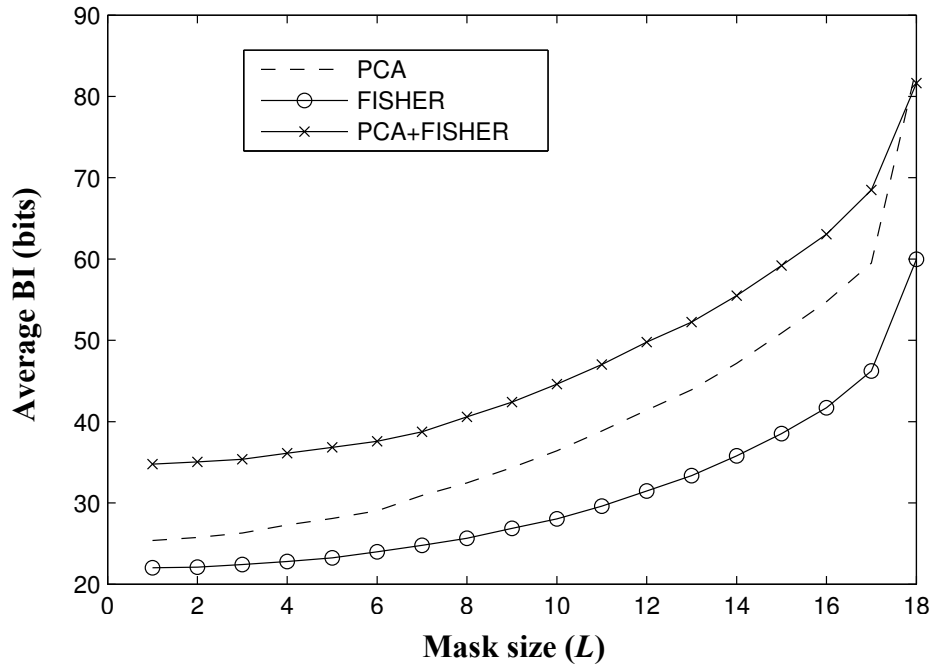
Figure 5.6: Average $D(p\|q)$ vs L (x-axis) for Np = 18. Each line represents the average of information calculated for a population of 16 individuals with 18 images each using PCA (middle), FLD (bottom) and a fusion of PCA and FLD features (top).
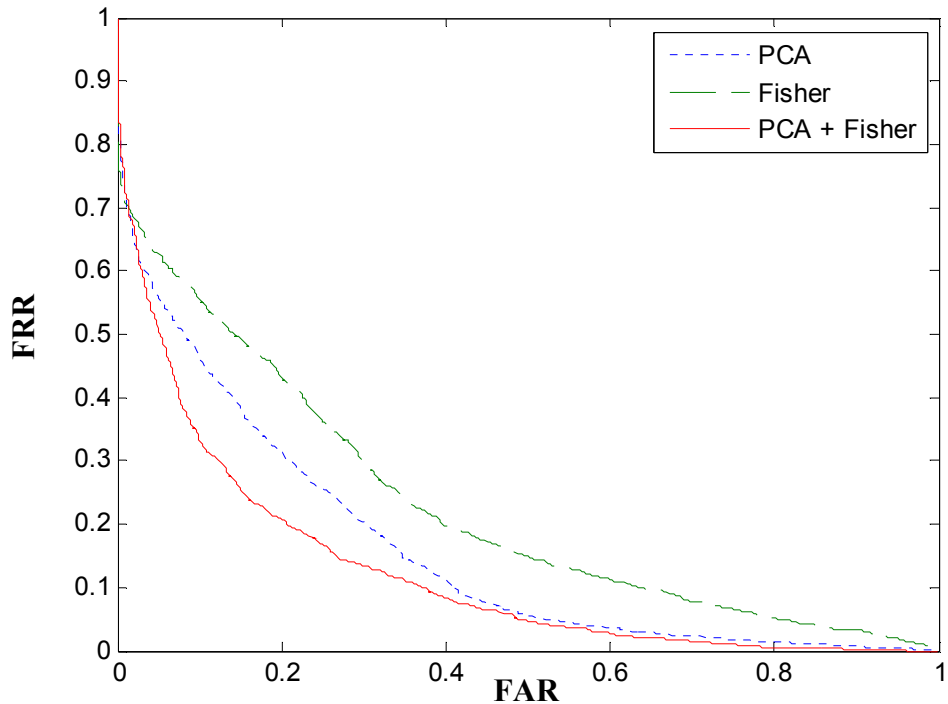
Figure 5.7: DET curves showing the FRR vs FAR for PCA, Fisher and fusion of PCA, and Fisher features, respectively. The relatively large error rates are a consequence of the use of a particularly difficult database, and the fact that the choice of difference metric is not a high performance face recognition algorithm. The purpose of this comparison is to show the effect of features fusion and classification on the EER for a specific system.

5.3.2 Degraded features

In this section, BI is computed for degraded features and information loss measured with respect to the original image. Equation (5.12) represents the blur degradation model used to generate degraded features where h is a space invariant Gaussian operator of size $n \times n$ and $\sigma = 3$, F is the original image and G is the resulting degraded image.

$$G(x, y) = \sum_{\alpha} \sum_{\beta} F(\alpha, \beta) h(x - \alpha, y - \beta) \qquad (5.12)$$

Using the degradation model described by equation (5.12), two different sets of images (φ_1 and φ_2) are generated. Each set of images is composed of 16 people with 18 images per individual for a total of 288. φ_1 is obtained by degrading half of each individuals face using different Gaussian operators while φ_2 is a set of images obtained as a result of blurring the entire face region. An example of images in φ_1 and φ_2 are seen in Figure 5.8. Using φ_1 and φ_2, new PCA, FLD and ICA features (g) are extracted using the original (non-degraded) principal component vectors. From the degraded features, ΔBI is computed for the degraded individual and population distributions using equation (5.11). This measure represents the amount of information lost as a function of the degradation level. Figure 5.9 shows ΔBI computed as function of the blur level for different images taken from φ_1 and φ_2. The x-axis represents 9 different levels (in increasing order) of Gaussian blur. As seen in Figure 5.9, the relative information loss in an image increases with the amount of system degradation. Interestingly, ΔBI tends to reach a steady state after some level of degradation (Figure 5.9b). This suggests that some features are

unaffected by the degradation process and represent a lower bound of information measure of an individual distribution. PCA features extracted using the most dominant eigenvalues of the system tend to be more robust against blur since they preserve valuable information at a large degradation level. It is important to note that in Figure 5.8b, ICA seems to be me robust to blur which is not a true representation of the actual information loss due to degradation at higher blur level. The reason behind this is the fact that ICA isn't a good scheme to use on Gaussian data such as the ones developed in this work since ICA maximizes non-Gaussianity and prefers fine features. Hence, this explains the unusual robustness of ICA against degradation at higher blur levels (Figure 5.9b).

(a)   (b)   (c)
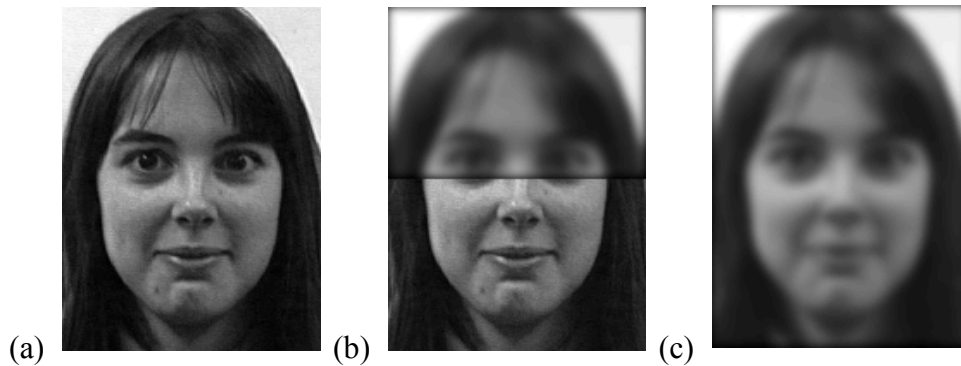
Figure 5.8: Degraded image obtained by applying a Gaussian blur to (b) a section of the original image (φ_1) and to (c) the entire image (φ_2).

(a)

(b)
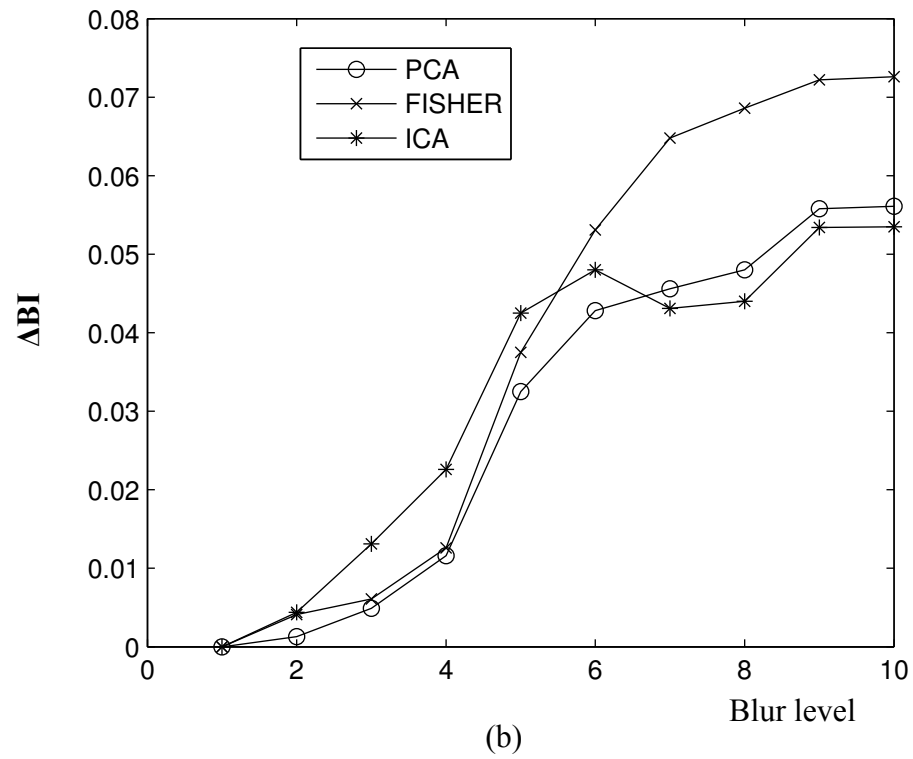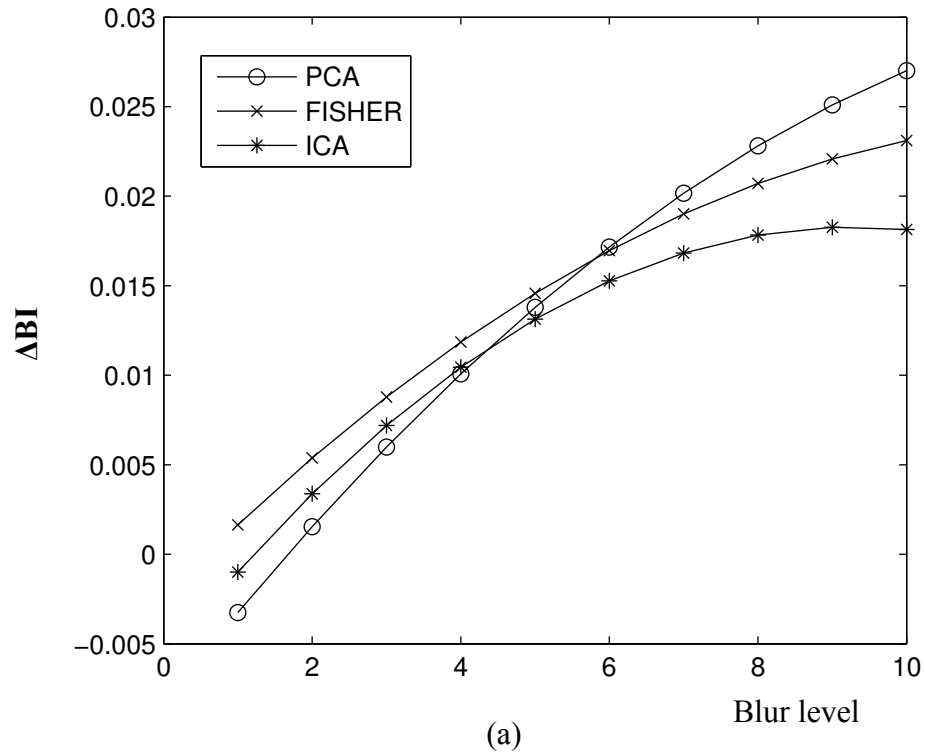
Figure 5.9: ΔBI as a function of an increasing blur level for images taken from (a) φ_1 **and (b)** φ_2

5.4 Biometric Iris Features Information

In this section we develop an algorithm to calculate biometric information based on a set of features, using the iris recognition system described in section (2.8) and the relative entropy measure developed in the section (5.2). The developed algorithm in this section is divided in the following steps: i. distribution modeling of iris biometric features, ii. relative entropy calculations, iii. ICA iris feature extraction and biometric information calculation. The iris regions used in the entropy calculation are obtained using the Masek and the enhanced iris segmentation techniques described in section (4.2).

In a generic biometric system, S biometric features are measured, to create a biometric feature vector $\mathbf{x}$ $(S \times 1)$ for each iris. For a person iris z in a subset of irises w, we have N_z feature samples, while we have N_w samples for a set of irises. Defining $\mathbf{x}$ as an instance of random variable X, we calculate the population feature mean μ_w

$$\mu_w = \underset{w}{E}[X] = \frac{1}{N_w} \sum_{i=1}^{N_w} \mathbf{x}_i \tag{5.13}$$

where the feature mean of an iris z, μ_z, is defined analogously, replacing w by z. The iris feature covariance matrix Σ_w can be written as follows:

$$\Sigma_w = \underset{w}{E}\left[(X - \mu_w)^t(X - \mu_w)\right] = \frac{1}{N_w - 1} \sum_{i=1}^{N_w} (\mathbf{x}_i - \mu_w)^t(\mathbf{x}_i - \mu_w) \tag{5.14}$$

The individuals iris feature covariance,Σ_z, is again defined analogously. One important general difficulty with direct information theoretic measures is that of data availability. Based on the Gaussian model, we can write:

$$z(\mathbf{x}) = \frac{1}{\sqrt{|2\pi\Sigma_z|}} exp\left(-\frac{1}{2}\left(\mathbf{x} - \mu_z\right)^t \Sigma_z^{-1}\left(\mathbf{x} - \mu_z\right)\right) \tag{5.15}$$

$$w(\mathbf{x}) = \frac{1}{\sqrt{|2\pi\Sigma_w|}} exp\left(-\frac{1}{2}\left(\mathbf{x} - \mu_w\right)^t \Sigma_w^{-1}\left(\mathbf{x} - \mu_w\right)\right) \tag{5.16}$$

From which we can calculate $D(z\|w)$.

$$D(z\|w) = \int z(\mathbf{x})\left(log_2 z(\mathbf{x}) - log_2 w(\mathbf{x})\right)d\mathbf{x}$$

$$= -k\left(ln|2\pi\Sigma_z| - ln|2\pi\Sigma_w| + 1 - \underset{z}{E}\left[\left(\mathbf{x} - \mu_w\right)^t \Sigma_w^{-1}\left(\mathbf{x} - \mu_w\right)\right]\right)$$

$$= k\left(ln\frac{|2\pi\Sigma_w|}{|2\pi\Sigma_z|} + trace\left((\Sigma_z + \mathbf{T})\Sigma_w^{-1} - \mathbf{I}\right)\right) \tag{5.17}$$

where $\mathbf{T} = (\mu_z - \mu_w)^t(\mu_z - \mu_w)$ and $k = log_2\sqrt{e}$.

This expression calculates the relative entropy in bits for Gaussian distributions $z(\mathbf{x})$ and $w(\mathbf{x})$. This expression corresponds to most of the desired requirements for a biometric feature information measure introduced in the section (5.2.2). The regularization scheme used for this method is the same as the one described in sections (5.2.3 and 5.2.4).

In order to measure the biometric feature information content of a biometric iris feature representation, we calculate the average biometric feature information for each iris in group of irises. This is a measure of the system biometric information (SBI) which can be calculated by the average IBI over the set of irises w.

$$SBI_{iris} = E_w[D(z||w)]$$

$$= \frac{1}{2}log_2|\Sigma_w\Sigma_z^{-1}| + tr(\Sigma_z\Sigma_w^{-1}) \tag{5.18}$$

Information in a feature representation of an iris is calculated using our described method for different irises. In order to test our algorithm, it is necessary to have multiple images of the same iris. For this reason, we used the CASIA database which includes 689 iris images taken using 108 subjects where 6 or 7 images were presented per class (i.e. subject's eye). The iris images were processed using the iris recognition and eyelash detection schemes described in section (4.2) from which we calculate the PCA (eigen-iris) features using the algorithm of (Grother (2000)) and the ICA iris features components using the algorithm described in (Xiang et al. (2004. For PCA and ICA feature decompositions, 327 separate feature vectors were computed and used for subsequent analysis. Figure 5.10 and Figure 5.11 illustrate the amount of biometric information calculated per PCA and ICA iris feature, respectively. Using the biometric information calculation procedure described in section (5.2), the sum of the biometric information over the PCA iris features extracted from the set of irises taken from the CASIA database give approximately 278 bits using Masek's algorithm. On the other hand, we computed 267 bits of information for the PCA iris features when using the

developed enhanced iris segmentation algorithm. The difference in bits can be explained by the fact that Masek's technique doesn't completely eliminate eyelash noise over the iris region and these pixels are falsely used as iris information. This will increase the biometric information since the algorithm takes eyelash as iris texture which then, compared to the rest of the irises in the set, makes it more unique or different.

In addition, Gabor features were used for the biometric information calculation. These features were decomposed using the ICA technique described in (Xiang et al. (2004)) in order to have N independent feature vectors. ICA has the advantage that it does not only decorrelates the signals but also reduces higher-order statistical dependencies in order to make the signals as statistically independent as possible. Since ICA maximizes non-gaussianity, it fits well to the assumptions that iris features tend to be non-gaussian. For the ICA features, an average of 288 bits was computed for $D(z\|w)$ using the Masek's segmentation algorithm and 277 bits using the enhanced segmentation algorithm. As noticed, the amount of information per iris feature is very close for PCA and ICA features. ICA features tend to contain more information since they fit the iris feature data model better.
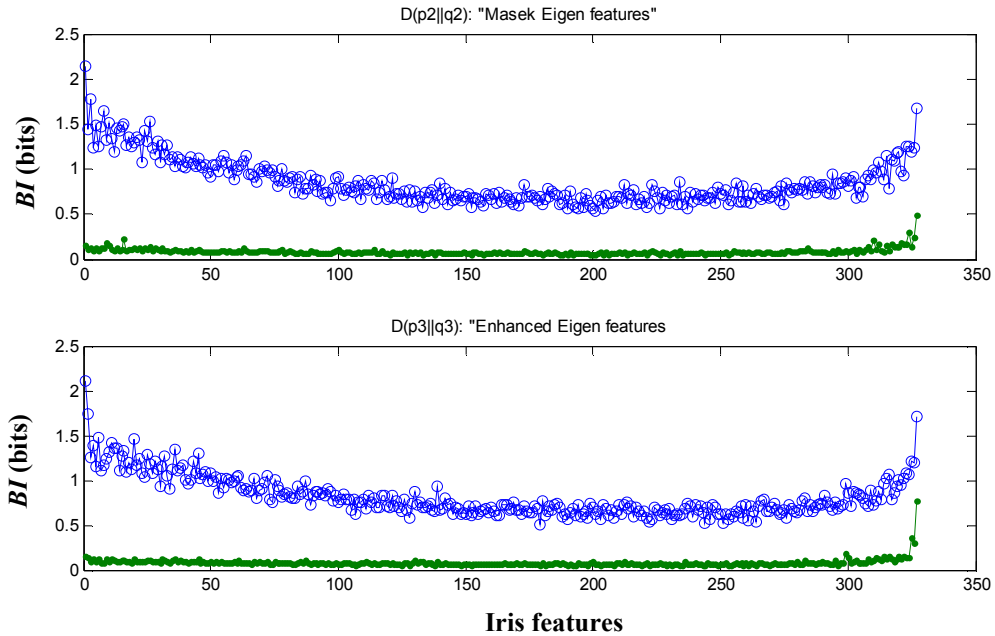
Figure 5.10: Biometric Eigen iris feature information computed for 327 iris features. The y-axis represents the biometric information for each feature (in bits) and the x-axis is the feature number. The top graph is calculated using the Masek's algorithm while the bottom graph is generated using the enhanced technique. The standard deviation is also plotted at the bottom of each graph.
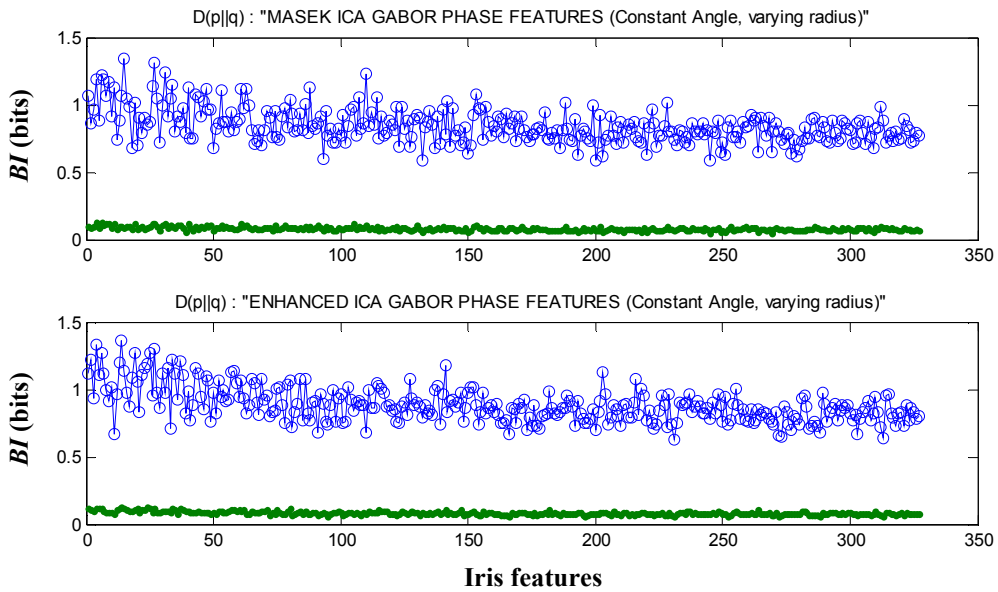
Figure 5.11: Biometric ICA iris feature information computed for 327 iris features where the features are extracted from the iris region at a constant angle/varying radius. The y-axis represents the biometric information for each feature (in bits) and the x-axis is the feature number. The top graph is calculated using the Masek's algorithm while the bottom graph is generated using the enhanced technique. The standard deviation is also plotted at the bottom of each graph.
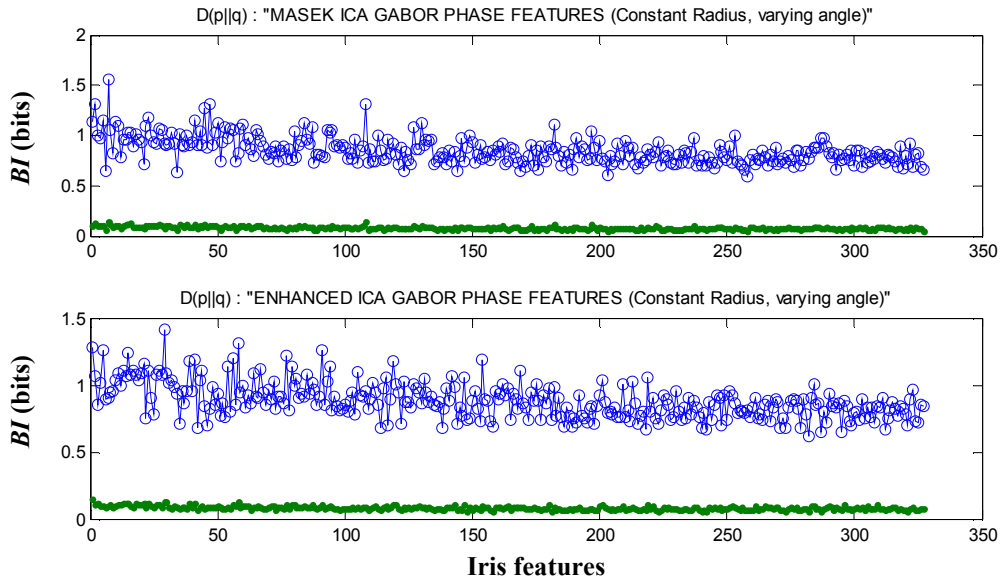
Figure 5.12: Biometric ICA iris feature information computed for 327 iris features where the features are extracted from the iris region at a varying angle/constant radius. The y-axis represents the biometric information for each feature (in bits) and the x-axis is the feature number. The top graph is calculated using the Masek's algorithm while the bottom graph is generated using the enhanced technique. The standard deviation is also plotted at the bottom of each graph.

5.5 Discussion

This work describes an approach to measure biometric feature information and the changes in biometric sample quality resulting from image degradations. A definition of biometric feature information is introduced and an algorithm to measure it proposed, based on a set of population and individual biometric features, as measured by a biometric algorithm under test. Biometric information is defined in terms of the reduction in uncertainty of the identity of a person resulting from a set of biometric feature measurements. Based on this definition, we show that this concept matches the information theoretic concept of relative entropy $D(p\|q)$, where p is the probability distribution of the person's features, and q is the distribution of features of the population.

Examples of its application were shown for two different face recognition algorithms based on PCA (Eigenface) and FLD feature decompositions. Subsequently, we introduced a measure of information loss as a function of image degradation. It is shown that the normalized mean square distance measure (ΔBI), based on the relative entropy, increases with the blur level but reaches a steady state after some amount of degradation which suggests that some features are unaffected by this degradation process.

Clearly, the framework developed in this work depends on accurate estimates of the population distributions q. Developing a good estimate of the "world model" is known to be a hard problem; in this work, we use the typical approach of assuming our database is an adequate representation of the population. The result of biometric feature information calculations (approximately 40 bits per face) is compatible with previous analyses of face recognition accuracy. From the FRVT results, we extrapolate the gallery size for an identification rate of 0.5 (Philips *et al.* (2003, 2007)). This is taken to be a rough model of the population for which the algorithm can reduce the identity uncertainty to 50%. For the top three face recognition algorithms described in Philips *et al.* (2003, 2007), the gallery sizes were 1.67×10^8, 3.53×10^7, and 2.33×10^6, corresponding to 27.3, 25.1, and 21.2 bits. These values correspond to over half the ones we calculated in this work which seems reasonable, since the FRVT database appears to be significantly more difficult than the one used here (Craw *et al.* (1999)), and current face recognition algorithms are not yet considered to be close to optimal. They seem to use approximately 1/2 to 2/3 of the available feature information.

In addition, this work describes an approach to measure biometric feature information for iris images segmented using the Masek and enhanced algorithms. It was shown that Masek's segmentation overestimates the eyelash noise in an iris image which tends to falsify the iris data by classifying eyelash noise as valid iris pixels (Xie (2007)). This will have an effect on the biometric information calculation since eyelash features add information to the iris image by making it more unique compared to the rest of the images. Examples of its application were shown for two different iris recognition algorithms based on PCA and ICA feature decompositions. The result of biometric feature information calculations (approximately 278 bits for PCA and 288 bits for ICA iris features using the Masek's code while obtaining 267 bits for PCA and 277 bits for ICA iris features using the enhanced segmentation algorithm) is compatible with previous analyses of iris recognition accuracy. Daugman (2002) states that the combinatorial complexity of the phase information of the iris across different persons spans about 249 degrees of freedom. Expressing this variation as discrimination entropy (Cover and Thomas (1991)) and using typical iris and pupil diameters of $11\ mm$ and $5\ mm$ respectively, the observed amount of statistical variability among different iris patterns corresponds to an information density of about $3.2\ bits/mm^2$ on the iris. From this, we can easily calculate that an average iris should have an average iris area of $\pi \times (5.5^2 - 2.5^2) = 75.39\ mm^2$ which ideally would give $(3.2 \times 75.39) = 241$ bits per iris. Using our developed biometric information calculation scheme, we found that, depending on the feature decomposition and iris segmentation technique, we obtain on average 283 bits of information for the iris decomposition features using the Masek's segmentation technique and 272 bits of iris information when applying the enhanced

technique prior to feature extraction. These results obtained using our algorithm supports Daugman's theory since our iris images have an average iris diameter ranging approximately from $11\ mm$ to $11.5\ mm$ which explains the difference in bits between our method and Daugman's who assumes the iris diameter to be $11\ mm$. For instance, a positive difference of $0.5\ mm$ in the iris diameter size results in an increase of 28.52 bits using Daugman's discrimination entropy measure. Hence, this explains the difference in numbers between our current results and Daugman's assumptions.

As an exploration of the implications of this work, an analogy can be made between a biometric system and a traditional communication system in terms of information capacity (Cover & Thomas (1991)). The signal source transmits one symbol from an alphabet; this corresponds to one person from a population to be identified. The symbol is encoded and sent across a channel and is subject to channel noise; similarly, biometric features from a person are measured, and are subject to variability due to noise in the measurement system and to inherent feature variability. Thus the biometric feature measurement system corresponds to the communication channel. The communications system receiver detects a signal and must decide which symbol was sent, corresponding to the role of the biometrics identification process. In this context, $D(p\|q)$ is the differential information of a single signal, and the average $D(p\|q)$, weighted by the probability of each signal p, is the channel capacity. Based on this analogy, we can say that biometric feature information is the channel capacity of a biometric measurement system.

In a general biometric system, the following issues associated with biometric features must be considered:

• Feature distributions vary. Features, such as minutiae ridge angles may be uniformly distributed over 0–2π, while other features may be better modeled as Gaussian. In this work, all features are modeled as Gaussian. This is valid model for most PCA and FLD features, but is not valid for any ICA features (since ICA is designed to maximize non-Gaussianity). On the other hand, a Gaussian model may be considered to estimate an upper bound for the entropy.

• Raw sample images need to be processed by alignment and scaling before features can be measured. Any variability in registration will dramatically increase the variability in measured features and decrease the biometric feature information measure.

• Feature dimensionality may not be constant. For example, the number of available minutiae points varies. The method presented in this work does not address this issue, since the dimensions of $p(\mathbf{x})$ and $q(\mathbf{x})$ must be the same. Generalized Entropy measures exist which may allow an extension of this approach to non-constant dimensional features. It is interesting to note that the biometric entropy is larger for some faces. Figure 5.5 shows a range of biometric information (from 32 to 47 bits) for different individuals, which may help explain why some people are potentially easier to recognize than others. This is perhaps some evidence for the "biometrics zoo" hypothesis (Doddington (1998)) which classifies users, in the context of a speaker recognition system, into different

groups based on their tendency to affect the FAR and FRR of a biometric system. In general, it states that some individuals possess more reliable/recognizable features (i.e. subjects with features that are well separated from others in the database) compared to other users who are intrinsically difficult to recognize and who can degrade the performance of a biometric system by increasing the FRR or FAR. In order to explore this effect, we plot the biometric feature information as a function of average feature variance for each person (Figure 5.13). A significant correlation ($p < .01$) is calculated for those features indicating that they contain less variability in those subjects with higher biometric feature information. The BI measure may help address many questions in biometrics technology, such as the following:

• Uniqueness of biometric features: A common question is "are fingerprints really unique?". While Pankanti *et al.* (2002) have recently provided a sophisticated analysis of this problem based on biometric feature distributions directly, a general approach based on information content would help address this question for other biometric modalities.

• Inherent limits to biometric template size requirements. A maximum compression of biometric features will be limited to the biometric feature information. This theoretical lower limit may be of use for ID card applications with limited data density.

• Feasibility of biometric encryption: Proposed biometric encryption systems use biometric data to generate keys (Uludag *et al.* (2004)), and thus the availability of

biometric feature information limits the security of cryptographic key generation (Ballard *et al.* (2007), Dodis *et al.* (2004)).

• Performance limits of biometric matchers: While some algorithms outperform others, it clear that there are ultimate limits to error rates, based on the information available in the biometric features. In this application, the biometric feature information is related to the discrimination entropy (Daugman (2003)).

• Biometric fusion: Systems which combine biometric features are well understood to offer increased performance (Ross *et al.* (2003)). It may be possible to use the measure of biometric feature information to quantify whether a given combination of features offers any advantage, or whether the fused features are largely redundant. The example of fusion of FLD and PCA (200 features) given here clearly falls into the latter category since it does not necessarily offer double the amount of information.

• Novel biometric features: Many novel biometric features have been suggested, but it is often unclear whether a given feature offers much in the way of identifiable information. Biometric information measurement may offer a way to validate the potential of such features.

• Privacy protection: It would be useful to quantify the threat to privacy posed by the release of biometric feature information, and also to be able to quantify the value of

technologies to preserve privacy, such as algorithms to de-identify face images (Newton *et al.* (2005), Zhu *et al.* (2007)).
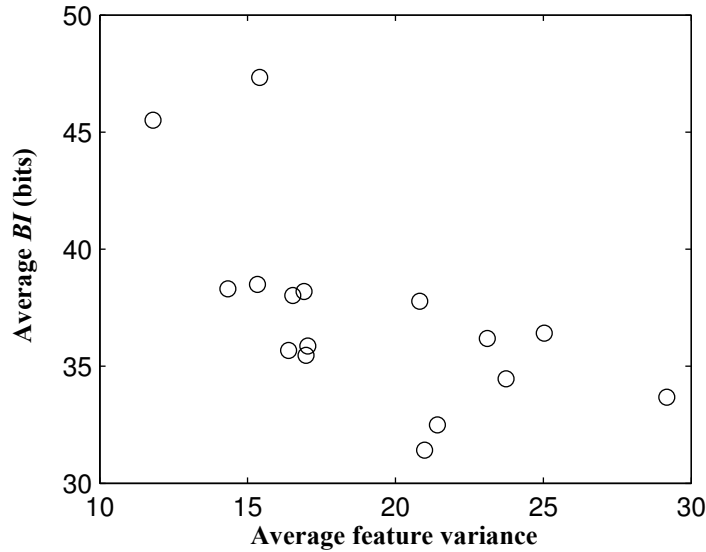
Figure 5.13: Average $D(p\|q)$ as a function of the mean feature variance (arbitrary units) (x-axis) for 16 different persons. The mean feature variance is computed by summing all the diagonal components of S_p matrix for each person. The correlation coefficient is -0.62, which is significant at $p < 0.01$.

5.6 Summary

This work describes an approach to measure biometric feature information and the changes in biometric sample quality resulting from image degradations. A definition of biometric feature information is introduced and an algorithm to measure it proposed, based on a set of population and individual biometric features, as measured by a biometric algorithm under test. Biometric information is defined in terms of the reduction in uncertainty of the identity of a person resulting from a set of biometric feature measurements and is measured using the relative entropy. Examples of its application

were shown for two different face recognition algorithms based on PCA and FLD feature decompositions. Subsequently, we introduced a measure of information loss as a function of image degradation. It is shown ΔBI, increases with the blur level but reaches a steady state after some amount of degradation which suggests that some features are unaffected by this degradation process. The result of biometric feature information calculations showed approximately an average of 40 bits of BI per face. In addition, this work describes an approach to measure biometric feature information for iris images segmented using the Masek and enhanced algorithms. Examples of its application were shown for two different iris recognition algorithms based on PCA and ICA feature decompositions. Biometric feature information calculations of approximately 278 bits for PCA, 288 bits for ICA iris features using the Masek's code and 267 bits for PCA, 277 bits for ICA iris features using the enhanced segmentation algorithm were obtained.

Chapter 6

Conclusion and Future Work

6.1 Discussion

Biometrics is a rising field of information technology that uses a subject's identifying biological traits in the goal to identify them. By calculating the physiological and behavioural characteristics using the individual's biological samples, it has been shown that information identifying each individual can be extracted in order to verify the identity of that individual in a population. The reason why biometrics is an attractive field is due to the fact that biometric traits cannot be forgotten or lost, they are difficult to copy, share and distribute and they require the person to be present at the time of authentication. Iris recognition technology is ranked as one of the best performing approaches to biometric recognition as compared with other biometric technologies such as fingerprint, hand geometry, speaker recognition and many more (Bolle *et al.* (1998)). Even though iris recognition is a relatively high performing technology, there are still some issues to be solved in order to further improve its accuracy and robustness.

In this thesis, new algorithms are developed to deal with low quality images for various applications in biometrics. A collection of techniques that can be applied for face and iris recognition in a non-cooperative environment is also presented. A novel scheme and new

algorithms are proposed for automatically detecting and recognizing human subjects via their face and eye traits at a long distance without cooperation. Face and iris recognition algorithms are widely used except that in most of them, images are taken from a cooperative individual under a controlled environment in order to provide satisfactory results (Ma *et al.* (2004)). Therefore, these techniques have limited capability of identifying non-cooperative subjects for applications such as surveillance, where the observed individuals are non-cooperating and/or non-habituated to the technology. Images taken from a non-cooperating individual tend to include more distortions and noise (i.e. low quality) hence the need of advanced algorithms to process low quality face and iris biometric images. The thesis objectives are to (i) use infrared illumination to improve eye and face tracking in low quality video images, (ii) develop improved identification of iris and eyelash features in low quality images, (iii) measure biometric sample quality in terms of biometric information for face features, (iv) measure information content in biometric iris and face features.

For the face tracking and eye detection algorithm, the first step is to locate the face in the image, detect the eyes and track the face based on pupil detection using IR illumination. The new algorithm for face and eye tracking extracts and tracks face and eye positions from surveillance type images with IR strobe taken under poor illumination. In the case where many reflections occur, the algorithm will find all possible eye locations and presents the best solution using multi-stage classification techniques. In order to reduce the set of possible eye region candidates, shape and geometric constraints are imposed in the classification process. A Kalman tracker is used to approximate eye location in bright

pupil images. If the image contains weak reflections, a local adaptive thresholding technique is used to extract the eye contour in order to estimate the pupil location. This improves the performance and accuracy of the system when dealing with faces at different orientation and with eye closure. Tested on 1800 IR images, the proposed system achieves a 99.5 % detection rate.

The second proposed algorithm is used on low quality eye/iris images where a major section of the iris region is occluded. The developed technique is intended to increase the biometric system's performance when dealing with low quality iris images, particularly when eyelash occlusions become severe. The developed iris recognition scheme is compared to the approach of Masek (1999) in order to observe the effect of the amount of valid iris image processed after noise detection on the system's performance assuming that more accurate iris segmentation (i.e. enhanced noise detection) results in better identification performance. The enhanced iris segmentation scheme is presented in chapter 4. The proposed method shows promising results for eyelash noise detection, accurate iris boundary extraction and ideal iris segmentation. This algorithm locates the iris region using logarithmic image enhancement and the Hough transform techniques, locates the iris boundary, extracts the exact iris contour, detects eyelash based on the local image statistics and block intensity and finally, proposes an ideal iris model for accurate iris recognition. The developed method overcomes the limitations encountered in other iris segmentation and eyelash detection techniques such that our method detects accurately separable and multiple eyelashes, extracts the exact iris contour and is illumination invariant. The developed method does not overestimate the eyelash noise in

the eye image, maximizing iris information. Using our technique, less iris noise and fewer eyelash occlusions are found in the normalized iris region compared to the approach of Masek (1999). The evaluation showed that this algorithm improves the error rates in DET curves except in very low FMR range. In addition, the decidability metric is calculated for both methods in order to measure the separation between the intra-class and inter-class Hamming distance distributions. It is seen that a higher decidability measure is obtained for the enhanced algorithm which implies that the iris recognition system implementing the enhanced eyelash detection scheme tend to have a better intra and inter-class distribution separation. This will result in lower false accept rate and false reject rate since it is easier to select the decision threshold that provides a good genuine-impostor distribution separation. The match score using the enhanced technique is better within the entire comparison range since it uses the most of the iris region in the pattern matching process. Masek's code neglects some valid iris pixels since it overestimates eyelash occlusion and noise pixels. This will result in a loss of valid iris pixels which will probably decrease the system's performance.

Finally, this work describes an approach to measure biometric feature information and changes in biometric sample quality resulting from image degradations. A definition of biometric feature information is introduced and an algorithm to measure it proposed, based on a set of population and individual biometric features, as measured by a biometric algorithm under test. Biometric information is defined in terms of the reduction in uncertainty of the identity of a person resulting from a set of biometric feature measurements. Based on this definition, we show that this concept matches the

information theoretic concept of relative entropy $D(p\|q)$, where p is the probability distribution of the person's features, and q is the distribution of features of the population. Examples of its application were shown for two different face recognition algorithms based on PCA (Eigenface) and FLD feature decompositions. Subsequently, we introduced a measure of information loss as a function of image degradation. We selected blur as a degradation process to test our algorithm. It is important to note that other type of degradations and distortions can also occur in a covert biometric system such as motion blur, head rotation, face occlusion, eyewear, non-uniform lighting, out-of-focus images and many more. It is shown that the normalized mean square distance measure (ΔBI), based on the relative entropy, increases with the blur level but reaches a steady state after some amount of degradation which suggests that some features are unaffected by this degradation process.

Clearly, the framework developed in this work depends on accurate estimates of the population distributions q. Developing a good estimate of the "world model" is known to be a hard problem; in this work, we use the typical approach of assuming our database is an adequate representation of the population. The result of biometric feature information calculations (approximately 40 bits per face) is compatible with previous analyses of face recognition accuracy. From the FRVT results, we extrapolate the gallery size for an identification rate of 0.5 (Philips *et al.* (2003, 2007)). This is taken to be a rough model of the population for which the algorithm can reduce the identity uncertainty to 50%. For the top three algorithms, the gallery sizes were 1.67×10^8, 3.53×10^7, and 2.33×10^6, corresponding to $27.3, 25.1$, and 21.2 bits. This value is over half that calculated here, and is reasonable, since the FRVT database appears to be significantly more difficult than the

one used here (Craw *et al.* (1999)), and current face recognition algorithms are not yet considered to be close to optimal. They seem to use approximately 1/2 to 2/3 of the available feature information.

Moreover, this work describes an approach to measure biometric feature information for iris images segmented using the Masek and the enhanced algorithms (Masek (1999)). It was shown that Masek's segmentation overestimates the eyelash noise in an iris image which tends to falsify the iris data by classifying eyelash noise as valid iris pixels. This will have an effect on the biometric information calculation since eyelash features add information to the iris image by making it more identifying compared to the rest of the images. Examples of its application were shown for two different iris recognition algorithms based on PCA and ICA feature decompositions. The result of biometric feature information calculations (approximately 278 bits for PCA and 288 bits for ICA iris features using the Masek's code while obtaining 267 bits for PCA and 277 bits for ICA iris features using the enhanced segmentation algorithm) is compatible with previous analyses of iris recognition accuracy. Daugman (2002) states that the combinatorial complexity of the phase information of the iris across different persons spans about 249 degrees of freedom. Expressing this variation as discrimination entropy (Cover and Thomas (1991)) and using typical iris and pupil diameters of $11\ mm$ and $5\ mm$ respectively, the observed amount of statistical variability among different iris patterns corresponds to an information density of about $3.2\ bits/mm^2$ on the iris. From this, we can easily calculate that an average iris should have an average iris area of $\pi \times (5.5^2 - 2.5^2) = 75.39\ mm^2$ which ideally would give $(3.2 \times 75.39) = 241\ bits$ per

iris. Using our developed biometric information calculation scheme, we found that, depending on the feature decomposition and iris segmentation technique, we obtain on average 283 bits of information for the iris decomposition features using the Masek's segmentation technique and 272 bits of iris information when applying the enhanced technique prior to feature extraction. These results obtained using our algorithm supports the value from Daugman (2002) since our iris images have an average iris diameter ranging approximately from $11\ mm$ to $11.5\ mm$ which explains the difference in bits between our method and Daugman's who assumes the iris diameter to be $11\ mm$. For instance, a positive difference of $0.5\ mm$ in the iris diameter size results in an increase of approximately $28.52\ bits$ using Daugman's discrimination entropy measure.

6.2 Future Work

Based on the results of this thesis, there are several promising avenues of research that are likely to yield useful results. For example, sophisticated methods can be developed to enhance circular detection by accurately locating the iris and pupil boundaries in the least amount of time, minimizing the identification error rates. It will be also interesting to study the biometric information theory in a way to analyze the information content with progressive image segmentation. It can give further insight into how the segmentation affects the biometric entropy for recognition. Does more iris mean additional discriminative information (in bits)?

Also, it is suggested to compare additional iris recognition algorithms in order to obtain new valuable information that will help improving the recognition accuracy of a typical

iris recognition system, according to different recognition strategies. Moreover, additional types of noise should be subject of further work, since this work dealt with low quality eye and face images but not necessarily with off-angle iris images which will obviously introduce new challenges to the recognition process.

Another idea will be to develop an accurate biometric identifier in a non-cooperative system. The algorithms and methods developed in this thesis can be used to understand the requirements to be able to physically implement a non-cooperative prototype system and to improve real-time algorithms for face and eye detection, face tracking and facial and iris recognition. Furthermore, since it is difficult to capture high-quality iris images with minimal user cooperation, the proposed methods in this thesis can be used to design a non-cooperative access control system for applications requiring high security. This system will identify individuals at a distance in an uncontrolled environment. When the subject is located within a capture zone, face and eye images will be captured using surveillance cameras. The subject can be located and tracked using advanced face detection and tracking techniques. In order to obtain high quality eye/iris images, a zoomed near infrared iris camera can be used to collect images of the targeted subject. The iris camera lens will automatically adjust its focal distance depending on the subject distance from the camera platform. From the acquired face and eye video frames, the proposed algorithms can be used to detect the subject's face, locate the eyes, reduce iris noise, segment the iris, generate a template and then identify the subject through typical pattern matching algorithms.

Another possible line of research is to use the entropy theory to analyze the information content with the progressive image segmentation proposed by Xie (2007). This will facilitates the understanding of the effects of iris noise segmentation on the biometric entropy for recognition.

Overall, all the developed techniques in this thesis could be used to improve an iris recognition system performance with low quality iris images. Such applications include security surveillance; face and eye tracking in poor lighting conditions, unsupervised capture of iris image under poor lighting conditions, iris capture for subjects on the move and many more. The results obtained in this thesis help to clarify future research directions in the effort to improve non-cooperative iris and face detection/recognition performance for low quality face and eye images.

Bibliography

Adler, A., Youmaran, R., Loyka, S. (2009).Towards a Measure of Biometric Feature Information. *Pattern Analysis and Applications*, **12**:261−270.

Adler, A. (2005). Vulnerabilities in biometric encryption systems. *Audio- and Video-based Biometric Person Auth.* NY, USA, 1100-1109.

Adler, A., Youmaran, R., Loyka, S. (2005). Information content of biometric Features. *Biometrics Consortium Conference Washington*, DC, USA.

Adler, A., Youmaran, R., Loyka S. (2005). Information content of biometric features. *Biometrics Consortium Conference*, Sep. 19-21, Washington, DC, USA.

Alter O, Brown PO, Botstein D.(2000). Singular value decomposition for genomewide expression data processing and modeling. *Proc Natl. Acad. Sci.,* **97**:10101−10106.

Asfaw, Y., Chen, B., Adler, A. (2002). Face detection using red-eye effect. Department of Electrical engineering, Montréal, Canada, 1211-1214.

Ballard, D.H. (1981). Generalizing the Hough transform to detect arbitrary shape, *Pattern Recognition*, **13**: 111-122.

Ballard, L.,Kamara, S.,Monrose, F., Reiter, M. (2007). On the Requirements of Biometric Key Generators, Technical Report TR-JHU-SPAR-BKMR-090707, John Hopkins University.

Boles, W., Boashash, B. (1998). A human identification technique using images of the iris and wavelet transform. *IEEE Transactions on Signal Processing*, **46** (4): 1185–1188.

Bolle, R., Pankanti, S. (1998). Biometrics, Personal Identification in Networked Society: Personal Identification in Networked Society. Kluwer Academic Publishers, Norwell, MA, USA.

Bovik, A.C. (2005). Handbook of Image and Video Processing. Elsevier Science & Technology.

Bradski, G.R. (1998). Computer vision face tracking for use in a perceptual user interface. *Intel Technology Journal*, 2nd Quarter.

Brady, N., Field, D. (2000). Local contrast in natural images: normalization and coding efficiency. *Perception*, **29** (9): 1041-1055.

Belhumeur, P.N., Hespanha, J.P., Kriegman, D.J. (1997). Eigenfaces vs. Fisherfaces: recognition using class specific linear projection, *Pattern Analysis and Machine Intelligence,* IEEE Transactions on, **19**:711 - 720.

Bovik, AL. (2000) "Handbook of Image and Video Processing", Academic Press Texas.

Bradski, G.R., (1998). Computer Vision Face Tracking For Use in a Perceptual User Interface. Workshop on Applications of Computer Vision.

Chau, M., Betke, M. (2005). Real time eye tracking and blink detection with USB cameras. Technical Report, Boston University Computer Science.

Chinese Academy of Sciences Institute of Automation. (2004).Casia iris image database. http://www.sinobiometrics.com

Chirillo, J., Blaul, S. (2003). Implementing biometric Security. Wiley Publishing, Inc.

Comaniciu, D., Ramesh, V., Meer, P. (2000). Real-time tracking of non-rigid objects using mean shift. *IEEE Conf. on Computer Vision and Pattern Recognition*, Hilton Head Island, South Carolina.

Comaniciu, D., Ramesh, V., Meer, P. (2003). Kernel-based object tracking. *IEEE Trans. Pattern Analysis and Machine Intelligence*. **25**(5):564–577.

Craw, I., Costen, N.P., Kato, T., Akamatsu, S. (1999). How should we represent faces for automatic recognition, *Pattern Analysis and Machine Intelligence,* IEEE Transactions on, **21**:725–736.

Conover, W.J. (1980). Practical Nonparametric Statistics, Wiley.

Cover, T.M., Thomas, J.A. (1991). Elements of Information Theory New York:Wiley.

Dansheng M. (2009). Face Tracking Algorithms: A Survey. Panasonic Singapore Lab, Singapore, Research Report.

Daugman, J. (1993) High confidence visual recognition of persons by a test of statistical independence. *IEEE Trans. Pattern Analysis and Machine Intelligence*, **15**:1148–1161.

Daugman, J. (2000). Biometric decision landscapes. Technical Report No. TR482, University of Cambridge Computer Laboratory.

Daugman, J. (2003). The importance of being random: Statistical principles of iris recognition, *Pattern Recognition*, **36**:279–291.

Daugman, J. (2004). How Iris Recognition Works. IEEE Transactions on Circuits and Systems for Video Technology, **14** (1): 21-304.

Daugman, J. (2004). Recognizing Persons by Their Iris Patterns. Lecture Notes in Computer Science, **3338**: 5-25.

Daugman, J. (2005). Technical Report of Results from 200 Billion Iris Cross Comparisons. University of Cambridge. UCAM-CL-TR-635.

Daugman, J., Downing, C. (2001). Epigenetic Randomness, Complexity and Singularity of Human Iris Patterns. *Biological Sciences*, vol. 268, no. **1477**: 1737-1740.

Deng, G., Cahill, L.W. (1993). Multiscale image enhancement using the logarithmic image processing model. Electronics Letters, **29**:803-804.

Deng, G., Cahill, L.W. (1994). Image Enhancement Using the Log-ratio Approach, Signals Systems and Computers, **1**:198-202.

Dessimoz, D., Richiardi, J., Champaud, C., Drygajlo, A. (2005). Multimodal biometrics for identity documents. Technical report, University of Lausanne.

Doddington, G., Liggett, W., Martin, A., Przybocki, M., Reynolds, D. (1998). Sheep, Goats, Lambs and Wolves: An Analysis of Individual Differences in Speaker Recognition Performance, *Proc. Int. Conf. Auditory-Visual Speech Processing*, Sidney, Australia.

Dodis, Y., Reyzin, L., Smith, A. (2004). Fuzzy Extractors and Cryptography, or How to Use Your Fingerprints, Proc. Eurocrypt'04. http://eprint.iacr.org/2003/235/

Dorairaj, V., Schmid, N., Fahmy, G. (2005). Performance evaluation of non-ideal iris based recognition system implementing global ICA encoding. *In Proceedings of the IEEE International Conference on Image Processing* (ICIP 2005, 285–288.

Draper, B.A., Baek, K., Bartlett, M.S., Beveridge, J.R. (2003). Recognizing faces with PCA and ICA, *Computer Vision and Image Understanding*, **91**:115-137.

Du, Y., Bonney, B., Ives, R., Etter, D., Schultz, R. (2005). Analysis of partial iris recognition using a 1D approach. In Proceedings of the IEEE International Conference on Acoustics, Speech and Signal Processing (ICASSP'05), 961–964.

Duc B., Fischer, S., Bigun, J. (1999). Face Authentication with Gabor Information on Deformable Graphs. *IEEE Transactions on Image Processing*, **8**(4).

Ebisawa, Y., Satoh, S., (1993). Effectiveness of pupil area detection technique using two light sources and image difference method. *Proceedings of the 15th Annual Int. Conf. of the IEEE Eng. in Medicine and Biology Society*, San Diego, CA, 1268–1269.

Fancourt, G., Bogoni, L., Hanna, K., Guo, Y., Wildes, R., Takahashi, N., Jain, U. (2005). Iris recognition at a distance. In Proceedings of the 2005 IAPR Conference on Audio and Video Based Biometric Person Authentication, 1–13.

Field, D. (1987). Relations between the statistics of natural images and the response properties of cortical cells. *Journal of the Optical Society of America*.

Freund, Y., Schapire, R.E. (1996). Experiments with a New Boosting Algorithm. *13ᵗʰ Conf. on Machine Learning,* 148-156.

Fromherz, T., Stucki, P., Bichsel, M. (1997). A Survey of Face Recognition", MML Technical Report, No 97.01, Dept. of Computer Science,Zurich.

Gejgu, P., Perka, M. (2003). Face tracking in color video sequences, Proceedings of the 19th spring conference on Computer.

Golfarelli, M., Maio, D., Maltoni, D. (1997). On the Error-Reject Tradeoff in Biometric Verification Systems, *Pattern Analysis and Machine Intelligence,* IEEE Transactions on, **19**:786-796.

Gonzalez, R.C., Woods, R.E. (2002). Digital Image Processing, Addison-Wesley Publishing Company.

Grother, P. (2000). Software Tools for an Eigenface Implementation, National Institute of Standards and Technology, http://www.nist.gov/humanid/feret/

Haro, A. ,Flickner, M., Irfan, E. (2000). Detecting and Tracking Eyes By Using Their Physiological Properties, Dynamics, and Appearance. *Computer Vision and Pattern Recognition Conference*, June 13-15.

Huang C., Ai, H., Li, Y., Lao, S. (2007). High-Performance Rotation Invariant Multiview Face Detection. Pattern *Analysis and Machine Intelligence, IEEE Transactions on*. **29** (4).

Huang, W., Mariani, R. (2000). Face detection and precise eyes location", *in: Proc. Int. Conf. on Pattern Recognition*.

Huang, J., Wang, Y., Tan, T., Cui, J. (2004). A New Iris Segmentation Method for Recognition, *Proceedings of the 17th International Conference on Pattern Recognition*, 1051-4651.

Hyvarinen, A. (1999). Fast and Robust Fixed-Point Algorithms for Independent Component Analysis. *IEEE Trans. Neural Networks* **10**:626–634.

Institute of Automation of the Chinese Academy of Sciences. (2003). CASIA V1.0. CASIA Iris Image Database, Beijing, China.

International Biometric Group (2005). Independent test of iris recognition technology. *http://www.biometricgroup.com/reports*.

ISO JTC1 SC37 Biometrics (2007). ISO 29794-1 Biometric Sample Quality, Committee Draft 1.

Jain, A.K., Ross, A., Prabhakar, S., (2004). An Introduction to Biometric Recognition. IEEE Transactions on circuits and systems for video technology, 14(1).

Jain, A., Hong, L., Pankanti, S. (2000). Biometric Identification. Communications of the Association for Computing Machinery, **43** (2): 90-98.

Kong, S.G., Heo, J., Abidi, B.R., Paik, J., Abidi, M.A.. (2005). Recent advances in visual and infrared face recognition: a review. *Computer Vision and Image Understanding*, **97**,1.

Kong, W.K., Zhang, D. (2001). Accurate Iris Segmentation Based on Novel Reflection and Eyelash Detection Model, *Proceedings of International Symposium on Intelligent Multimedia, Video and Speech Processing*, 263-266.

Kosmerlj, M. (2004). Passport of the Future: Biometrics against Identity Theft? MSc thesis, Gjovik University College, NISlab.

Kovesi, P. (1997). Image Features From Phase Congruency, *Journal of Computer Vision Research*, **1**:1-27.

Kryszcuk, K., Drygajlo, A. (2005). Gradient-based image segmentation for face recognition robust to directional illumination. In Visual communications and image processing 2005: 12-15, Beijing, China.

Kryszcuk, K., Drygajlo, A. (2006). On combining evidence for reliability estimation in face verification. In. Proc. Of the EU-SIPCO 2006, Florence.

Kuncheva, L.I., Whitaker, C.J., Shipp, C.A., Duin, R.P.W. (2000). Is independence good for combining classifiers?. Int'l Conf. on Pattern Recognition (ICPR), **2:**168–171.

Lee, T.W. (1999). Nonlinear approaches to independent component analysis, Proc. American Institute of Physics.

Li, S., Jain A. (Eds.). (2005). Handbook of Face Recognition. Springer.

Li, Y., Ai, H., Yamashita, T., Lao,S., Kawade, M. (2008). Tracking in Low Frame Rate Video: A Cascade Particle Filter with Discriminative Observers of Different Life Spans, *Pattern Analysis and Machine Intelligence, IEEE Transactions on* **30** (10).

Ma, L., Tan, T., Zhang, D., Wang, Y. (2004). Local Intensity Variation Analysis for Iris Recognition. *Pattern Recognition*, **37:**1287-1298.

Mansfield A.J., Wayman, J.L.(2002). Best Practices in Testing and Reporting Performance of Biometric Devices, Version 2.01. Centre for Mathematics and Scientific Computing, National Physical Laboratory, Queens Road, Teddington, Middlesex, TW11 OLW.

Masek, L., Kovesi, P. (2003). MATLAB Source Code for a Biometric Identification System Based on Iris Patterns. School of Computer Science and Software Engineering. University of Western Australia, Perth, Australia.

Masek, L. (2003). Recognition of Human Iris Patterns for Biometric Identification. Master's thesis, School of Computer Science and Software Engineering, University of West Australia, Perth, Australia.

Montgomery, T.M. (2007). Iris image, "Anatomy, Physiology and Pathology of the Human Eye". Available:
http://www.tedmontgomery.com/theeye/eyephotos/IrisNevus.html

Morimoto, C.H. ,Koons, D.,Amir, A.,Flickner,M. (1998). Pupil Detection and Tracking Using Multiple Light Sources. *Technical Report RJ-10117*, IBM Almaden Research Center, San Jose, Ca. http://domino.watson.ibm.com/library/cyberdig.nsf/Home.

Newton, E.M., Phillips, P.J. (2007). Meta-Analysis of Third-Party Evaluations of Iris Recognition. Technical Report NISTIR 7440, National Institute of Standards and Technology, Gaithersburg, MD.

Newton, E.M., Sweeney, L., Malin, B. (2005). Preserving Privacy by De-Identifying Face Images, *IEEE Trans. Knowledge Data Eng.* **17**: 232–243.

Niblack, W. (1986). An Introduction to Image Processing", Prentice-Hall, Englewood Cliffs, NJ, 115–116.

Nixon, M. (1985). Eye spacing measurement for facial recognition", *in: Proc. of the Society of Photo-Optical Instrument Engineers*.

Ojala, T., Pietikäinen, M., Harwood, D. (1996). A Comparative Study of Texture Measures with Classification Based on Feature Distributions. *Pattern Recognition* **19**(3):51-59.

Pan, G., Wu, Y., Wu, Z., Liu, W. (2003). 3D face recognition by profile and

surface matching. *Neural Networks, IEEE,* **3**:2169–2174.

Pankanti, S., Prabhakar, S., Jain, A.K. (2002). On the Individuality of Fingerprints, *Pattern Analysis and Machine Intelligence,* IEEE Transactions on, **24**:1010–1025.

Papageorgiou, C., Oren, M., Poggio, T. (1998). A general framework for object detection. International Conference on Computer Vision.

Pentland, A., Moghaddam, B., Starner, T. (1994). View-based and modular eigenspaces for face recognition. *Proc. IEEE Conf. on Computer Vision and Pattern Recognition*, Seattle, WA.

Phillips, P.J., Martin, A., Wilson, C.L., Przybocki, M. (2000). An Introduction to Evaluating Biometric Systems," Computer, **33**(2):56-63.

Phillips, J. The Face Recognition Grand Challenge (FRGC). http://www.frvt.com/FRGC/. Phillips, P.J., Grother, P., Micheals, R.J., Blackburn, D.M., Tabassi, E., Bone, J.M. (2003). FRVT 2002: Evaluation Report, NIST. http://www.frvt.org/DLs/FRVT_2002_Evaluation_Report.pdf

Phillips, P.J., Scruggs, T.W., OToole, A.J., Flynn, P.J., Bowyer, K.W., Svhott, C.L., Sharpe, M. (2007). FRVT 2006: Evaluation Report, NIST. http://www.frvt.org/FRVT2006/docs/FRVT2006andICE2006LargeScaleReport.pdf

Poursaberil, A., Araabi1, B. N. (2006). Iris Recognition for Partially Occluded Images: Methodology and Sensitivity Analysis. EURASIP Journal on Advances in Signal Processing, 25-38.

Proenca, H.P. (2006). Towards Non-Cooperative Biometric Iris Recognition. University of Beira Interior. Department of Computer Science.

Ritter, N., Owens, R. (1999). Location of the Pupil-Iris Border in Slit-Lamp Images of the Cornea. International Conference on Image Analysis and Proceedings, **00**: 740-745.

Ritter, N., Cooper, J.R. (2003). Locating the iris: A first step to registration and identification. In Proc. 9th IASTED *International Conference on Signal and Image Processing*, 507-512.

Ross, A., Jain, A. (2003). Information Fusion in Biometrics, *Pattern Recognition Letters*, **24**:2115-2125.

Rukhin, A., Malioutov, I. (2005). Fusion of Biometric Algorithms in the Recognition Problem. *Pattern Recognition Letters*, **26** (5): 679-684.

Sandström, M. (2004) Liveness Detection in Fingerprint Recognition Systems. MSc thesis, Linköpings tekniska högskola.

Sarnoff Corporation. Iris On The Move, 2005. http://www.sarnoff.com/

Schuckers, S. A. C. (2002). Spoofing and Anti-Spoofing Measures. *Information Security Technical Report*, **7**(4), 56–62.

Soutar, C., Roberge, D., Stoianov, A., Gilroy, R., Vijaya, B. (1998). Biometric Encryption using image processing, *Proc. SPIE Int. Soc. Opt. Eng.,* **3314** 178-188.

Sung, E., Chen, X., Yang, J. (2002). Towards non-cooperative iris recognition systems. In Proceedings of the seventh International Conference on Control, Automation, Robotics and Vision (ICARV'02), 990–995.

Swaminathan, G., Venkoparao, V., Bedros, S., Rowley, H. (2007). Multiple appearance models for face tracking in surveillance videos. Advanced Video and Signal Based Surveillance. IEEE Conference AVSS 2007.

Tabassi, E., Wilson C.R., Watson, C.I. (2004). Fingerprint Image Quality, NISTIR 7151.

Tisse, C.L., Torres, L., Robert, M. (2002). Person Identification Technique using Human Iris Recognition. *International Conference on Vision Interface*. Calgary, Canada, 294-299.

Tajbakhsh, N., Araabi, B.N., Soltanianzadeh, H. (2008). Feature fusion as a practical solution toward non-cooperative iris recognition. *Information Fusion, 11th International Conference on.* Control & Intell. Process. Center of Excellence, Univ. of Tehran. 1-7.

Turk, M., Pentland, A. (1991). Eigenfaces for recognition, *J. Cognitive Neuroscience*, **3**:71-86.

Turk, M., Pentland, A. (1991). Face Recognition Using Eigenfaces. *Proceedings of the IEEE Computer Society Conference on Computer Vision and Pattern Recognition*, June Maui, Hawaii, 586-591.

Uludag, U., Pankanti, S., Prabhakar, S., Jain, A.K. (2004). Biometric Cryptosystems: Issues and Challenges, *Proc. IEEE* **92**:948–960.

Viola, P., Jones, M. (2001). Robust Real-time Object Detection. Second International Workshop on Statistical and Computational Theories of Vision - Modeling, Learning, Computing and Sampling.

Wang, C., Li, Z. (2008). A New Face Tracking Algorithm Based on Local Binary Pattern and Skin Color Information. *Computer Science and computational Technology*, ISCSCT'08. International Symposium on. **2**: 20-22.

Wang, Y., Zhu, Y., Tan, T. (2002). Personal Identification Based on Iris Recognition, Acta Automatica Sinica, **28**:1-10.

Wang, P., Ji, Q. (2005). Learning Discriminant Features for Multi-View Face and Eye Detection. *IEEE International Conference on Computer Vision and Pattern Recognition* (CVPR), San Diego, CA.

Wayman, J. (1999). Error Rate Equations for the General Biometric System. IEEE Transactions on Robotics and Automation Magazine, **6**: 35-48.

Wayman, J.S. (2001). A Definition of Biometrics. *http://www.engr.sjsu.edu/biometrics/nbtccw.pdf*.

Wayman, J.S. (2004). The cotton ball problem, *Biometrics Conference*, Washington DC, USA.

Wayman, J., Jain, A., Maltoni, D., Maio, D. (2005). Biometric Systems: Technology, Design and Performance Evaluation. Springer-Verlag London Limited.

Wildes, R., Asmuth, J.C., Green, G.L. (1996). A machine Vision System for Iris Recognition. *Machine Vision and Applications*, **1**(9): 1432-1769.

Wildes, R. (1997) Iris recognition: An emerging biometric technology. *Proc. IEEE*, **85**:1348–1363.

Xiang, C., Fan, X.A., Lee, T.H. (2004). Face recognition using recursive Fisher linear discriminant, *Communications, Circuits and Systems international Conference on*.

Xie, L. (2007). Algorithms for Recognition of Low Quality Iris Images. Master's thesis, Carleton University, Ottawa.

Adler, A., Youmaran, R., Loyka, S. (2009). Towards a Measure of Biometric Feature Information. *Pattern Analysis & Applications*, 12:261−270.

Youmaran, R., Adler, A. (2008). Measuring Information Content in Biometric Features. Book chapter in Biometrics: Theory, Methods, and Applications N.V. Boulgouris, K.N. Plataniotis, and E.Micheli-Tzanakou (Eds), In press: Wiley/IEEE 2008.

Youmaran, R., Adler, A. (2008). Using Infrared Illumination to Improve Eye & Face Tracking in Low Quality Video Images. *24th Queen's Biennial Symposium on Communications*, QBSC 2008, Kingston, Canada.

Youmaran, R., Lipeng, X., Adler, A. (2008). Improved Identification of Iris and Eyelash Features, *24th Queen's Biennial Symposium on Communications*, QBSC 2008, Kingston, Canada.

Youmaran, R., Adler, A. (2006). Measuring Biometric Sample Quality in Terms of Biometric Information. *Biometrics Consortium Conference 2006*, Sep. 19-21, Baltimore, MD, USA.

Youmaran, R., Adler, A. (2006). Towards a measure of biometric information. Can. *Conf. Computer Elec. Eng. (CCECE),* Ottawa, Canada, May 7-10.

Yuan, X., Shi, P. (2004). An Iris Segmentation Procedure for Iris Recognition, *Sinobiometrics*, 546-553.

Zhao, W., Chellappa, R., Philips, P.J., Rosenfeld, A. (2003). Face Recognition: A Literature Survey", *ACM Computing Surveys*.

Zhang, J., Yan, Y., Lades, M. (1997). Face Recognition: Eigenface, Elastic Matching, and Neural Nets. *Proceedings of the IEEE*, **85**(9),1423–1435.

Zhu, Y., Tan, T., Wang, Y.W. (2000). Biometric Personal Identification based on Iris Patterns. 15th International Conference on Pattern Recognition, **2**: 801-804.

Zhu, Z., Ji, Q. (2005). Robust real-time eye detection and tracking under variable lighting conditions and various face orientations. *Computer Vision and Image Understanding*, **1**: 124-154.

Zhu, Y., Dass, S. C., Jain, A. K. (2007). Statistical Models for Assessing the Individuality of Fingerprint, *IEEE Transactions on Information Forensics and Security*, **2**, No. 3, 391-401.